Genetic regulation of maize floral development - insights from the transcriptome and translatome

By

Hailong Yang

July, 2022

Director of Dissertation: Beth Thompson, PhD

Major Department: Department of Biology

ABSTRACT

Flowers are produced by floral meristems, groups of stem cells that give rise to floral organs. In grasses, including the major cereal crops, flowers (florets) are contained in spikelets, which contain one to many florets, depending on the species. Floral development in plants is regulated by gene expression. Understanding gene expression regulation in maize floral development is critical to regulate floret fertility in other grasses and potentially useful to engineer more productive cereal crops.

In this work, I focus on gene expression regulation at transcriptome and translatome level to gain insights into floral development. To transcriptionally gain insight into the functional differences between florets with different fates, I examined gene expression in upper and lower floral meristems in maize ear using laser capture microdissection coupled with RNA sequencing. Differentially expressed genes were involved in hormone regulation, cell wall, sugar and energy homeostasis. Furthermore, cell wall modifications and sugar accumulation differed between the upper and lower florets. Finally, a novel boundary domain between upper and lower florets was

identified, which might be important for floral meristem activity. A model is proposed, in which growth is suppressed in the lower floret by limiting sugar availability and upregulating genes involved in growth repression.

To gain insight into microRNA regulation in maize floral development, I examined the translatome of a maize microRNA biogenesis mutant and normal siblings using ribosome profiling and RNA sequencing. My results indicated microRNAs in maize regulate both mRNA decay and translation repression. Importantly, translation repression by microRNAs is broad but magnitude is small in maize. Furthermore, translation is broadly affected beyond direct microRNA targets when microRNAs are perturbed. Thus, translation regulation is likely a critical regulator gene expression during floral development.

Genetic regulation of maize floral development - insights from the transcriptome and translatome

A Dissertation

Presented To

The Faculty of the Interdisciplinary Program in Biology, Biomedicine

and Chemistry: Biology

Department of Biology, Harriot College of Arts and Sciences

East Carolina University

Submitted in Partial Fulfillment

of the Requirements for the Degree

Doctor of Philosophy in Interdisciplinary Biology, Biomedicine and Chemistry

by

Hailong Yang

July, 2022

Genetic regulation of maize floral development - insights from the transcriptome and translatome

By

Hailong Yang

APPROVED BY:

Director of Dissertation _____

Beth Thompson, PhD

Committee Member _____

Elizabeth Ables, PhD

Committee Member _____

Brett Keiper, PhD

Committee Member _____

Eric Anderson, PhD

Committee Member _____

Patrick Horn, PhD

Chair of the Department of Biology _____

David Chalcraft, PhD

Dean of the Graduate School _____

Paul J. Gemperline, PhD

Acknowledgement

I would first like to greatly thank my advisor, Beth Thompson, for leading, guiding, and sharing her exciting scientific insight with me. Without her support, I am hardly able to make this way in my PhD. I would also like to highly appreciate the help from my committee, especially Brett Keiper, Eric Anderson, Patric Horn, Elizabeth Ables, for suggestions, discussion, and help during my PhD time.

I also want to thank members of Thompson labs and Scitech 575 labs both past and present. In particular, I want to say thank you to Jessica Wilson, Anastasia Amoiroglou, Katherine Novitzky, Daniel Maynard, Leasia Glover, Kimberly Rispress, Kate Nukunya, Queying Ding, Allison Beachum, and other folks for technical discussion, help, and advice along the way.

I would like to thank friends and colleagues who helped me with my PhD life and scientific projects: Prakitchai (Non) Chotewutmontri, Gita Arvind Gajjar, Madelaine Bartlett, Clinton Whipple, Michael Brewer, Julie Marik, Cathy Herring, Jim Holland, Cindy Kukoly, Ross Sozzani, Angel de Balaguer, Kristen Andrew, Wasseem Chaya, Emily Tate, Tom Fink, David Pearsall family, Don Holbert family, Julie Green, …

In the end, I cannot make it without the support from my family. I want to greatly thank my wife (Danfeng Wu) for encouraging and accompanying me for almost six years in the USA. I also want to appreciate love and support from my family's members, my mother, father, brothers, and my close relatives.

Table of Contents

List of Tables

List of Figures

Chapter 1

Genetic and physiological control in floret fertility

Grass crops provide staple foods and biomaterials around the world. Quality and production of grass crops are critical for the ever increasing human and livestock populations. A key determinant of grass quality and yield is floral fertility. Grass flower (floret) abortion/sterility is regulated by many biological mechanisms like floral transition, flowering time, floral fate, and floral organogenesis. As one main leading cause of floral sterility and reproductive success, the fate of floral meristems and floral organs controlled by key genes and physiological processes still seems elusive. In this review we focus on two themes on floral fertility or abortion: key genes and physiological modules, and outline the emerging framework to engineer floret fertility.

Flower morphology of grass crops

Grass flowers (florets) are contained in grass-specific structures, called spikelets, which are repetitive small branch structures in the grass inflorescence. Each spikelet contains two glumes and one or more florets depending on the grass species. Here, we focus on florets from barley, maize, and wheat spikelets: barley spikelets contain one floret; maize spikelets contain two florets; wheat spikelets usually contain 4-5 florets (Figure 1).

Barley and wheat inflorescences consist of a central spike that produce spikelets with bisexual florets. Barley produces triple spikelets, in which the central floret develops earlier than two lateral florets; the lateral florets are sterile, and the only functional floret is in the central spikelet (Figure 1A). For wheat spikelet development, wheat inflorescence meristem becomes determinate with a single terminal spikelet at the apical spike. Barley and wheat spikelets contain one and 4-5 florets with two glumes, respectively (Figure 1B). The lemma with long projecting

tips called awn and palea enclose two lodicules, three stamens, and one pistil whose two styles are tipped with a biforked and hairy stigma (Ferrante et al., 2013; McKim et al., 2018).

Maize is a monecious plant, which has male and female inflorescences in separate positions on the same plant (Figure 1C). Both male (tassel) and female (ear) inflorescences (ear) are patterned similarly except that tassel also has the lateral branches. Spikelets are produced in pairs and each spikelet contains two glumes and two florets. One of two florets is aborted when the ear spikelet matures. Tassel spikelets contain two fully functional florets. Each floret contains two bract-like organs, the lemma and palea, two lodicules (analogous to petals), three stamens and three carpels. Florets in both the tassel and ear are intially bisexual and sex determination occurs through stamen arrest in the ear and carpel abortion in the tassel (Thompson and Hake, 2009; Yang et al., 2022).

Grass inflorescence development is dependent on the activity of meristems. Meristems serve as stem cell pools and can be determinate (stem cells are consumed in the production of primordia) or indeterminate (stem cells remain after production of primordia). In general, when grass plants transit from vegetative stage to reproductive stage, shoot apical/axillary meristem transforms into inflorescence meristem (IM). IMs of maize and barley are indeterminate and wheat IM is determinate. Maize IM will produce spikelet pair meristems (SPM), which in turn initiate two spikelet meristems (SM). Maize tassel IM will also produce branch meristems containing spikelet pair meristem. However, IM of barley and wheat produces a series of double spikelet ridges. Each barley spikelet ridge contains triple spikelet meristems: two lateral spikelet meristems and one central spikelet meristem. Each wheat ridge produces one single spikelet meristem. Maize and barley spikelet meristems are determinate: maize and barley SM gives rise

to two and one floral meristems (FM), respectively. In contrast, spikelet meristems of wheat are indeterminate (Sakuma and Schnurbusch, 2020). Wheat spikelet meristems can produce up to about 12 floral meristems, but usually have five or fewer fertile florets at anthesis (Ghiglione et al., 2008; Sakuma et al., 2019).

Genetic control in floret fertility

Floret fertility is important and can be a major contributor to yield. Recent decades have witnessed a growing genetic characterization in genes controlling floral sterility or fertility.

In barley, *six-rowed spike (vrs)* genes are required for lateral floret fertility (Lundqvist, 2014). To date, five *VRS* loci have been identified, all of which encode translational regulators. *VRS1* encodes a homeodomain-leucine zipper I (HD-ZIP) transcription factor and orthologous to maize *GRASSY TILLERS1 (GT1*). In wild barley, *VRS1* RNA is present in immature floral primordia and developing carpels of lateral florets. *VRS1* knockouts completely convert sterile lateral florets into fertile florets (Komatsuda et al., 2007; Sakuma et al., 2013).

In wheat, *Grain Number Increase1* (*GNI1*) encodes an ortholog of barley *VRS1* and maize *GT1*, HD-Zip I transcription factor. Transcripts of *GNI1* were detected in the distal end of wheat spikelets and the rachilla that bear the florets or floral primordia. Knockdown of *GNI1* increased the fertile florets in wheat spikelets, probably by inhibiting the aborting fate of floral primordia (Sakuma et al., 2019).

There are two genetic modifiers (*VRS4* and *VRS5*) likely acting upstream of the *VRS1* pathway in barley. *vrs4* mutants also have complete fertile lateral florets with additional indeterminate florets. *VRS4* belongs to one of LATERAL ORGAN BOUNDARIES (LOB)

transcription factors and is orthologous to maize *RAMOSA2* (*RA2*). Similar to the localization of maize *RA2* RNA in axillary meristems (Bortiri et al., 2006), *VRS4* expression is also restricted to axillary meristems and mainly lateral florets of early developing spike. Later, *VRS4* RNA is localized in the central and lateral floret (Koppolu et al., 2013). *VRS5* (also called *INTERMEDIUM-C/INT-C*) encodes a TEOSINTE BRANCHED1/CYCLOIDEA/PROLIFERATING CELL NUCLEAR ANTIGEN FACTOR (TCP) transcription factor and is orthologous to maize *TEOSINTE BRANCHED1* (*TB1*). *vrs5* mutants have partial fertile conversion in lateral florets of the spike, where typically middle to upper part of rachis have fertile lateral florets (Ramsay et al., 2011). Resembling the specific expression of maize *TB1* in lateral meristems and primordia (Hubbard et al., 2002), *VRS5* RNA is strictly confined to lateral floret of the middle-upper spike (Thiel et al., 2021), consistent with *vrs5* mutant phenotypes.

Unlike *VRS1,* which is expressed exclusively in barley lateral florets, *VRS2* (encodes a SHORT INTERNODES/SHI transcriptional factor) is expressed throughout the central and lateral floret, and lemma primordia. *vrs2* mutants only rescue the fertile lateral florets at center of barley spike, coupled with fertile, extra lateral florets and sterile lateral florets in the base and tip of the spike, respectively (Youssef et al., 2017).

Barley *VRS3* encodes a putative H3K9me2/me3 demethylase with a conserved zinc finger and Jumonji C & N domain and is considered as a transcription activator. In the early development of barley spike, *VRS3* RNA is localized in the outer glumes of lateral floret and later is detected in rachis vascular tissues. *vrs3* mutants promote the partial fertile conversion of

lateral floret in barley spike: lateral fertile floret mainly in upper spike and extra lateral fertile florets mainly in central spike (Bull et al., 2017; van Esse et al., 2017).

Recent laser capture microdissection sequencing (LCM-seq) of barley floral meristems also identified a regulator in floret fertility called *SPL14*, which encodes a SQUAMOSA PROMOTER BINDING (SBP)-box transcription factor and is co-orthologous to maize *UNBRANCHED2* and *UNBRANCHED3*. Barley *SPL14* has high expression in the lateral floret and *spl14* mutants have variable fertile lateral florets. LCM-seq also further confirmed that *VRS1-5* displayed higher expression in lateral florets, consistent with previously reported RNA *in situ* hybridization (Thiel et al., 2021).

In maize, jasmonic acid (JA) genes are required for floret fertility, predominantly by sex determination pathway. JA-deficient mutants often produce tasselseed phenotype (sterile male florets and unaborted pistil) and sometimes unaborted lower floret in the ear. In maize, abortion of the lower floret is initiated by carpel abortion and this appears to use the same molecular mechanisms - at leats in part - that controls pistil abortion in tassel florets. Recessive mutants, *tasselseed1*(*ts1*) and *ts2,* and dominant *Ts5* mutant have the tasselseed phenotype and two fertile florets in ear spikelets. The *ts1* mutant is caused by downregulation of a JA biosynthesis enzyme whereas *Ts5* mutant is dominant and is caused by overexpression of a JA catabolic enzyme (so the effect is to reduce JA) (Emerson, 1920; Nickerson and Dale, 1955; Irish and Nelson, 1993; Irish et al., 1994; Lunde et al., 2019; Wang et al., 2020). Double mutants in the redundant JA biosynthetic mutants, *oxo-phytodienoate reductase7* (*opr7*); *opr8*, f also have similar tasselseed phenotypes resembling *ts1* and *ts2*, caused by reduced JA levels (Yan et al., 2012). In contrast, the recessive mutant *silkless1* (*sk1*) has normal tassel florets but eliminated pistils in the ear

florets by inappropriately accumulating JA to promote pistil abortion in the ear (Jones, 1925; Hayward et al., 2016). Phenotypic analysis of double mutants from *ts1;ts2*, *ts1;Ts5*, *ts2;Ts5*, *ts2; sk1*, *Ts5; sk1* also genetically suggested their direct or indirect physiological roles of JA biosynthesis and metabolism in maize floret fertility (Irish et al., 1994; Calderon-Urrea and Dellaporta, 1999; Lunde et al., 2019). RNA localization also suggests JA genes have potential roles in floret fertility. *TS1* RNA has broad expression in maize plants and, in the inflorescence, is specifically located in the base of spikelets, suggesting its non-cell autonomous mediation in adjacent floral development (Acosta et al., 2009). *TS5* RNA has high ectopic expression in pistil primordia in *Ts5* mutant inflorescences (Wang et al., 2020). Although *ts2* mutant is not clearly caused by direct regulation of JA genes, strong expression of *TS2* (encoding a short-chain alcohol dehydrogenase) was detected in the subepidermal cells of the tassel and ear gynoecium, implying its function in carpel abortion (DeLong et al., 1993; Calderon-Urrea and Dellaporta, 1999). *SK1* has highest expression in the ear but with no detectable RNA localization, indicating that *SK1* protects pistil development of ear upper florets from the elimination of JA pathway (Hayward et al., 2016).

Brassinosteroid (BR) biosynthetic mutants including *nana plant1* (*na1*) and *na2* also display feminized tassels with male floret defects. *NA1* RNA is expressed throughout stamen development and in the outer layer of aborting or pre-aborted carpel, suggesting BR roles in male and female floral organ development (Hartwig et al., 2011; Best et al., 2016).

Epigenetic state changes also likely regulate the floret fertility. An epigenetic mutant called *required to maintain repression 6* (*rmr6*) also has the *tasselseed* phenotype and two fertile florets

in ear spikelets, suggesting maintenance of epigenetic states controls the maize floret fertility (Parkinson et al., 2007).

A maize ortholog of barley *VRS1* and wheat *GNI1*, *GT1* also encodes a class I homeodomain leucine zipper transcription factor. Similar to the expression of barley *VRS1* and wheat *GNI1*, *GT1* also has strong expression in degenerating carpel primordia of maize florets and *gt1* mutant displayed sterile depressed carpel in tassel florets. However, GT1 protein appears to act as a non-cell-autonomous way, implying possible interactions with other molecules to exert functions (Whipple et al., 2011). Recent analysis of the *grassy tillers1; ramosa3* (*gt1;ra3*) double mutant showed bisexual tassels with two perfect florets (sterile derepressed carpel and fertile stamens) and two fertile florets of ear spikelets, suggesting interaction of *GRASSY TILLERS1 and RAMOSA3* has a unique carpel programming in floret fertility (Klein et al., 2022).

Although we have found genes involved in floret fertility, none of them seem to be a master regulator of floret fertility *per se* rather than they are general regulators for growth. If there are not master regulators of floret fertility, then the physiology that underlies floret fertility would be intriguing to consider.

Downstream physiological modules potentially control floret fertility

Gene expression studies to investigate floret fertility have revealed a similar set of physiological processes that likely contribute to floret fertility. Multiple core downstream physiological hubs work as synergistic or antagonistic signals to control floret fertility.

Hormone and sugar homeostasis controls the barley floret fertility. Higher cytokinin and sugar availability are responsible for floret fertility. Upregulation of cytokinin biosynthesis and sugar

transport genes (increasing cytokinin level and sugar availability) are required for fertile lateral florets of barley *vrs2* and *vrs4* (Koppolu et al., 2013; Youssef et al., 2017). Instead, upregulation of cytokinin degradation and sugar availability inactivate genes (decreasing cytokinin level and sugar availability, e.g. upregulation of UDP-glycosyltransferase to conjugate sugar and trehalose-6-phosphate phosphatase to decrease trehalose-6-phosphate and increase trehalose) are required for the extreme suppressed lateral florets of *deficiens* mutant (overexpression of *VRS1*) (Sakuma et al., 2017). Downregulation of trehalose biosynthesis genes is also observed in developing fertile lateral florets in *vrs4* mutant (Koppolu et al., 2013). Lower levels of auxin is also required for floret fertility. Indeed, downregulation of auxin biosynthesis is also required for fertile lateral florets of *vrs2*. Metabolite and hormone analysis confirmed higher level of sucrose and cytokinin as well as lower level of auxin were present in the developing *vrs2* mutant spike compared to wild type, especially in the basal and central part of *vrs2* spike where lateral florets were not suppressed (Youssef et al., 2017).

Metabolism and other physiological modules also potentially control the barley floret fertility. Downregulation of amino acid metabolism is required for fertile lateral florets of *vrs2* whereas upregulation of amino acid metabolism and glutathione S-transferase/GST activity are required for the extreme suppressed lateral florets of *deficiens* mutant (overexpression of *VRS1*) (Youssef et al., 2017; Sakuma et al., 2017). Cell wall modification potentially also controls the floret fertility in barley. Cell wall modification genes (e.g. pectin modification) were differentially regulated in barley *deficiens* and in *vrs4* mutants (Koppolu et al., 2013; Sakuma et al., 2017). Taken together, qualitative or quantitative variation in sugar, hormone, cell wall, metabolites

regulation likely serve as epicenters of downstream physiology regulation, which are potentially critical for barley lateral floret fertility.

In maize, conserved physiological modules are also required for floret fertility. LCM-seq in upper floral meristem and lower floral meristem also unveiled that core common physiological processes including hormone homeostasis, sugar metabolism, cell wall remodeling were involved in maize floret fertility. Remarkably, cell wall remodeling and pectin modification in particular is associated with program cell death in carpel abortion (Yang et al., 2022). Pectin modification has been extensively studied in organ primordia initiation of Arabidopsis (Peaucelle et al., 2008; Peaucelle et al., 2011). However, pectin modification in program cell death of maize flowers might uncover another significant role of cell wall remodeling in flower fertility.

Apart from core common physiological modules by LCM-seq, physiological studies in JA reveal that higher JA level is required for floret fertility in maize. Hormone and metabolite measurement of tassels authenticated JA deficiency of *ts1*, *Ts5,* and transgenic gain-of-function *SK1* plants as well as *opr7*; *opr8* double mutant. Moreover, exogenous JA application rescued male floret fertility in feminized tassels of *ts1*, *ts2*, *Ts5*, and gain-of-function *SK1* single mutants as well as *opr7*; *opr8* double mutant, tangibly establishing direct requirement of the downstream JA pathway to mediate maize floret fertility (Acosta et al., 2009; Yan et al., 2012; Hayward et al., 2016; Lunde et al., 2019; Wang et al., 2020). Another two downstream hormones are brassinosteroid (BR) and gibberellic acid (GA). Hormone measurement and exogenous treatment in *na1* mutant suggest deficiency of endogenous BR leads to the male sterility by failing to suppress the pistil development in *na1* mutant tassels (Hartwig et al., 2011). Genetic analysis of double mutants between *na2* mutant and GA-deficient mutants revealed that the BR pathway is

dependent on the GA pathway. Exogenous application of GA in *na2* mutant enhanced the severity of tasselseed phenotypes, implying BR shares some common physiological modules with GA to control the floret fertility (Best et al., 2016).

A handful of data has been investigated in controlling wheat floret fertility by downstream physiology. Wheat *GNI1* transcription factor is orthologous to maize *GT1* and barley *VRS1* and it might maintain part of conserved physiological regulation in floret fertility. Indeed, RNA-seq of *GNI1* knockdown and wild type revealed downstream nitrogen and sucrose metabolism as well as in G protein dynamics, which might account for increased fertile florets in *GNI1* knockdown mutant (Sakuma et al., 2019).

Relationship between genetic control and physiological modules

Most studies in grass floret fertility have mainly focused on characterization of key regulators. Barley key regulators have evidently turned out to be transcription factors like VRS1, 2, 4, 5 and SPL14, or epigenetic regulators like VRS4. Systemic findings on transcription regulators lead to a major premise in barley: complex transcription regulatory networks are required for downstream physiology. Part of the reason could probably be the evolution of transcription regulation, especially transcription factors. As one of principal contributors to transcription regulatory complexity, evolutionary mechanisms of transcription factors are involved in changes inside or outside of DNA-binding domain sequence and changes in the gene regulatory network upstream or downstream of the transcription factors (Romani and Moreno, 2021). Reasonably, dynamic downstream physiological adaptation requires upstream transcription regulatory complexity.

Common transcription regulatory networks may contribute to similar core downstream physiological modules. Large-scale transcriptomic analysis in *vrs1*, *vrs2*, and *vrs4* mutants shared several core downstream physiological modules, probably due to three molecular mechanisms of transcription factors: share common downstream targets or interchangeable targets; share similar interaction networks like protein-protein or metabolite-metabolite or protein-metabolite; involve similar distal or proximal chromatin remodeling. Supporting the third mechanism, RNA-seq of developing lateral florets from *vrs3* epigenetic mutant versus wild type also unveiled same striking alteration of physiology pathways like sugar homeostasis and hormone balance, likely by direct or indirect alteration of chromatin state of VRS1, VRS2, VRS4, and VRS5 transcription factors (Bull et al., 2017; van Esse et al., 2017). Genetic interaction of *vrs* single/double mutants, comparative transcriptome or expression analysis, and protein-protein interaction also support the hypothesis that VRS transcription factors not only direct common downstream physiological targets or interchangeable targets like cytokinin biosynthesis, but also share similar interaction networks, potentially through one of downstream integrators, VRS1 (Koppolu et al., 2013; van Esse et al., 2017; Zwirek et al., 2019; de Souza Moraes et al., 2022).

However, none of these above are master regulators of floret fertility. Barley and wheat *VRS* are general regulators of growth that can be and are deployed in multiple developmental contexts. While some of the upstream regulators are conserved (i.e. *VRS1*/*GT1* regulates floret fertility in barley), what is conserved in regulating floret fertility are the downstream physiological processes. Physiological modules controlling maize floret fertility appear to lack upstream transcription factors like barley or wheat. One possibility is that maize orthologs of

barley *VRS* genes do not independently control the floret fertility to a large extent, partially due to the possible evolutionary complexity from hermaphroditism to monoecy. Barley and wheat mature flowers are hermaphrodite (i.e. bisexual floral organs are in the same flower); maize mature flowers are monoecious (i.e. male and female floral organs in the sperate flowers but in the same plant). Monoecy is considered to evolve from bisexual-flowered ancestors (Torices et al., 2011). This evolutionary complexity might require maize orthologs to partner with other regulators to fully mediate floret fertility. Partner regulators could be upstream epigenetic regulators, parallel transcription factors, or downstream physiological controllers. Maize orthologs of barley six-rowed *VRS* genes like *GT1* (ortholog of *VRS1*), *RA2* (ortholog of *VRS4*), and *TB1* (ortholog of *VRS5*) have been characterized as domestication genes mainly controlling lateral or axillary events (Bortiri et al., 2006; Studer et al., 2011; Whipple et al., 2011). Comparable to barley *VRS* pathway, genetic interaction of double mutant *gt1; tb1*, expression analysis, and metabolite measurement also confirmed that GT1 functions in the downstream of TB1 to regulate the downstream physiology including sugar metabolism (like sucrose and trehalose metabolism) and hormone homeostasis (like JA, gibberellic acid, and abscisic acid). Level of JA and its intermediates, and expression of JA biosynthetic genes like *TS1* and *OPR8* were also downregulated in vegetative tiller buds of *gt1* and *tb1* mutants. Likewise, sucrose, fructose, and trehalose-6-phosphate as well as expression of sugar transport like *SWEET15b* and trehalose biosynthetic genes like *RAMOSA3* (trehalose-6-phosphate phosphatase) were upregulated in vegetative tiller buds of *gt1* and *tb1* mutants (Whipple et al., 2011; Dong et al., 2019). Maize physiological modules appear to be preserved like the barley *VRS* pathway but are prominent in the regulation of vegetative tiller growth, in agreement with the major domesticated

functions of GT1 and TB1. *gt1* mutants have weak carpel suppression phenotypes and are sterile (Whipple et al., 2011). Noticeably, when *gt1* genetically interacted with downstream trehalose biosynthetic mutant, *ra3*, *gt1;ra3* double mutant enhanced the capacities to mediate carpel suppression and strongly prevented the floret abortion. Subsequent misregulation of sugar metabolism, hormone homeostasis, and cell wall remodeling appeared to function in *gt1;ra3* mutant flower fertility (Klein et al., 2022). These data suggest that maize orthologs of barley *VRS* genes might require downstream physiological regulators to recruit conserved physiological programs to fine-tune the complexity of floret fertility in maize. This seems to partially explain incompetence of maize orthologs of barley *VRS* in fully control the floret fertility. Another explanation is direct downstream physiological modification due to the fact that floret fertility in maize has been primarily controlled by hormone-related genes. Recent LCM-seq in the upper floral meristem and lower floral meristem in maize ear also supports direct downstream physiology in maize floret fertility regulation (Yang et al., 2022).

The emerging perspective to engineer grass floret fertility

Identifying key regulators and downstream physiological networks responsible for increased floret fertility will help biologists and crop breeders develop new approaches and generate more opportunities for enhancing grain yield in staple crops. Unquestionably, characterization of novel regulators is necessary to understand regulation of floret fertility. In fact, perfect regulators are very few, so it is also essential to investigate other possible ways.

One approach is to combine upstream transcription factors and downstream physiological regulators. Grasses, including staple crops, contain large-size genomes where multi-level regulation of floret fertility is only partially explained by a limited number of key regulator genes

like transcription factors. Although transcription factors could interact with *cis*-regulatory targets or other regulators, it usually causes other unexpected phenotypical penalty in floret fertility. In barley *VRS* genes, only *vrs1* mutant has the complete fertile lateral floret in the whole spike (Komatsuda et al., 2007). *vrs2-5* mutants do not contain complete-fertile lateral florets and sometimes also produce indeterminate florets (Ramsay et al., 2011; Koppolu et al., 2013; Bull et al., 2017; van Esse et al., 2017; Youssef et al., 2017). Likewise, maize *gt1* and *tb1* mutants also have dramatic vegetative tillers. Interestingly, maize tiller domestication genes like GT1 and TB1 retain part of ancestral function in the floret fertility. *gt1* and *ra3* mutants have the weak derepressed carpels and they are sterile (Whipple et al., 2011; Klein et al., 2022). *tb1* mutant converts normal ear shoots (female inflorescence) into male inflorescence in the axil of plant stalk (Hubbard et al., 2002). Undoubtedly, transcription regulators have widespread physiological targets, raising one genetic possibility to precisely engineer floret fertility without severe phenotypic penalty. A forward genetic attempt combining GT1 transcription factors with RA3 sugar gene confers a pioneer successful approach to fine-tune maize floret fertility (Klein et al., 2022). Double mutant from *tb1* (ortholog of barley *VRS5*) and downstream JA-related mutant, *ts2*, recover the normal ear shoots (female inflorescence) in the axil of plant stalk (Hubbard et al., 2002).

Another approach is exploring novel alleles of key regulators to increase floret fertility. Incompetence of floret fertility in barley or maize might also be explained by strong alleles of key regulators. Key regulators of barley, wheat, or maize are generally transcription factors. Coincidently, crop domestication genes are also commonly transcription factors (Doebley, 2006). Domestication of crops like barley, wheat, or maize is to increase floret fertility and produce

more seeds. To acquire desirable phenotypes, best or strong alleles are favorably selected and genetic diversity is dramatically reduced (Doebley et al., 2006). For example, analysis of barley *vrs1* mutant alleles showed that complete deletion of the *VRS1* coding sequence produced the fully six-rowed barley spikes (Komatsuda et al., 2007). Intriguingly, changes in crop domestication genes are sometimes caused by changes in upstream regulatory regions of transcription factors rather than null allele or loss-of-function (Doebley et al., 2006). For example, seven alleles of barley *vrs1* mutant were caused by regulatory regions variation rather than coding sequencing change (Komatsuda et al., 2007). This provides another thread to edit the regulatory regions to create weak alleles. Recent advances in maize and tomato (Rodríguez-Leal et al., 2017; Liu et al., 2021) showed that promoter editing using CRISPR/Cas9 can create weak alleles to avoid undesirable phenotypic penalties. In fact, promoter editing is one epigenetic way to precisely control tissue-specific expression. Alternatively, making combinations of different alleles might offset the undesirable traits caused by strong alleles. For example, barley double mutant analysis among *vrs3*, *vrs4* or *vrs5* alleles could increase lateral floret fertility. Double mutants like *vrs1vrs3*, *vrs1vrs4*, and *vrs1vrs5* have more complete fertile lateral florets than their single *vrs3, vrs4*, and *vrs5* parent and phenotypically comparable to *vrs1* (Zwirek et al., 2019).

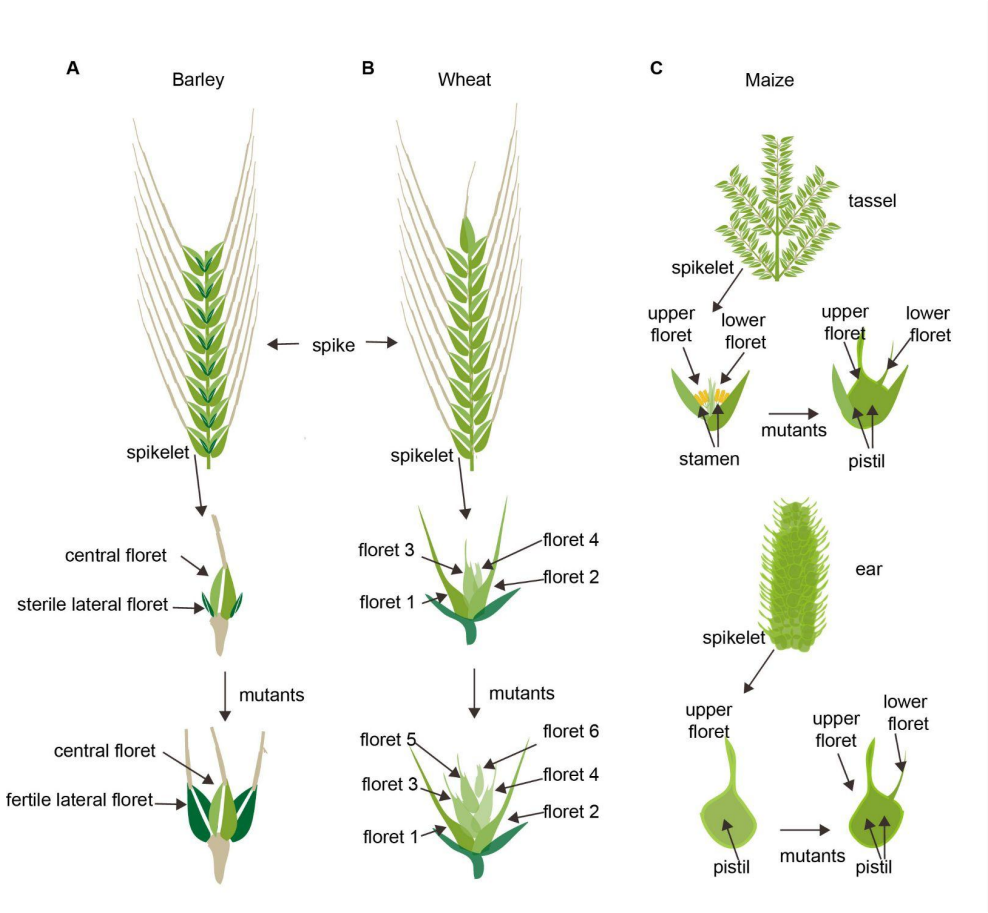

Figure 1. Flower morphology of barley, wheat, and maize.

A. Normal barley inflorescence called spike (top panel), normal triple spikelets containing one fertile central floret and two sterile lateral florets (middle panel), and mutant triple spikelets containing one fertile central floret and two fertile lateral florets (bottom panel). B. Normal wheat inflorescence called spike (top panel), normal spikelets containing about four fertile florets (middle panel), and mutant spikelets containing six fertile lateral florets (bottom panel). C. Normal male maize inflorescence called tassel (top first panel), normal male spikelets containing two fertile male florets with stamens and mutant male spikelets containing two female florets with pistils (top second and third panel), normal female maize inflorescence called ear (top fourth panel), and normal female spikelets containing one fertile female floret (upper floret) with one pistil and mutant female spikelets containing two female florets (upper floret and lower floret) with pistils (last two panels).

Reference

Acosta IF, Laparra H, Romero SP, Schmelz E, Hamberg M, Mottinger JP, Moreno MA, Dellaporta SL (2009) tasselseed1 is a lipoxygenase affecting jasmonic acid signaling in sex determination of maize. Science **323**: 262–265

Best NB, Hartwig T, Budka J, Fujioka S, Johal G, Schulz B, Dilkes BP (2016) nana plant2 Encodes a Maize Ortholog of the Arabidopsis Brassinosteroid Biosynthesis Gene DWARF1, Identifying Developmental Interactions between Brassinosteroids and Gibberellins. Plant Physiol **171**: 2633–2647

Bortiri E, Chuck G, Vollbrecht E, Rocheford T, Martienssen R, Hake S (2006) ramosa2 encodes a LATERAL ORGAN BOUNDARY domain protein that determines the fate of stem cells in branch meristems of maize. Plant Cell **18**: 574–585

Bull H, Casao MC, Zwirek M, Flavell AJ, Thomas WTB, Guo W, Zhang R, Rapazote-Flores P, Kyriakidis S, Russell J, et al (2017) Barley SIX-ROWED SPIKE3 encodes a putative Jumonji C-type H3K9me2/me3 demethylase that represses lateral spikelet fertility. Nat Commun **8**: 936

Calderon-Urrea A, Dellaporta SL (1999) Cell death and cell protection genes determine the fate of pistils in maize. Development **126**: 435–441

DeLong A, Calderon-Urrea A, Dellaporta SL (1993) Sex determination gene TASSELSEED2 of maize encodes a short-chain alcohol dehydrogenase required for stage-specific floral

organ abortion. Cell **74**: 757–768

Doebley J (2006) Plant science. Unfallen grains: how ancient farmers turned weeds into crops. Science **312**: 1318–1319

Doebley JF, Gaut BS, Smith BD (2006) The Molecular Genetics of Crop Domestication. Cell **127**: 1309–1321

Dong Z, Xiao Y, Govindarajulu R, Feil R, Siddoway ML, Nielsen T, Lunn JE, Hawkins J, Whipple C, Chuck G (2019) The regulatory landscape of a core maize domestication module controlling bud dormancy and growth repression. Nat Commun **10**: 3810

Emerson RA (1920) HERITABLE CHARACTERS OF MAIZE II.—PISTILLATE FLOWERED MAIZE PLANTS1. Journal of Heredity **11**: 65–76

van Esse GW, Walla A, Finke A, Koornneef M, Pecinka A, von Korff M (2017) Six-Rowed Spike3 (VRS3) Is a Histone Demethylase That Controls Lateral Spikelet Development in Barley. Plant Physiol **174**: 2397–2408

Ferrante A, Savin R, Slafer GA (2013) Floret development and grain setting differences between modern durum wheats under contrasting nitrogen availability. J Exp Bot **64**: 169–184

Ghiglione HO, Gonzalez FG, Serrago R, Maldonado SB, Chilcott C, Curá JA, Miralles DJ, Zhu T, Casal JJ (2008) Autophagy regulated by day length determines the number of fertile florets in wheat. Plant J **55**: 1010–1024

Hartwig T, Chuck GS, Fujioka S, Klempien A, Weizbauer R, Potluri DPV, Choe S, Johal GS, Schulz B (2011) Brassinosteroid control of sex determination in maize. Proc Natl Acad Sci U S A **108**: 19814–19819

Hayward AP, Moreno MA, Howard TP 3rd, Hague J, Nelson K, Heffelfinger C, Romero S, Kausch AP, Glauser G, Acosta IF, et al (2016) Control of sexuality by the -encoded UDP-glycosyltransferase of maize. Sci Adv **2**: e1600991

Hubbard L, McSteen P, Doebley J, Hake S (2002) Expression patterns and mutant phenotype of teosinte branched1 correlate with growth suppression in maize and teosinte. Genetics **162**: 1927–1935

Irish EE, Langdale JA, Nelson TM (1994) Interactions betweentassel seed genes and other sex determining genes in maize. Developmental Genetics **15**: 155–171

Irish EE, Nelson TM (1993) DEVELOPMENT OF TASSEL SEED 2 INFLORESCENCES IN MAIZE. American Journal of Botany **80**: 292–299

Jones DF (1925) HERITABLE CHARACTERS OF MAIZE. Journal of Heredity **16**: 339–342

Klein H, Gallagher J, Demesa-Arevalo E, Abraham-Juárez MJ, Heeney M, Feil R, Lunn JE, Xiao Y, Chuck G, Whipple C, et al (2022) Recruitment of an ancient branching program to suppress carpel development in maize flowers. Proc Natl Acad Sci USA. **119**: e2115871119

Komatsuda T, Pourkheirandish M, He C, Azhaguvel P, Kanamori H, Perovic D, Stein N,

Graner A, Wicker T, Tagiri A, et al (2007) Six-rowed barley originated from a mutation in a homeodomain-leucine zipper I-class homeobox gene. Proceedings of the National Academy of Sciences **104**: 1424–1429

Koppolu R, Anwar N, Sakuma S, Tagiri A, Lundqvist U, Pourkheirandish M, Rutten T, Seiler C, Himmelbach A, Ariyadasa R, et al (2013) Six-rowed spike4 (Vrs4) controls spikelet determinacy and row-type in barley. Proc Natl Acad Sci U S A **110**: 13198–13203

Liu L, Gallagher J, Arevalo ED, Chen R, Skopelitis T, Wu Q, Bartlett M, Jackson D (2021) Enhancing grain-yield-related traits by CRISPR–Cas9 promoter editing of maize CLE genes. Nature Plants **7**: 287–294

Lunde C, Kimberlin A, Leiboff S, Koo AJ, Hake S (2019) Tasselseed5 overexpresses a wound-inducible enzyme, ZmCYP94B1, that affects jasmonate catabolism, sex determination, and plant architecture in maize. Communications Biology. doi: 10.1038/s42003-019-0354-1

Lundqvist U (2014) Scandinavian mutation research in barley - a historical review. Hereditas **151**: 123–131

McKim SM, Koppolu R, Schnurbusch T (2018) Barley Inflorescence Architecture. Compendium of Plant Genomes 171–208

Nickerson NH, Dale EE (1955) Tassel Modifications in Zea Mays. Annals of the Missouri Botanical Garden **42**: 195

Parkinson SE, Gross SM, Hollick JB (2007) Maize sex determination and abaxial leaf fates are canalized by a factor that maintains repressed epigenetic states. Dev Biol **308**: 462–473

Peaucelle A, Braybrook SA, Le Guillou L, Bron E, Kuhlemeier C, Höfte H (2011) Pectin-induced changes in cell wall mechanics underlie organ initiation in Arabidopsis. Curr Biol **21**: 1720–1726

Peaucelle A, Louvet R, Johansen JN, Höfte H, Laufs P, Pelloux J, Mouille G (2008) Arabidopsis phyllotaxis is controlled by the methyl-esterification status of cell-wall pectins. Curr Biol **18**: 1943–1948

Ramsay L, Comadran J, Druka A, Marshall DF, Thomas WTB, Macaulay M, MacKenzie K, Simpson C, Fuller J, Bonar N, et al (2011) INTERMEDIUM-C, a modifier of lateral spikelet fertility in barley, is an ortholog of the maize domestication gene TEOSINTE BRANCHED 1. Nat Genet **43**: 169–172

Rodríguez-Leal D, Lemmon ZH, Man J, Bartlett ME, Lippman ZB (2017) Engineering Quantitative Trait Variation for Crop Improvement by Genome Editing. Cell **171**: 470–480.e8

Romani F, Moreno JE (2021) Molecular mechanisms involved in functional macroevolution of plant transcription factors. New Phytol **230**: 1345–1353

Sakuma S, Golan G, Guo Z, Ogawa T, Tagiri A, Sugimoto K, Bernhardt N, Brassac J, Mascher M, Hensel G, et al (2019) Unleashing floret fertility in wheat through the

mutation of a homeobox gene. Proc Natl Acad Sci U S A **116**: 5182–5187

Sakuma S, Lundqvist U, Kakei Y, Thirulogachandar V, Suzuki T, Hori K, Wu J, Tagiri A, Rutten T, Koppolu R, et al (2017) Extreme Suppression of Lateral Floret Development by a Single Amino Acid Change in the VRS1 Transcription Factor. Plant Physiol **175**: 1720–1731

Sakuma S, Pourkheirandish M, Hensel G, Kumlehn J, Stein N, Tagiri A, Yamaji N, Ma JF, Sassa H, Koba T, et al (2013) Divergence of expression pattern contributed to neofunctionalization of duplicated HD-Zip I transcription factor in barley. New Phytol **197**: 939–948

Sakuma S, Schnurbusch T (2020) Of floral fortune: tinkering with the grain yield potential of cereal crops. New Phytol **225**: 1873–1882

de Souza Moraes T, van Es SW, Hernández-Pinzón I, Kirschner GK, van der Wal F, da Silveira SR, Busscher-Lange J, Angenent GC, Moscou M, Immink RGH, et al (2022) The TCP transcription factor HvTB2 heterodimerizes with VRS5 and controls spike architecture in barley. Plant Reprod. doi: 10.1007/s00497-022-00441-8

Studer A, Zhao Q, Ross-Ibarra J, Doebley J (2011) Identification of a functional transposon insertion in the maize domestication gene tb1. Nat Genet **43**: 1160–1163

Thiel J, Koppolu R, Trautewig C, Hertig C, Kale SM, Erbe S, Mascher M, Himmelbach A, Rutten T, Esteban E, et al (2021) Transcriptional landscapes of floral meristems in barley.

Sci Adv. doi: 10.1126/sciadv.abf0832

Thompson BE, Hake S (2009) Translational biology: from Arabidopsis flowers to grass inflorescence architecture. Plant Physiol **149**: 38–45

Torices R, Méndez M, Gómez JM (2011) Where do monomorphic sexual systems fit in the evolution of dioecy? Insights from the largest family of angiosperms. New Phytol **190**: 234–248

Wang F, Yuan Z, Zhao Z, Li C, Zhang X, Liang H, Liu Y, Xu Q, Liu H (2020) Tasselseed5 encodes a cytochrome C oxidase that functions in sex determination by affecting jasmonate catabolism in maize. J Integr Plant Biol **62**: 247–255

Whipple CJ, Kebrom TH, Weber AL, Yang F, Hall D, Meeley R, Schmidt R, Doebley J, Brutnell TP, Jackson DP (2011) grassy tillers1 promotes apical dominance in maize and responds to shade signals in the grasses. Proc Natl Acad Sci U S A **108**: E506–12

Yang H, Nukunya K, Ding Q, Thompson BE (2022) Tissue-specific transcriptomics reveal functional differences in floral development. Plant Physiol **188**: 1158–1173

Yan Y, Christensen S, Isakeit T, Engelberth J, Meeley R, Hayward A, Emery RJN, Kolomiets MV (2012) Disruption of OPR7 and OPR8 reveals the versatile functions of jasmonic acid in maize development and defense. Plant Cell **24**: 1420–1436

Youssef HM, Eggert K, Koppolu R, Alqudah AM, Poursarebani N, Fazeli A, Sakuma S, Tagiri A, Rutten T, Govind G, et al (2017) VRS2 regulates hormone-mediated

inflorescence patterning in barley. Nat Genet **49**: 157–161

Zwirek M, Waugh R, McKim SM (2019) Interaction between row-type genes in barley controls meristem determinacy and reveals novel routes to improved grain. New Phytol **221**: 1950–1965

Chapter 2

Tissue-specific transcriptomics reveal functional differences in floral development

This is a pre-copyedited, author-produced version of an article accepted for publication in Plant Physiology following peer review. The version of record [Hailong Yang, Kate Nukunya, Queying Ding, Beth E Thompson*, Plant Physiology, Volume 188, Issue 2, February 2022, Pages 1158–1173] is available online at: https://doi.org/10.1093/plphys/kiab557.

Introduction

Flowers are essential for plant reproduction and also form fruits and seeds, which are consumed as food. Flowers are produced by floral meristems, undifferentiated groups of stem cells that generate floral organs (Bartlett and Thompson, 2014). Grass flowers (florets) are contained in spikelets, which contain two bracts (glumes) and one to many florets depending on the species. Like other grass flowers, maize florets are highly derived structures. Within two enclosing organs, the lemma and palea, maize flowers contain two lodicules (homologous to petals), three stamens and three carpels, two of which fuse to form the silk (Figure 1).

Maize produces two inflorescences, the tassel and ear, which produce male and female flowers, respectively (Cheng et al., 1983). Unlike Arabidopsis, in which the inflorescence meristem (IM) directly initiates floral meristems (FM) on its flanks, grass IMs produce a series of higher order meristems before initiating FM. Upon the transition to flowering, the shoot apical meristem (tassel) or an axillary meristem (ear) transitions to an indeterminate IM; the IM initiates ordered rows of spikelet pair meristems (SPM), which in turn gives rise to two spikelet meristems (SM) (Figure 1G) (Thompson and Hake, 2009; Whipple, 2017). The SM first initiates the proximal/lower FM (LFM) in the axil of a lemma on the abaxial side of the SM (Figure 1, H-L). The origin of the distal/upper FM (UFM) is less clear; one model proposes that the UFM is also initiated as an axillary meristem by the SM whereas the second model proposes the SM is itself converted to the UFM (Irish, 1997; Chuck et al., 1998).

Both the tassel and ear initiate bisexual flowers and early floral development is very similar in upper and lowers florets (Irish and Nelson, 1989). Carpels abort via programmed cell death in the tassel and stamens arrest shortly after anther formation in the ear (Cheng et al., 1983). In the

ear, lower floret abortion is initiated by programmed cell death similar to the carpel abortion program in the tassel in the carpel (Cheng et al., 1983). Thus, mature ear spikelets contain a single female floret, whereas mature tassel spikelets contain two male florets (Figure 1, A-F).

Spikelets containing sterile or aborted florets are common in the grasses, including cereal crops. In some species, (e.g. maize and barley), floret abortion/sterility is genetically preprogrammed and invariable between individuals whereas in other species (e.g. wheat), the number of aborted florets in a spikelet is variable and influenced by the environment. A few regulators of floral abortion have been identified (i.e. jasmonic acid in maize, *vrs* genes in barley, and *GNI1* in wheat); however, the importance of floral abortion is still unknown and we know almost nothing about the processes downstream of these high level regulators (Sakuma and Schnurbusch, 2020). To gain insight into the functional differences between florets with different developmental fates, we used laser capture microdissection (LCM) coupled with RNA-seq to globally survey gene expression in UFM and LFM of maize ears.

Results

The upper floral meristem and lower floral meristem have distinct gene expression profiles

Gene expression is dynamic during floral development and to ensure we isolated upper and lower FM at similar developmental stages, we isolated FM from ear primordia after initiation of lemma, but before stamen primordia (Figure 2, A-F). LFM development is delayed relative to the UFM (Cheng et al., 1983), and therefore LFM were dissected from older spikelets than UFM. Principal component analysis (PCA) and Pearson's correlation analysis confirmed UFM and LFM biological samples clustered together and had high reproducibility (Supplemental Figure 1). Approximately 700 genes were differentially expressed between UFM and LFM (238

UFM-enriched, 456 LFM-enriched; FC ≥2 and q <0.05; Figure 2G). Importantly, our data included three UFM-enriched genes with known RNA expression patterns (Supplemental Figure 2). *zmm8*/GRMZM2G102161 and *zmm14*/GRMZM2G099522 encode MADS-box transcription factors that are broadly expressed in the meristem and floral organs of the upper floret, but not detected in the lower floret (Cacharron et al., 1999; Du et al., 2021). *barren stalk1 (ba1)*/GRMZM2G397518 encodes a bHLH protein required for axillary meristem initiation and is expressed in a diffuse pattern in UFM and in a group of cells at the UFM/LFM boundary, but not detected in LFM (Gallavotti et al., 2004).

To gain insight into the biological function of differentially expressed genes (DEGs), we predicted gene function using MapMan (Schwacke et al., 2019), gene ontology (GO) enrichment analysis (Gene Ontology Consortium, 2015), and CornCyc, which predicts metabolic pathways (Schläpfer et al., 2017) (Figure 2, H-J). To facilitate the interpretation of hierarchical GO enrichment groups, we used the Cytoscape plug-in, Enrichment Map, to construct functional GO networks (Merico et al., 2010). In general, the UFM was enriched for genes in functional groups associated with growth and primary metabolism, including RNA synthesis and processing, protein synthesis, vesicle trafficking, nucleotide metabolism, and sugar response and transport (Figure 2, H and I). In contrast, the LFM was enriched for genes in functional groups associated with secondary metabolism and dormancy, including phytohormones, protein degradation, amino acid catabolism, and cell wall-related genes (Figure 2, H-J).

We further examined select functional groups to gain insight into the functional patterns of DEGs (Supplemental Figure 2-4). DEGs in the RNA biosynthesis group contains several classes of transcription factors (TFs) with well-known roles in plant growth and development, including

APETALA2/ETHYLENE RESPONSIVE FACTOR (AP2/ERF), myeloblastosis (MYB), homeobox, basic helix-loop-helix (bHLH), TEOSINTE BRANCHED1/CYCLOIDEA/PROLIFERATING CELL NUCLEAR ANTIGEN FACTOR (TCP), and WRKY TFs (Supplemental Figure 2). DEGs also included TFs with known functions in maize floral development, including *ba1*/GRMZM2G397518 (Gallavotti et al., 2004), *GRF-interacting factor1 (gif1)*/GRMZM2G180246 (Zhang et al., 2018), *zmm8*/GRMZM2G102161 and *zmm14*/GRMZM2G099522 *(Du et al., 2021)* in the UFM and *branched silkless1 (bd1)*/GRMZM2G307119 *(Chuck et al., 2002)*, *gnarley1 (gn1)*/GRMZM2G452178 (Foster et al., 1999a; Foster et al., 1999b), *teosinte branched1 (tb1)*/AC233950.1_FG002 (Hubbard et al., 2002), *Wavy auricle in blade1 (Wab1)*/*branched angle defective1 (bad1)*/GRMZM2G110242 (Hay and Hake, 2004; Bai et al., 2012; Lewis et al., 2014), and *zfl2*/GRMZM2G180190 (Bomblies et al., 2003) in the LFM.

DEGs in the phytohormone group function in metabolism and signaling of multiple hormones, including cytokinin, auxin, gibberellin (GA) and jasmonic acid (JA) (Figure 2, H-J; Supplemental Figure 3). Of the four cytokinin-related genes in our DEGs set, two cytokinin biosynthesis genes (*czog1*/GRMZM2G168474, GRMZM2G008726) were UFM-enriched and two A-type ARR negative regulators of cytokinin signaling (*crr2*/GRMZM2G392101, GRMZM2G179827) were LFM-enriched, suggesting that cytokinin signaling may be higher in UFM relative to LFM. In contrast, auxin, GA and JA-related genes were predominantly enriched in LFM. JA is required for lower floret abortion in the ear (DeLong et al., 1993; Acosta et al., 2009; Lunde et al., 2019; Wang et al., 2020) and three JA biosynthesis genes were LFM-enriched (*lox9*/GRMZM2G017616; *tasselseed1 (ts1)*/GRMZM2G104843; GRMZM2G168404). Seven

auxin-related DEGs were LFM-enriched and functioned in auxin synthesis (*tar2*/GRMZM2G066345), transport (*pin3*/GRMZM2G149184; GRMZM2G085236; GRMZM2G037386) and signaling (*aas8*/GRMZM2G053338; *iaa37*/GRMZM2G359924; *bif4*/GRMZM5G864847). GA-related DEGs were also LFM-enriched and function in the GA synthesis (*ga20ox1*/AC203966.5_FG005), inactivation (*ga2ox3*/GRMZM2G022679; *ga2ox9*/GRMZM2G152354), and signaling (*gras46*/GRMZM2G001426; GRMZM2G040278; GRMZM2G440543). The LFM was also enriched for three genes encoding Gibberellic Acid Stimulated Arabidopsis (GASA) cysteine-rich polypeptides (*gsl1*/GRMZM2G062527; GRMZM2G077845; GRMZM2G150688), which in Arabidopsis, are induced by GA and have broad functions in defense and development (Roxrud et al., 2007; Zhong et al., 2015). These gene expression profiles suggest that hormone accumulation and signaling differs between UFM and LFM of maize ears, with high cytokinin in the upper floret and high auxin, GA and JA in the lower floret.

We investigated the spatial expression of DEGs by RNA *in situ* hybridization in developing spikelets with more than 45 genes and determined specific expression patterns for 10 genes. AC217050.4_FG006 (encodes a 14-3-3 protein, $\log_2$FC = 1.124), *AP2/EREBP transcription factor 26 (ereb26)*/GRMZM2G317160 ($\log_2$FC = -1.162), and *chromatin complex subunit A 101 (chr101)*/GRMZM2G177165 ($\log_2$FC = -1.251) were broadly expressed in both upper and lower FM (Figure 3, A-C); AC217050.4_FG006 and *chr101*/GRMZM2G177165 were also present in stamen and carpel primordia (Figure 3, A and C; Supplemental Figure 5). As previously shown, *gif1*/GRMZM2G180246 ($\log_2$FC = 1.063) was expressed in a ring around developing UFM and at the base of palea in upper florets (Zhang et al., 2018), and showed a similar expression pattern

in lower florets (Figure 3D). GRMZM2G101682 (grass-specific gene of unknown function, $log_2FC = -1.009$) was also expressed in both UFM and LFM (Figure 3E), with strong expression restricted to the outermost cell layer. We also observed expression in the outer cell layer of SM, stamen and carpel primordia (Figure 3E and Supplemental Figure 5). In developing shoots, GRMZM2G101682 is localized to the L1 layer of boundary regions between initiating organs and the preligular band of developing leaves, but is not expressed in the mersitem itself (Johnston et al., 2014). *Histone H1-like*/GRMZM2G069911 ($log_2FC = -1.233$) and GRMZM2G180870 (*XYLOGLUCAN ENDOTRANSGLUCOSYLASE/HYDROLASE 9* (*XTH9)* homolog, $log_2FC = -1.059$) were expressed in punctate patterns characteristic of genes involved in cell division (Figure 3, F and G; Supplemental Figure 6) (Asai et al., 2002; Kim et al., 2007; Ikeda-Kawakatsu et al., 2009). In the SAM, stem cells at the tip of the meristem have lower cell division rates compared to cells in axillary primordia (Satterlee et al., 2020). If this pattern of cell division also occurs in FM, enrichment of cell division genes in the LFM could reflect the axillary meristem of LFM, whereas the UFM is likely converted from the SM. Alternatively, because UFM were larger than LFM at the time of dissection, we likely captured a higher proportion of "tip stem cells" (with lower cell division rates) in UFM relative to LFM samples. Finally, three genes were localized to a unique boundary region between the upper and lower florets. GRMZM2G114552 ($log_2FC = 2.616$) encodes a Bowman-Birk type trypsin inhibitor (*BBTI*) and was expressed in a discrete domain on the abaxial side of UFM but not detectable in LFM (Figure 3H). *BBTI* was also expressed at the boundaries of initiating SPM, SM, and at the base of palea in the upper floret (Supplemental Figure 7). A *pectate lyase* homolog, GRMZM2G131912 ($log_2FC = -1.281$), and *arginine decarboxylase1 (adc1)*/GRMZM2G396553

(log_2FC = -1.216) were present in discrete domains on the adaxial side of the LFM at the boundary with the upper floret (Figure 3, I and J; Supplemental Figure 7). *BBTI, adc1,* and *pectate lyase* were also expressed in this boundary region in tassel florets (Supplemental Figure 7), indicating that this boundary expression is not unique to the ear.

Pectin modification is dynamic during spikelet development and differs between upper and lower florets

GO and MapMan functional analyses indicated that DEGs belonged to several functional groups (Figure 2), several of which made sense based on their well-established roles in development (i.e. transcription, development, morphogenesis, hormones), however, other functional groups were more surprising. We were particularly intrigued by enrichment of cell wall-related genes in LFM and sugar-related genes in UFM, and thus further investigated these functional groups.

Our DEG set included 20 MapMan-annotated cell wall-related genes, 18 of which were enriched in LFM (Figure 4). Indeed, RNA *in situ* hybridization confirmed that GRMZM2G131912 (*pectate lyase* homolog), is expressed in the lower floret, adjacent to the UFM/LFM boundary (Figure 3I). Cell wall-related DEGs were involved in synthesis or modification of all major cell wall components, including cellulose (one gene), lignin (two genes), hemicellulose (four genes), and pectin (five genes), as well as arabinogalactan proteins (six genes) and expansins (two genes) (Figure 4A). Most of these genes are involved in synthesis and modification of the primary cell wall, which is synthesized and continuously deposited around dividing or expanding cells, including meristems (Cavalier et al., 2008; Keegstra, 2010; Sampathkumar et al., 2019).

Differential expression of cell wall-related genes suggested that UFM and LFM have different cell wall compositions and/or modifications. Therefore, we stained the major cell wall components in developing spikelets, including cellulose (calcofluor white/fluorescent brightener 28), lignin (phloroglucinol-HCl), and pectin (ruthenium red). To confirm our staining protocols accurately reflected cell wall composition, we first stained vasculature tissue, where cell wall composition is well-characterized (Supplemental Figure 8) (Chen et al., 2006; Verhertbruggen et al., 2009; Pesquet et al., 2013; Hu et al., 2017; Torode et al., 2018). Lignin is predominantly found in secondary cell walls, which only form after cells have stopped expansion (Zhong et al., 2019). As expected for meristematic tissue, lignin staining was weak or undetectable in inflorescence primordia (Supplemental Figure 8), with no indication of floret-specific accumulation. Cellulose accumulated at the periphery of all cells and appeared similar in both florets (Supplemental Figure 8). We visualized pectin using ruthenium red, which preferentially stains acidic pectin (Ruzin, 1999), and observed striking differences in pectin distribution between UFM and LFM. Ruthenium red strongly stained the L1 layer of SM and glume primordia; staining persisted in the L1 of UFM, however was much weaker or absent in LFM (Figure 4B).

To examine pectin composition in more detail, we used two monoclonal antibodies, LM19 and LM20, which recognize the low methylesterified (acidic) and high methylesterified forms of homogalacturonan (HG), the most abundant pectic polysaccharide (Verhertbruggen et al., 2009). We observed dynamic LM19 staining during floral development, suggesting that HG methylesterification is developmentally regulated (Figure 4, C-H). LM19 (low methylesterification) strongly stained the L1 layer of SM and glume primordia, similar to

ruthenium red staining (Figure 4C). LM19 also stained cells at the base of glumes, and strongly stained incipient and initiating floral organ primordia (Figure 4, D-G). We observed weak staining at the base of the LFM, and occasionally observed a couple of brightly staining cells that appeared to correspond to palea primordia (Figure 4G).

LM20 (high methylesterified HG) showed a dramatically different staining pattern than LM19 (Figure 4, I-N). LM20 weakly stained the periphery of most or all cells in developing spikelets and intensely stained the apical surface of the L1 layer of SM and young UFM (Figure 4, I-K). LM20 staining persisted throughout UFM development, but its localization became more punctate and primarily accumulated at cell junctions (Figure 4, K-M). In LFM, LM20 also stained cell peripheries, often forming puncta at cell junctions (Figure 4, J-M). Although variable, we never observed strong LM20 staining in LFM as we did in UFM.

We next asked if differential pectin accumulation also occurred in spikelets where the lower floret does not abort. Specifically, we examined tassel spikelets, which produce two staminate florets, and *ra3; gt1* ear spikelets, in which the lower floret does not abort and produce two pistillate florets (Klein et al., 2021). Pectin preferentially accumulated in the upper floret of tassel and *ra3; gt1* ear spikelets, similar to what we observed in normal ear spikelets (Supplemental Figure 9). In the upper floret of tassel spikelets, however, LM19 also strongly stained aborting carpels (Figure 5, A-C). Indeed, demethylesterified pectin was generally associated with carpel abortion; LM19 strongly stained aborting carpels in the lower florets of both tassels and ears (Figure 5, D-I). Lower florets of *ra3; gt1* double mutants, however, lacked intense LM19 staining characteristic of aborting carpels and resembled initiating and elongating carpels in upper florets (Figure 5, J-L). Together, these results indicate that pectin is dynamically

regulated during floral development and pectin modification differs between upper and lower FM. Both methylesterified and demethylesterified pectin preferentially accumulate in the upper floret, even in spikelets where the lower floret does not abort. Demethylesterified pectin strongly accumulates in incipient and initiating organ primordia of UFM, indicating pectin may also play a role in organ initiation in maize. Finally, demethylesterified pectin is strongly associated with aborting carpels in the lower floret of ears and both florets in tassels.

Sugar-related genes and starch are differentially regulated between upper and lower floral meristems

The ability to coordinate energy and carbon availability with plant growth is critical. Hexose sugars generated through photosynthesis in source tissues are converted to sucrose for transport to sink tissues and starch for storage. Carbohydrates are required not only to provide chemical energy required for plant growth, but also to generate nucleotides and construct cell walls around newly divided and expanding cells (Sampathkumar et al., 2019). GO and MapMan analysis indicated UFM were enriched for genes involved in carbohydrate/sugar transport and response (Figure 2, H and I), while the LFM was enriched for multiple members of the SNF1-related protein kinase 1 (SnRK1) signaling pathway (Figure 6, A and B).

The SnRK1 pathway is a key regulator of plant growth and energy homeostasis (Baena-González et al., 2007) and is regulated both by trehalose-6-phosphate (T6P) levels (Baena-González and Lunn, 2020) and interactions with FCS-like zinc finger (FLZ) proteins (Nietzsche et al., 2014; Jamsheer K et al., 2018b; K et al., 2019). Trehalose is present in trace amounts in plants and its primary role is likely in sugar sensing and signaling, rather than chemical energy storage (Wingler, 2002; Figueroa and Lunn, 2016). The trehalose precursor,

T6P, is synthesized from UDP-glucose and glucose-6-P by T6P synthase (TPS) and thought to be the active signaling molecule; T6P is converted to trehalose by trehalose-6-phosphate phosphatases (TPPs) (Cabib and Leloir, 1958). T6P levels are positively correlated with sucrose levels and T6P sensing may be a key mechanism by which plants monitor sucrose availability (Figueroa and Lunn, 2016). The maize genome contains 13 TPP genes, of which *ramosa3 (ra3)/tpp10/*GRMZM2G014729 is the most extensively studied and is required for SPM and SM determinacy in the inflorescence and carpel abortion in florets (Satoh-Nagasawa et al., 2006). Interestingly, *ra3* promotes meristem determinacy at least in part independent of its enzymatic activity and likely functions in transcriptional regulation (Claeys et al., 2019; Demesa-Arevalo et al., 2021). Both *ra3* and *tpp3*/GRMZM2G117564 were LFM-enriched, suggesting that sugar signaling could be critical in the LFM. *Ra3* functions redundantly with the HD-ZIP TF, *grassy tillers1 (gt1)* to repress carpel growth in tassel florets. Particularly relevant to this work, the lower floret fails to abort in *ra3; gt1* double mutants, demonstrating that our approach identified genes with functional differences in the upper and lower florets (Klein et al., 2021).

The plant-specific *FLZ* gene family is defined by the presence of a ~50 amino acid FLZ domain, which interacts with SnRK1 (K and Laxmi, 2014; Jamsheer K et al., 2018b). While the function of many *FLZ* genes is unknown, they have been implicated in ABA, sugar, and energy response in Arabidopsis (K and Laxmi, 2015; Jamsheer K et al., 2018a) and are thought to act as adapters between SnRK1 and other proteins (Tsai and Gazzarrini, 2014; Jamsheer K et al., 2018b; K et al., 2019). Based on MapMan annotations, the maize genome contains 39 *FLZ* genes in the “multiprocess regulation” functional group, 28 of which were expressed in our FM samples. Strikingly, nearly one-third (8/28) of the FM-expressed *FLZ* genes were DE between

UFM and LFM, all of which were LFM-enriched ($p<4.7e10-7$ in a two-sided Fisher's Exact test) (Figure 6). All core components of the SnRK1 signaling pathway were expressed in our FM samples, but only *FLZ* genes were differentially expressed between UFM and LFM (Figure 6A).

Determining sugar accumulation and distribution *in situ* is challenging due to a lack of dyes or other mechanisms to detect specific sugars. Most sugar analysis requires grinding tissue and measuring overall sugar levels, which precludes the cellular-level resolution required to detect spatial differences in sugar accumulation. Starch, the major storage carbohydrate in plants, however, can be easily visualized by iodine staining (Zhang et al., 2019). In the inflorescence, starch accumulates at the base of developing SM, but not in the SM itself (Figure 6C). After LFM initiation, starch begins to accumulate at the base of UFM, near the boundary with LFM (Figure 6, D and E). Starch accumulation intensifies and becomes more defined at the boundary between UFM and LFM in older spikelets (Figure 6, E-G). Strikingly, we did not observe detectable starch in LFM at any stage of spikelet development (Figure 6, C-G). We observed similar starch accumulation in tassels (Supplemental Figure 8, N-R) and in *ra3; gt1* ears (Supplemental Figure 8, S-W), in which both upper and lower florets fully develop, indicating starch distribution is carefully regulated in developing spikelets of both male and female inflorescences and sugars accumulate differently in UFM and LFM independent of lower floret abortion.

Discussion

Upper and lower floral meristems are not developmentally equivalent

Floral meristems are typically regarded as functionally equivalent, regardless of where they are initiated on the plant. In Arabidopsis, for example, all FM form as axillary meristems on the

flanks on an inflorescence meristem, produce identical flowers, and appear to have the same developmental potential (Liu et al., 2009). In maize, spikelet meristems are often depicted as initiating two equivalent FM (Figure 1G), however this depiction is misleading and upper and lower FM are likely functionally divergent from the time of initiation. The Andropogoneae tribe, which includes maize along with the key crops sorghum and sugarcane, produce paired spikelets with two florets per spikelet. Upper and lower florets in the Andropogoneae are typically dimorphic; the upper floret is often hermaphroditic whereas the lower floret is usually reduced or sterile (Le Roux and Kellogg, 1999). Ear spikelets, in which the lower floret aborts, may be more representative of the Andropogoneae and findings more relevant to other species in the tribe. Floral abortion and sterility are common in the cereals and the mechanisms that regulate lower floret growth in maize may also apply to other cereal crops.

We sought to understand the functional differences of the upper and lower florets by globally surveying gene expression in the UFM and LFM of maize ears. Both UFM and LFM expressed a broad set of genes, including genes previously implicated in floral development and/or meristem function. Approximately 3.5% of genes are differentially expressed between UFM and LFM (Figure 2G), which is consistent with previous molecular and genetic analyses. At least two maize mutants differentially affect the upper and lower florets. In *bearded-ear (bde)* mutants, UFM are indeterminate whereas LFM initiate additional floral meristems and lose FM fate (Thompson et al., 2009). In *restorer of fertility2 (rf2)* mutants, stamens arrest in lower, but not upper florets (Liu et al., 2001). Microarray analysis indicates that approximately 9% of genes are differentially expressed in equivalently staged anthers from the upper and lower florets (Skibbe et al., 2008); thus, floret-specific gene expression persists even in differentiated floral organs.

These data support the model that UFM and LFM use distinct gene regulatory networks and have divergent developmental fates from the very earliest stages of development.

The divergent developmental fates of UFM and LFM may be due in part to their distinct ontogenies. The LFM is clearly an axillary meristem and associated with formation of auxin maxima and with novel expression of shoot and floral meristem markers, such as *knotted1 (kn1)* and *bde,* respectively (Figure 1, H-N) (Jackson et al., 1994; Gallavotti et al., 2008; Thompson et al., 2009). In contrast, formation of the UFM is not associated with an auxin maximum, which supports the model that the UFM is not an axillary meristem but rather that the SM is converted to the UFM (Gallavotti et al., 2008). We found the LFM was enriched for auxin-related genes (Figure 2, H and J; Supplemental Figure 3), which could reflect the axillary meristem identity of LFM, but not UFM.

Transcriptional regulatory networks also differ between upper and lower florets. One of the largest groups of DE genes identified in our analysis were transcriptional regulatory proteins, which included TF classes with key functions in plant development (i.e. TCP, WRKY, homeobox, AP2/ERF). These experiments were motivated in part by the *bde* mutant phenotype, which as previously mentioned, promotes FM determinacy in the upper floret and FM fate in the lower floret. *bde* encodes a MADS-box TF and we hypothesized that these floret-specific phenotypes were caused by disruption of distinct BDE-containing complexes in the UFM and LFM, resulting in misregulation of different target genes (Thompson et al., 2009). Surprisingly, *zmm8* and *zmm14* were the only two DE MADS-box genes identified in our samples (Supplemental Figure 2), both of which were previously shown to be strongly UFM-enriched and have been hypothesized to act as upper floret selector genes (Cacharron et al., 1999). Recent

analysis of *zmm8;zmm14* double mutants, however, indicate that *zmm8/zmm14* promote FM meristem determinacy in both florets and do not have floret-specific functions (Du et al., 2021). Although *zmm8/zmm14* are highly UFM-enriched in our data, they are also expressed in LFM. Combined with the fact that we did not identify clear candidates for lower floret selector genes, these data suggest that upper versus lower floret selector genes may not exist. We favor the hypothesis that the developmental history and anatomy of upper versus lower florets lead to physiological differences between the florets (i.e. energy availability or hormone status), which can cause floret-specific mutant phenotypes and ultimately determine UFM versus LFM fate.

Genes associated with growth repression are enriched in the lower floral meristem

Plants must be able to alter growth and development in response to both internal and external cues, including energy status. Sugar, mainly in the form of glucose and fructose, is produced by photosynthesis in source tissues and transported as sucrose to sink tissues, such as developing seeds. Once localized to sink tissues, sucrose can be converted to glucose and used for chemical energy, as a structural component of cells (e.g. cell walls) or stored for later use. Sugar is also an important signaling molecule and functions in diverse processes. The lower floret is enriched for genes involved in growth repression, and our data suggests low sugar availability in the lower floret may contribute to this growth repression. Indeed, increased sucrose in wheat decreases floral abortion, suggesting that sugar signaling and homeostasis can regulate floral abortion in cereal crops (Ghiglione et al., 2008).

The conserved SnRK1 protein kinase (homologous to yeast Snf1 and animal AMPK1) is a key mechanism by which plants sense nutrient availability and maintain energy homeostasis. SnRK1 stimulates pathways that inhibit growth and increase catabolism in response to energy

starvation (Baena-González et al., 2007). SnRK1 senses energy status primarily through repression by T6P, which is a proxy for carbon availability (Smeekens, 2015; Figueroa and Lunn, 2016). Our data suggest a model in which low sugar availability in the lower floret suppresses growth via the SnRK1 signaling pathway (Figure 7). The LFM is enriched for RNAs encoding two TPP enzymes (*ra3/tpp10* and *tpp3*) (Figure 6B), consistent RA3 localization at the UMF/LFM boundary (Satoh-Nagasawa et al., 2006; Klein et al., 2021). The UFM is enriched for *tpp12*, consistent with data showing that *ra3* and *tpp12* expression is inversely correlated (Claeys et al., 2019). In other developmental contexts, the RA3 (and other TPPs) primarily function in transcriptional regulation and not direct modulation of T6P levels (Claeys et al., 2019; Demesa-Arevalo et al., 2021). Regardless, RA3/TPPs likely regulate or respond to sugar levels, suggesting that sugar levels are carefully regulated in the spikelet.

Both the UFM and LFM express RNAs corresponding to all core components of the SnRK1 signaling pathway, most of which are not differentially expressed (Figure 6A). The LFM, however, showed enrichment of eight *FLZ* genes (Figure 6, A and B), which likely act as adaptors for SnRK1, and *FLZ* RNA levels respond to sugar, hormones and abiotic stress (K and Laxmi, 2015; Jamsheer K et al., 2018a). In addition to SnRK1 subunits, FLZ interacts with developmental regulators, including homologs of LFM-enriched genes (TCP, homeobox TFs, GAI, DELLA) (Nietzsche et al., 2016; K et al., 2019). Thus, LFM-enriched *FLZ* genes may direct SnRK1 to specific targets that function in floral development. The LFM also showed enrichment of genes involved in protein degradation and amino acid catabolism (Figure 2, H and I; Supplemental Figure 4), consistent with active SnRK1 in LFM. High T6P levels have been correlated with increased expression of genes involved in primary metabolism (Oszvald et al.,

2018), and indeed, the UFM was enriched for genes involved in RNA processing and protein biosynthesis (Figure 2H).

T6P also promotes starch accumulation, the major storage carbohydrate in plants (Figueroa and Lunn, 2016). Starch gradually accumulates during spikelet development (Figure 6, C-G), presumably increasing the strength of the inflorescence as a sink tissue. Starch does not accumulate throughout the spikelet, but rather accumulates in a defined region at the boundary between the upper and lower floret and appears to be excluded from the lower floret. In animals, the SnRK1 homolog, AMPK1, binds and is negatively regulated by glycogen (Janzen et al., 2018), which is analogous to starch in plants, raising the intriguing possibility that SnRK1 directly binds and is regulated by starch. Starch accumulation is similar in spikelets where the lower floret does not abort (Supplemental Figure 8, N-W), suggesting that low starch does not directly signal floral abortion, but may be important for general growth repression of the lower floret.

In addition to its function in sugar signaling and homeostasis within a tissue, T6P can affect sugar utilization and distribution at the whole plant level and is a key regulator of the source/sink balance (Figueroa and Lunn, 2016). The interaction between source and sink tissues affects timing of senescence and many DEGs in our data set have been implicated in senescence. For example, the UFM-enriched senescence-inducible chloroplast stay-green protein, GRMZM2G091837, is associated with delayed senescence (Li et al., 2020), whereas the LFM-enriched *Malate synthase 1* (*Mas1/*GRMZM2G102183) and arabidopsis *FLZ* genes are induced in senescing tissues (Yandeau-Nelson et al., 2011; K and Laxmi, 2015; Jamsheer K et al., 2018a). Furthermore, we noted overlap between genes that regulate natural variation of

senescence in maize (Sekhon et al., 2019) and our DEGs, including glutathione S-transferases (GSTs; 5 LFM-enriched, 2 UFM-enriched, 3 senescence-associated) (Supplemental Figure 4); indeed *gst41*/GRZM2G097989 overlapped both lists. The cell wall has also emerged as a significant contributor to senescence, which can act as a secondary sink and may affect the source/sink balance (Sekhon et al., 2012; Sekhon et al., 2019). The arabidopsis senescence-inducible promoter, p*SAG12,* is sufficient to drive transcription in the lower floret and indeed p*SAG12*-induced expression of the cytokinin biosynthesis gene, *isopentenyl transferase1 (ipt1)* in the lower floret inhibits floret abortion (Young et al., 2004). While not directly implicated in senescence, we also noted the LFM was enriched for two Rapid Alkalinization Factor (RALF)/RALF-like (RALFL) peptides, which are associated with repressed growth (Blackburn et al., 2020).We propose the LFM executes a senescence-like program to repress growth in the lower floret (Figure 7).

Plant growth requires the synthesis of new cell walls as cells divide and modification of existing cell walls to allow for cell expansion. In eudicots, pectin composition and modification is developmentally regulated and has been implicated in multiple aspects of plant growth and development (Saffer, 2018). Pectins are complex galacturonic acid-rich polysaccharides, of which homogalacturonan (HG) is the most abundant (Harholt et al., 2010). HG is deposited in the cell wall in a highly methylesterified form and can be demethylesterified by pectin methylesterseses (PMEs); in Arabidopsis, demethylesterification of HG regulates primordia initiation and phyllotaxy (Peaucelle et al., 2008; Peaucelle et al., 2011). Grass cell walls contain significantly less pectin than eudicot cells walls (~5% in grasses vs 20-35 % in eudicots) (Vogel, 2008) and what role, if any, pectin modification plays in primordia initiation and phyllotaxy in

grasses is unclear. Our data show that demethylesterified pectin is clearly associated with floral organ primordia initiation in the UFM (Figure 4, C-H), strongly suggesting that pectin's role in organ initiation is conserved in grasses. Furthermore, we show that demethylesterified pectin strongly accumulates in aborting carpels (Figure 5). While, it is unclear if this pectin demethylesterification is a trigger for or the result of carpel abortion, these data clearly show that pectin is dynamically modified during maize floral development and may be critical for floret fertility.

Does the UFM/LFM boundary affect FM activity?

Boundary regions between meristems and initiating primordia are essential to separate groups of cells with different developmental fates and can also affect the activity of adjacent cell populations (Wang et al., 2016; Richardson and Hake, 2018). In grass inflorescences, meristem determinacy is controlled by groups of genes expressed in regions adjacent to the mersitem that form boundaries with organ primordia. For example, the *ramosa* regulatory module functions at the base of SPM and is required to restrict SPM determinacy (Eveland et al., 2014). Similarly, *bd1* and *indeterminate spikelet1* (*ids1*) transcription factors are expressed at the base of the SM and limit SM determinacy (Chuck et al., 1998; Chuck et al., 2002). In barley *compositum1* (*com1*) mutants, determinate spikelets on the main rachis are transformed into indeterminate branches due to defective boundary formation. The *ra3* ortholog, along with other sugar and cell wall-related genes are misexpressed in *com1* mutants, suggesting that sugar signaling and cell wall changes are critical for boundary formation (Poursarebani et al., 2020). Thus, boundary regions adjacent to meristems may function as novel signaling centers that regulate meristem activity (Whipple, 2017), although the mechanism is unclear.

Our data suggest that a similar boundary program may function at the UFM/LFM boundary. First, *RA3* is localized to the boundary (Satoh-Nagasawa et al., 2006; Klein et al., 2021) and overlaps with starch accumulation (Figure 6, C-G). We also identified the *com1* ortholog, *Wab1/bad1,* as a LFM-enriched gene in our samples (Supplemental Figure 2). Because of the small size of LFM, we likely isolated boundary genes in our LFM samples that were excluded from UFM samples in which we were able to isolate the "tips" of the meristems. Our data also suggest cell walls are differentially regulated in UFM and LFM (Figure 4). Indeed, *pectate lyase* was localized to a discrete domain at the UFM/LFM boundary (Figure 3I and Supplemental Figure 7) and boundary regions are often characterized by stiffer cell walls (Richardson and Hake, 2018). *Arginine decarboxylase1 (adc1)*, a key enzyme required for synthesis of the polyamines, is also expressed at the UFM/LFM boundary (Figure 3J and Supplemental Figure 7). Polyamines have diverse functions in plants ranging from stress responses to growth and development, including flower bud formation (Chen et al., 2018). *ba1* is also expressed in the domain at the UFM/LFM boundary and later below the palea (Gallavotti et al., 2004). Finally, *BBTI* is expressed in the upper floret at the UFM/LFM boundary and at the base of the palea (Figure 3H and Supplemental Figure 7). The palea expression of *BBTI* and *ba1* is particularly intriguing; in barely, *com1* is also expressed in palea and *com1* mutants have enlarged palea cells with thinner cell walls (Poursarebani et al., 2020). Thus, palea may also have important boundary functions or alternatively, boundary regulatory modules may be redeployed in palea development.

Understanding the genetic and physiological processes that regulate floret abortion and sterility is a necessary first step to engineer maize and other cereal crops with increased floret

fertility. Our data suggest that upper versus lower floral meristem fate in maize is not determined by master regulatory genes, but rather by differences in core physiological processes that coordinate sugar availability, energy homeostasis and plant growth. This foundational work provides important insights into the downstream processes that likely regulate floret abortion and provides a rich set of candidate genes to potentially increase floret fertility in cereal crops and enhance yield.

Materials and Methods

Laser Capture Microdissection, RNA isolation and amplification

Ear primorida (1-2 cm) were dissected from greenhouse grown (16 h light at 27°C, 8 h dark at 21°C) B73 plants and immediately fixed and embedded for LCM as previously described (Takacs et al., 2012). Longitudinal sections (8 μm) were made using a Reichert-Jung (Leica) 2030 rotary microtome and mounted on Zeiss Membrane Slide (1.0 polyethylene naphthalate); LCM was performed using the Zeiss PALM MicroBeam System. A minimum 350,000 μm^2 tissue was dissected for each of six replicates (three UFM and three LFM; 1-2 ear primordia used per replicate). Because LFM are developmentally delayed relative to UFM, LFM samples were dissected from later stage spikelets than UFM samples. Total RNA was extracted using Arcturus PicoPure RNA Isolation kit (Applied Biosystems) and DNase treated using the Qiagen RNase-free DNase set. RNA was amplified (Epicenter TargetAmp 2-Round aRNA Amplification Kit 2.0, Epicentre Biotechnologies), DNase-treated (RapidOut DNA Removal kit, ThermoFisher Scientific) and purified (RNeasy MinElute Cleanup Kit, Qiagen). Quality and size of aRNA was assessed using Bioanalyzer 2100 (Agilent Technologies).

RNA-seq and data analysis

Library construction (TruSeq Stranded mRNA Sample Prep LS kit) and RNA-seq was performed on an Illumina HiSeq 2500 system by Genomic Sciences Laboratory at North Carolina State University. Raw data was trimmed and low quality reads were filtered out using trim_galore. Reads were mapped to the maize genome (V3) using Tophat2 (v2.1.0) (Kim et al., 2013) with parameters: --library-type fr-secondstrand --b2-very-sensitive -i 20 and quantified using the htseq-count package with default parameters except: --stranded=yes (Anders et al., 2015). Count tables were analyzed using DESeq2 in the R environment for differential expression analysis (Love et al., 2014). Genes with a minimum read count of 10 in at least two biological replicates, fold change ≥ 2 and adjusted p-value <0.5 were considered differentially expressed. Principal component analysis was performed using DESeq2 (Love et al., 2014) in the R environment and correlation analysis was performed using R package "psych" pairs.panels function.

Gene ontology was analyzed using g:Profiler (Raudvere et al., 2019) with default options except statistical settings: Benjamini-Hochberg FDR and All known genes. Gene enrichment maps were generated using Cytoscape (version 3.7.1) plug-in, Enrichment Map (Merico et al., 2010), with default options except FDR q-value cutoff = 0.05, connectivity = second degree sparse, and size of functional category = 1 to 5000. Functional groups were predicted using MapMan 3.6.0RC1 (X4 annotation), with the maize v3 mapping file (retrieved from Mercator4 Fasta validator with the protein option) (Schwacke et al., 2019). CornCyc 9.0 was used to predict metabolic pathways (Schläpfer et al., 2017). Gene ID description analysis was analyzed with g:Profiler g:Convert functional tab (Raudvere et al., 2019).

RNA *in situ* hybridization and histochemistry

Inflorescence primordia (1-2 cm) for RNA *in situ* hybridization, lignin/cellulose staining, and immunohistochemistry, were fixed and embedded as described in (Thompson et al., 2009) and sectioned (10 μm) using a Microm HM315 Microtome. Inflorescence primordia for ruthenium red and starch staining were directly frozen with optimal cutting temperature (OCT) embedding medium on dry ice and sectioned (60-80 μm) with a Microm HM550 Cryostat Microtome at -20 °C.

RNA *in situ* hybridization was performed as described previously (Jackson, 1992), with the following modifications. Pronase digestion was performed for 25 minutes at 37 °C; incubated in blocking solution (Sigma Roche) for 1 hour at room temperature before incubation with anti-DIG antibody (1:4000-5000 in blocking solution). After antibody incubation, slides were washed with Buffer A without Triton-X100. Slides were imaged using an Olympus BX-41 compound light microscope and processed using Adobe Photoshop. Probes were generated as described in (Bortiri et al., 2006), using primer sequences listed in Supplemental Table 1.

For pectin, lignin, and cellulose staining, cryosections and rehydrated sections were stained as previously described (Gunawardena et al., 2007; Pradhan Mitra and Loqué, 2014) except staining was performed at room temperature in the dark. Phloroglucinol-HCl-stained samples were immediately imaged with Olympus BX-41 compound light microscope. Calcofluor white/fluorescent brightener 28-stained samples were visualized with an Olympus IX2-DSU Confocal Compound Light Microscope using eDAPI or emDAPI filters. Lugol's Iodine Solution (Electron Microscopy Sciences) was used to stain starch, washed with 90% isopropanol or ethanol and mounted with histoclear. Maize stem tissue was processed in parallel for all stains.

Immunofluorescence labeling was modified from (Xue et al., 2013). Briefly, rehydrated sections were blocked using 1×PBS with 5% BSA for 30 minutes at room temperature and stained with primary antibodies, LM19 and LM20 (Kerafast, diluted 1:10) overnight at 4°C. After washing in 1×PBS (three washes, five minutes each) sections were incubated for two hours at room temperature with goat anti-Rat IgG (H+L) Alexa Fluor 488 secondary antibody (ThermoFisher Scientific, diluted 1:200). Antibodies were diluted in 1×PBS with 5% BSA and incubated in the dark. Sections were washed three times (five minutes each) with 1×PBS, incubated with 0.02% Toluidine Blue O (1×PBS) for five minutes to quench autofluorescence, and rinsed twice with 1×PBS prior to mounting with antifade medium (Hinnant et al., 2017). Slides were stored at 4°C in the dark prior to imaging with a Zeiss LSM700 laser scanning microscope. Negative controls lacking primary antibody were processed in parallel. Images were processed in Adobe Photoshop and false colored using the Blue Orange icb look up table in ImageJ (Schneider et al., 2012).

Accession numbers

RNA sequencing data were deposited into NCBI Sequence Read Archive under accession number PRJNA717335.

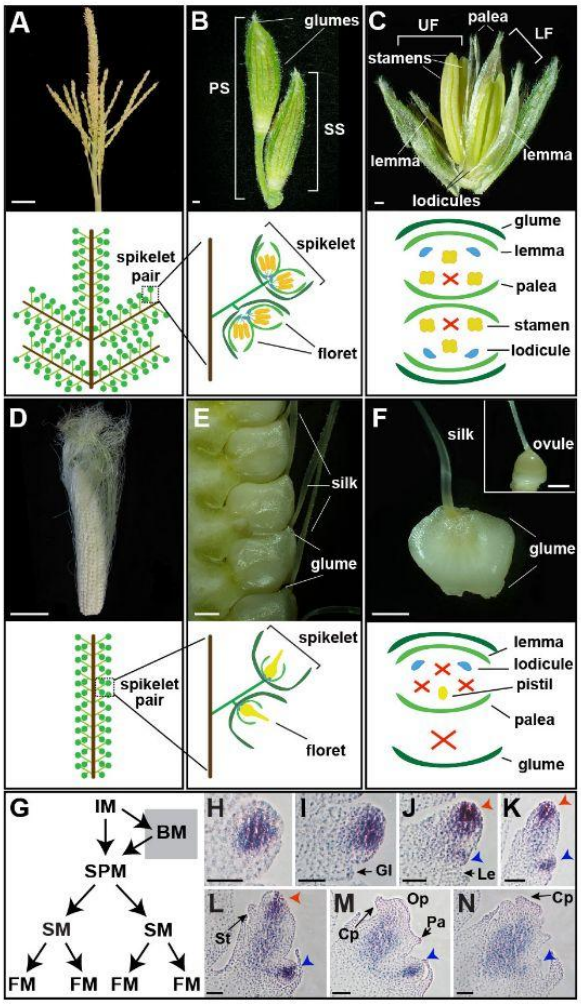

Figure 1. Normal maize floral development.

(A) Mature tassel, the male inflorescence. (B) Pair of tassel spikelets. (C) Dissected tassel spikelet, exposing two male florets. (D) Mature ear, the female inflorescence. (E) Mature ear spikelets. (F) Dissected ear spikelet, containing a single female floret. Inset is a mature ovule with glumes and other floral organs removed. (G) Diagram depicting meristems in the inflorescence. (H-N) RNA *in situ* hybridization of the meristem marker, *kn1*, in developing ear spikelets; Red and blue arrowheads indicate upper and lower floral meristems, respectively. PS, pedicellate spikelet; SS, sessile spikelet; UF, upper floret; LF, lower floret; IM, inflorescence meristem; BM, branch meristem; SPM, spikelet pair meristem; SM, spikelet meristem; FM, floral meristem; Gl, glume; Op, ovule primordia; Cp, carpel primordia; Lo, lodicule; St, stamen; Le, lemma. Scale bars: (A, D) = 5 cm, (B, C, E, F) = 500 μm, (H-N) = 50 μm.

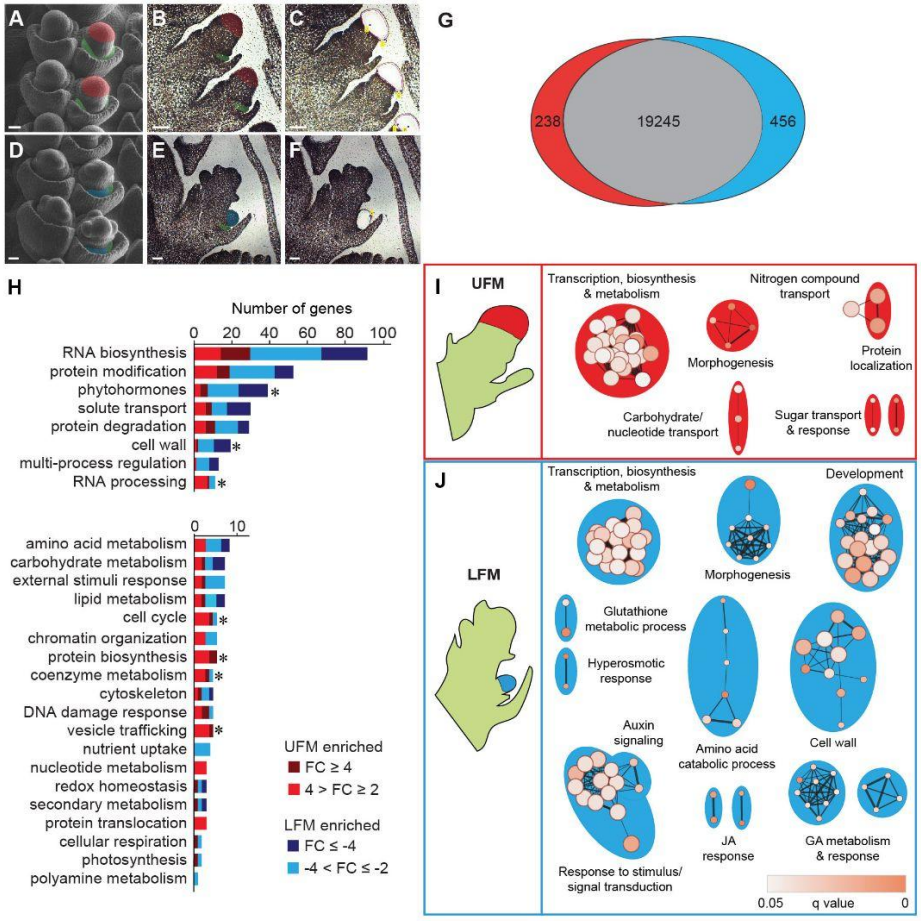

Figure 2. Maize upper and lower floral meristems are enriched for genes belonging to distinct functional groups.

SEMs of spikelets at developmental stages of UFM (A) and LFM (D) dissections. Representative images of FM before (B, E) and after (C, F) LCM. False coloring indicates UFM (red), LFM (blue) and lemma primordia (green). (G) Venn diagram depicting DEG ($q < 0.05$ and fold change ≥ 2) in UFM (red) and LFM (blue). (H) Distribution of DEG in MapMan-annotated functional groups. Note difference in scale of the X-axis. * indicates $p < 0.05$ in Wilcoxon rank sum test. Genes unassigned to a functional group (99 UFM-enriched and 227 LFM-enriched) are not shown. (I, J) GO-enrichment maps for UFM and LFM DEGs. Nodes (circles) indicate significantly enriched GO terms. Node size is proportional to number of DEGs in each node; node color indicates statistical significance. Edges (lines) link similar GO terms. Edge thickness is proportional to the number of DEGs shared between GO terms. Node clusters were manually labeled based on corresponding GO terms in each cluster. Scale bars = 50 μm.

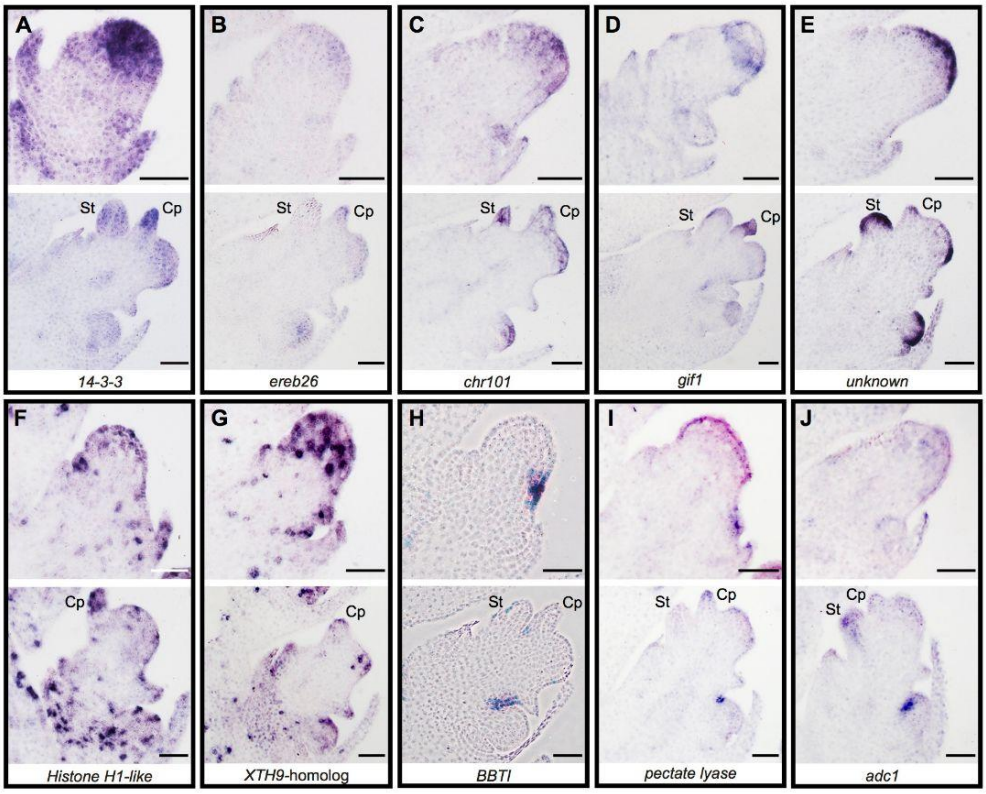

Figure 3. UFM and LFM DEGs have distinct RNA expression patterns.

(A) AC217050.4_FG006, 14-3-3 protein. (B) GRMZM2G317160/*ereb26*. (C) GRMZM2G177165/*chr101*. (D) GRMZM2G180246/*gif1*. (E) GRMZM2G101682, unknown function. (F) GRMZM2G069911, *histone H1-like*. (G) GRMZM2G180870, *AtXTH9* (*XYLOGLUCAN ENDOTRANSGLUCOSYLASE/HYDROLASE 9*) homolog. (H) GRMZM2G114552/*BBTI*, Bowman-Birk type (proteinase/bran trypsin) inhibitor. (I) GRMZM2G131912, *pectate lyase* homolog. (J) GRMZM2G396553/*adc1*. Developmental stages at which UFM (top) and LFM (bottom) were dissected are shown for each gene. St: Stamen; Cp: carpel primordium. Scale bars = 50 μm.

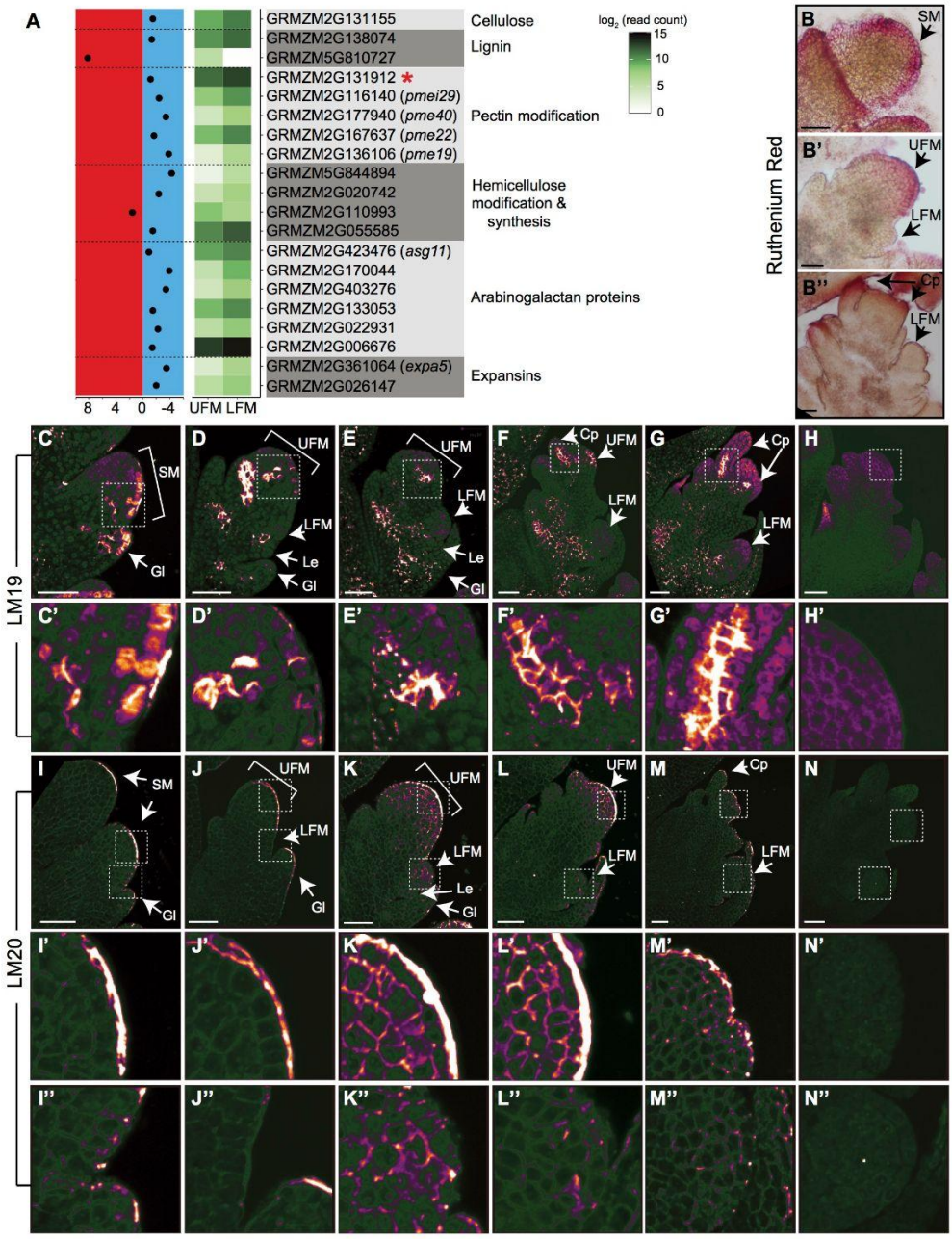

Figure 4. The UFM and LFM have distinct cell wall compositions.

(A) Expression profiles for DEG in the MapMan Cell Wall functional group. Left panel indicates $\log_2$(fold change) for each gene. UFM-enriched genes are plotted on the left (red) and LFM-enriched genes on the right (blue). Middle panel shows an expression heatmap. Red * indicates gene with known RNA *in situ* hybridization patterns. Ruthenium red staining of acidic pectin in SM (B), early (B') and late (B'') ear florets. (C-G) LM19 immunostaining of low methylesterified HG in developing spikelets. (H) Negative control lacking primary antibody to show background autofluorescence using the same laser settings as (C-G). White boxes indicate

zoomed in areas shown in (C'-H'). (I-M) LM20 immunostaining of high methylesterified HG in developing spikelets. (N) Negative control lacking primary antibody to show background autofluorescence using the same laser settings as (I-M). White boxes indicated zoomed in areas corresponding to UFM (I'-N') and LFM (I''-N''). Weak, diffuse cytoplasmic signal in (C-N) is background autofluorescence, which varies due to incomplete quenching. Micrographs were false colored using ImageJ (Orange Blue icb look-up table) to visualize signal intensity. Scale bars = 50 μm.

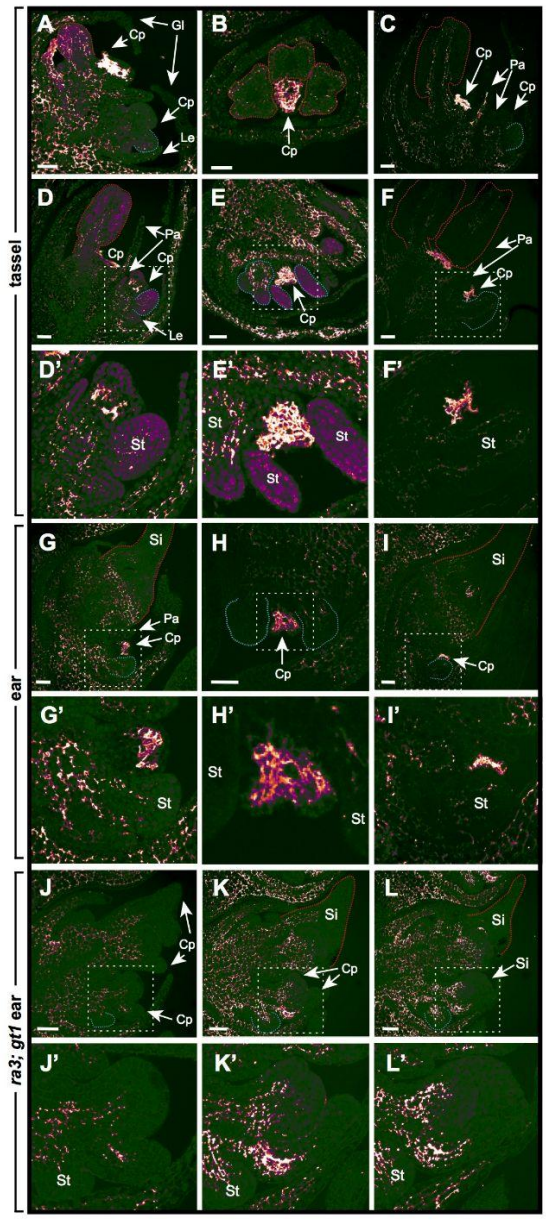

Figure 5. Pectin demethyletserification is associated with aborting carpels.

LM19 immunostaining of low methylesterified HG in aborting carpels in the upper (A-C) and lower (D-F) florets of tassel spikelets, and lower florets of ear spikelets (G-I). In ra3;gt1 mutant ear spikelets, where the lower floret does not abort, LM19 stains initiating carpel primordia, but lacks the intense staining associated with aborting carpels. White boxes indicate zoomed in areas corresponding to regions shown in (D'-L'). Red and blue dashed lines outline stamen primordia in upper and lower florets, respectively. Silks in the upper floret are also outlined in red in G, I, K and L. LM19 staining use the same laser settings as Figure 4, C-G. Cp, carpel primordia; Gl, glume; Le, lemma; Pa, palea; Si, silk; St, stamen primordia. Scale bars = 50 μm.

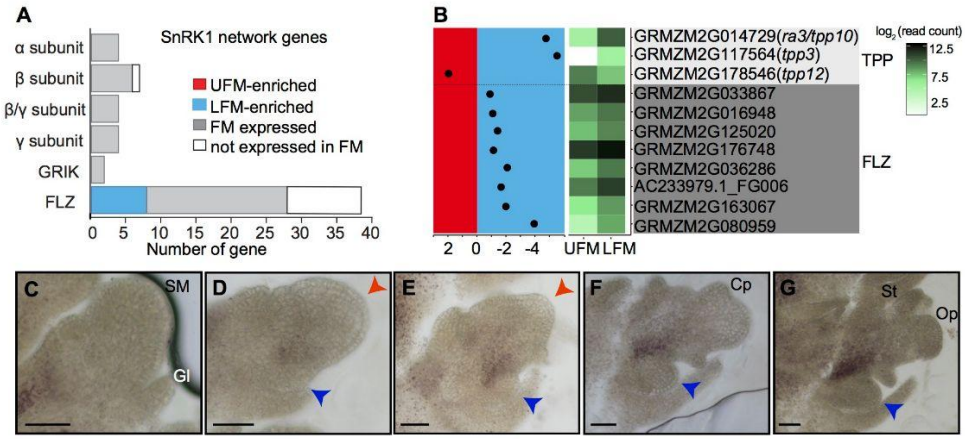

Figure 6. Sugar metabolism likely differs in UFM and LFM.

(A) Summary of predicted SnRK1 signaling network genes expressed in FM samples. (B) Expression profiles for sugar-related DEG; layout is the same as cell wall-related genes in Fig 4. (C-G) Starch accumulates at the boundary between the UFM and LFM in developing spikelets. Red and blue arrowheads indicate UFM and LFM respectively. Scale bars = 50 μm.

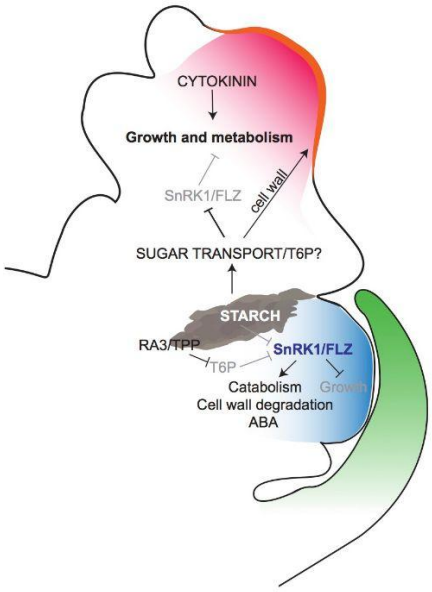

Figure 7. A model for growth regulation in developing florets.

In UFM (red), high cytokinin and sugar availability promote growth and metabolism, including synthesis of new cell walls (orange). In LFM (blue), low sugar availability activates the SnRK1/FLZ pathway to repress growth and increase catabolism. Starch accumulates at the UFM/LFM boundary and may supply sugar to the UFM and/or be important for boundary formation.

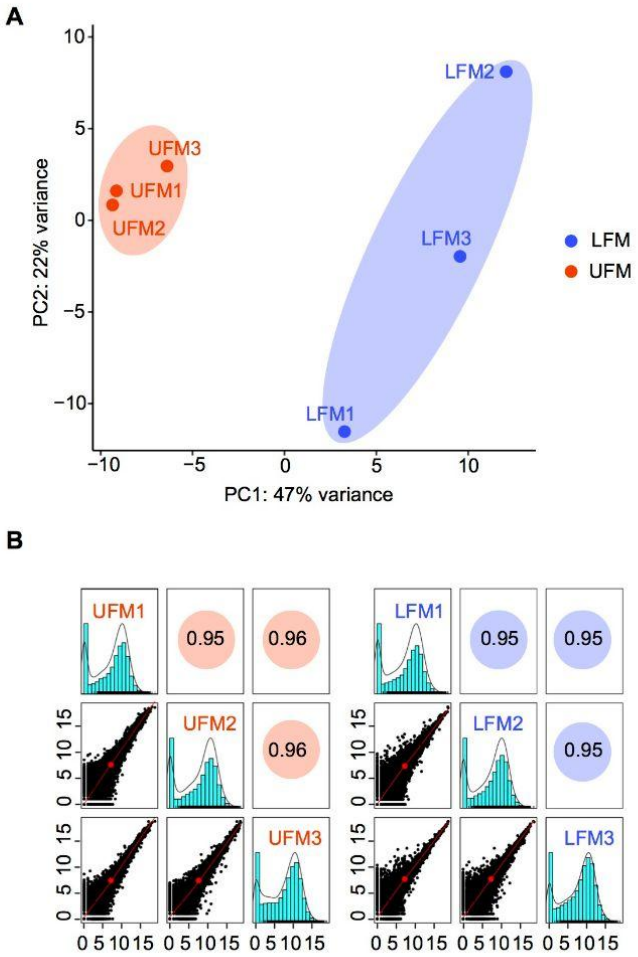

Supplemental Figure S1. Cluster and reproducibility analysis of LFM and UFM biological replicates.

(A) PCA analysis of expression profiles in UFM and LFM biological replicates. (B) Reproducibility of FM biological replicates using transformed expression values (log_2 read count). Histogram shows the number of genes (Y-axis) in transformed read count categories (X-axis) of each biological replicate. Circles/numbers indicate Pearson's coefficient matrix of pairwise comparison among biological replicates; scatterplots are pairwise comparisons of expression values among biological replicates. X and Y axes in scatterplots are log_2(read count) for two different biological replicates. UFM, upper floral meristem; LFM, lower floral meristem.

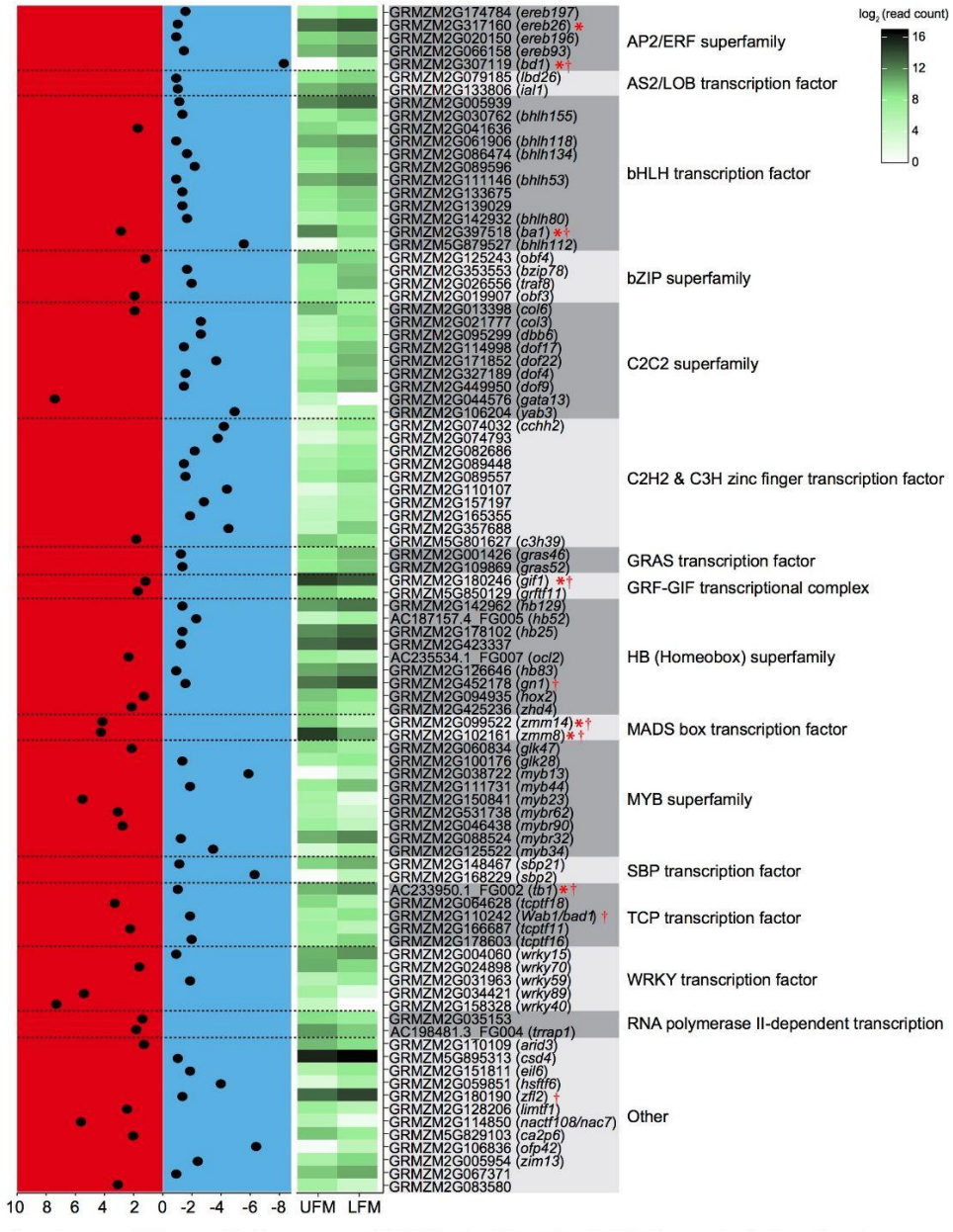

Supplemental Figure S2. Summary of DEG in the MapMan RNA biosynthesis functional group.

Left panel indicates $\log_2$ (fold change) for each gene. UFM-enriched genes are plotted on the left (red) and LFM-enriched genes on the right (blue). Middle panel shows expression heatmap based on the $\log_2$ (read count). Red * indicates genes with known RNA in situ hybridization patterns; red † indicates genes associated with mutant phenotype. UFM, upper floral meristem; LFM, lower floral meristem.

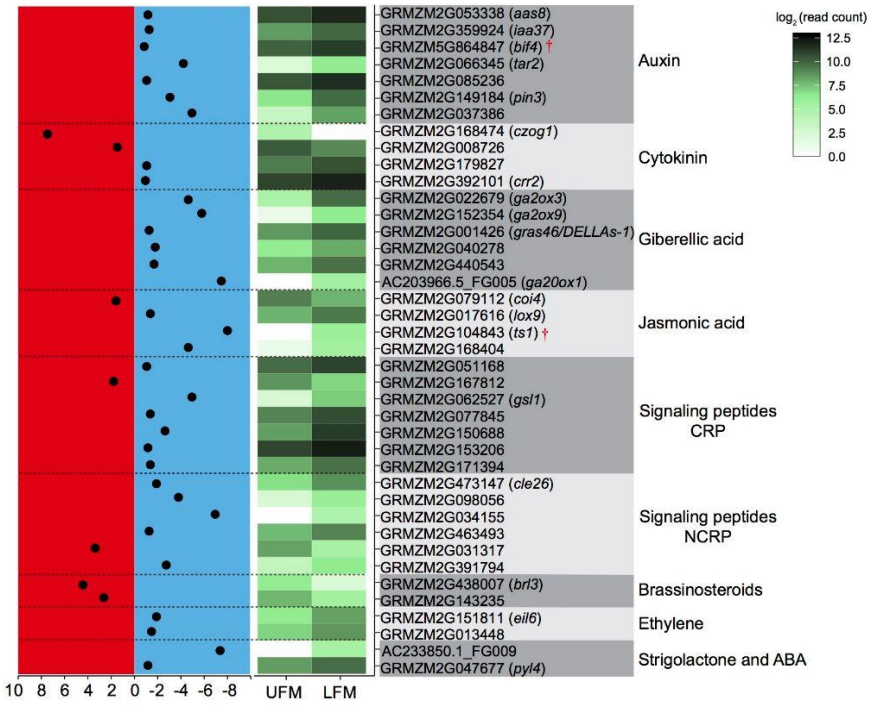

Supplemental Figure S3. Summary of DEG in the MapMan phytohormone functional group.

Left panel indicates $\log_2$ (fold change) for each gene. UFM-enriched genes are plotted on the left (red) and LFM-enriched genes on the right (blue). Middle panel shows expression heatmap based on the $\log_2$(read count). Red † indicates genes associated with mutant phenotype. UFM, upper floral meristem; LFM, lower floral meristem; CRP, cysteine-rich peptide; NCRP, non-cysteine-rich peptide; ABA, abscisic acid.

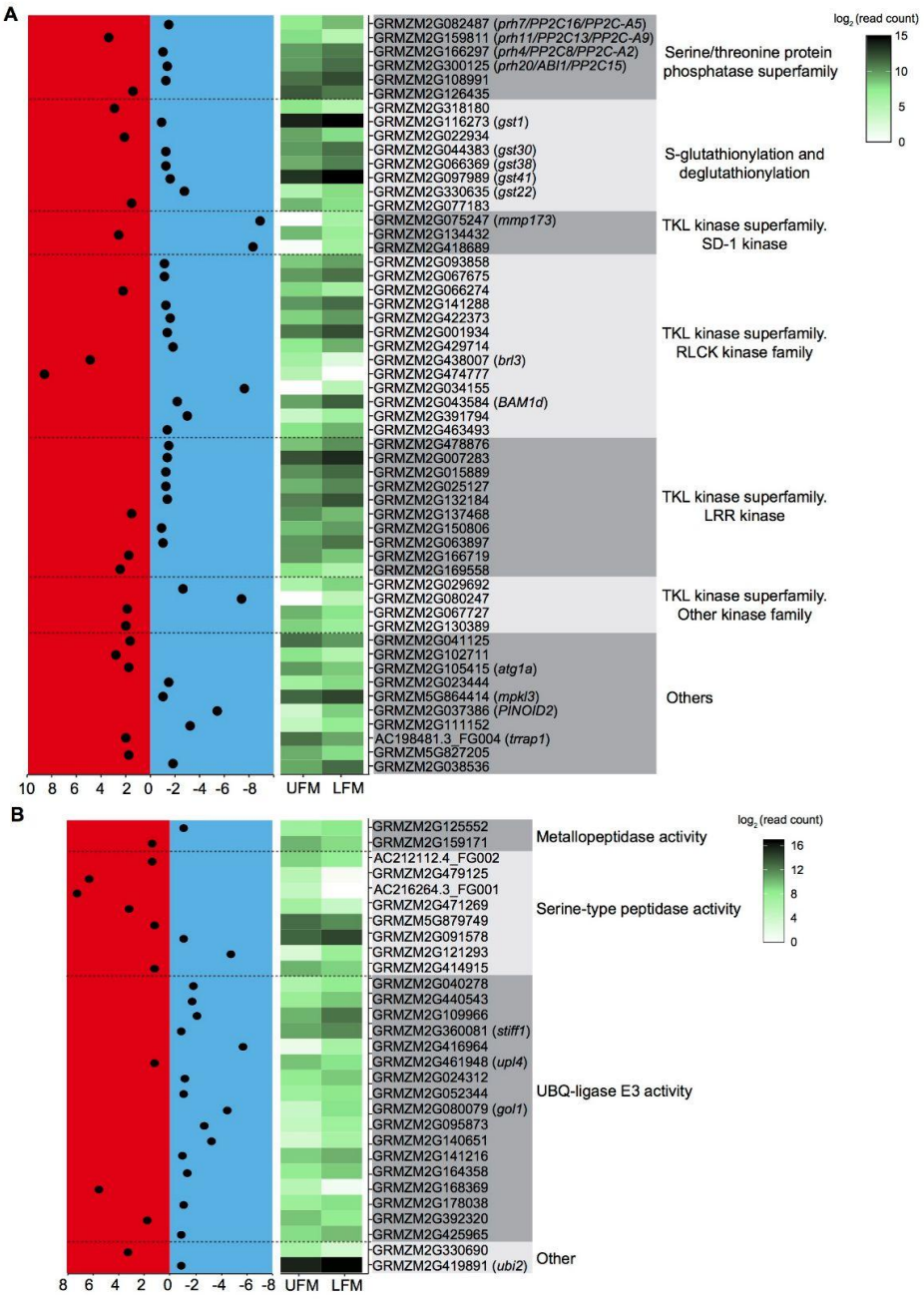

Supplemental Figure S4. Summary of DEG in MapMan protein modification (A) and degradation (B) functional groups.

Left panel indicates $\log_2$ (fold change) for each gene. UFM-enriched genes are plotted on the left (red) and LFM-enriched genes on the right (blue). Middle panel shows expression heatmap based on the $\log_2$ (read count). UFM, upper floral meristem; LFM, lower floral meristem; SD, S domain; TKL, tyrosine kinase-like; RLCK, receptor-like cytoplasmic kinase; LRR, leucine-rich repeat; UBQ, ubiquitin.

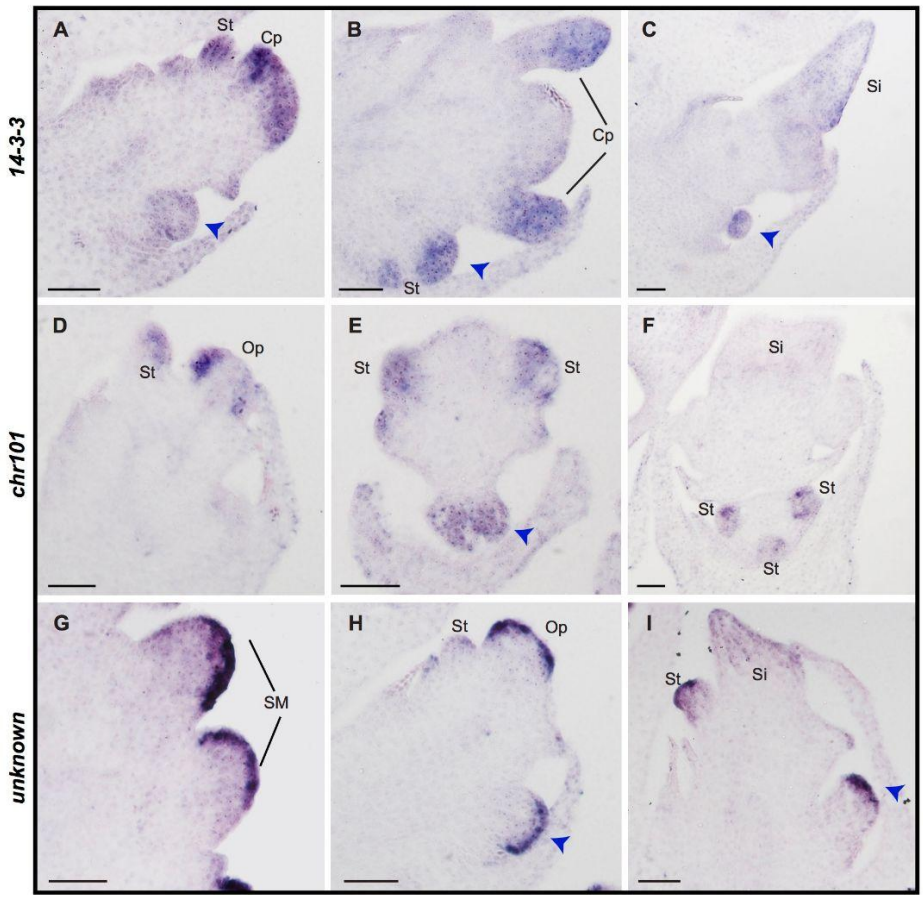

Supplemental Figure S5. RNA in situ hybridization of AC217050.4_FG006, *chr101*/GRMZM2G177165, and GRMZM2G101682 in developing inflorescences.

AC217050.4_FG006 (encodes a 14-3-3 protein) is expressed in UFM, stamen and carpel primordia in the upper floret, and weakly in palea primordia (A). Expression persists in initiating carpels, but not in ovule primordium. AC217050.4_FG006 is also expressed in FM and stamen primordia of the lower floret (C). In late stage spikelets, AC217050.4_FG006 is weakly in the silk and LFM (B). *chr101* is expressed in stamen and ovule primordia of the upper floret (D-E) and in the LFM (E). *chr101* is also expressed in stamen primordia in the lower floret, but no longer detectable in the upper floret (F). GRMZM2G101682 is strongly expressed in the L1 layer of SM (G), ovule (H), and stamen (I) primordia, and in LFM throughout spikelet development (H-I). Blue arrowheads indicate LFM. UFM, upper floral meristem; LFM, lower floral meristem; Cp, carpel primordia; Op, ovule primordia; St, stamen; Si, silk; SM, spikelet meristem. Scale bars = 50 μm.

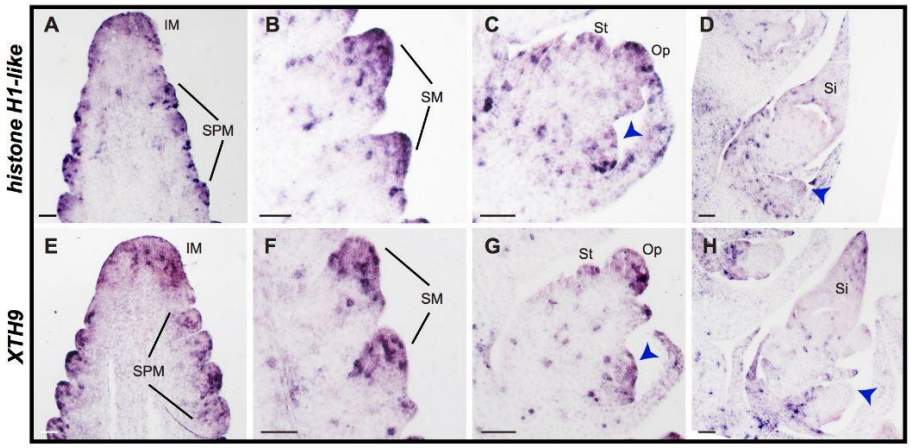

Supplemental Figure S6. RNA in situ hybridization of *histone H1-like*/GRMZM2G069911 and *XTH9* homolog/GRMZM2G180870 in developing inflorescences.

Histone H1-like/GRMZM2G069911 (A-D) and GRMZM2G180870 (*XTH9* homolog, E-H) are expressed in a punctate pattern in all inflorescence meristems and organ primordia including the IM (A, E), SPM (A, E), SM (B, F), glume and floral organ primordia (B-D, F-H). Blue arrowheads indicate LFM. LFM, lower floral meristem; IM, inflorescence meristem; SPM, spikelet pair meristem; SM, spikelet meristem; Op, ovule primordia; St, stamen; Si, silk. Scale bars = 50 μm.

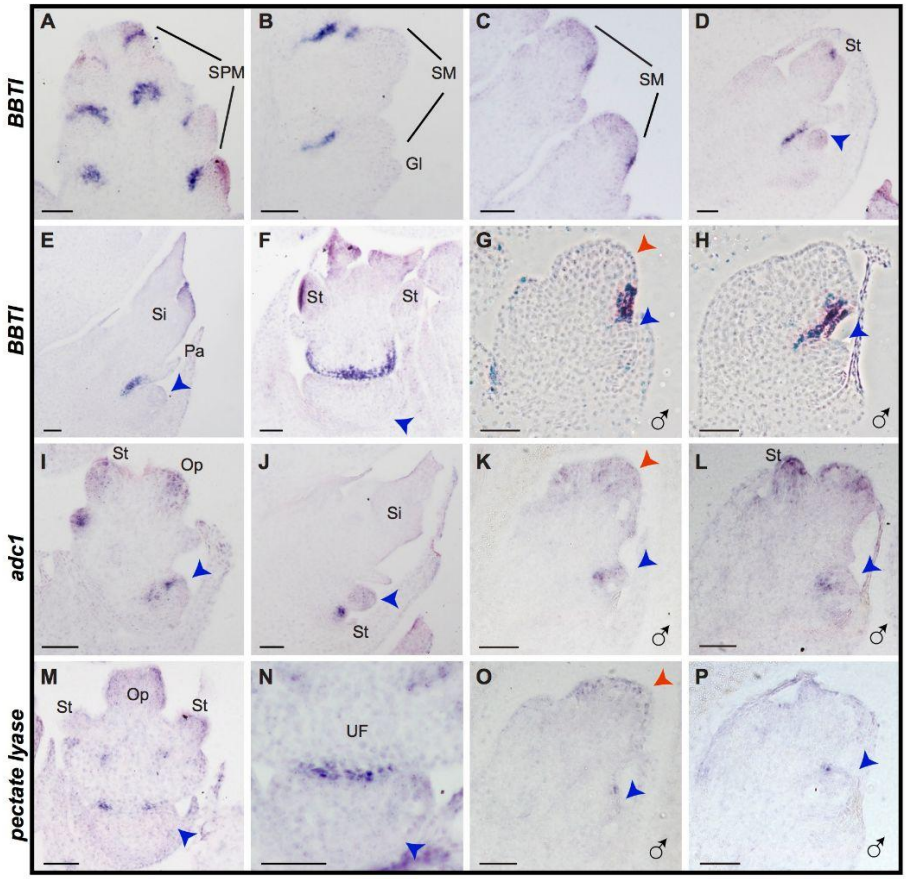

Supplemental Figure S7. RNA in situ hybridization of *BBTI*, *adc1* and *pectate lyase* in developing inflorescences.

BBTI is expressed at the base of developing SPM (A) and SM (B), and on the abaxial side of late stage SM (C). During floral development, *BBTI* persists on the abaxial side of the UFM and ultimately localizes to the base of the palea at the boundary with the lower floret (D-F). *BBTI* is also expressed at the UFM/LFM boundary in tassel spikelets (G-H). *adc1* is expressed in the stamen primordia and ovule primordia (I-J). In older spikelets, its expression is restricted to FM and stamen primordia of the low floret (J). *adc1* is also expressed at the UFM/LFM boundary of developing tassel spikelets (K-L). GRMZM2G131912 (pectate lyase homolog) is expressed at the boundary upper and lower florets (M-N), and at the UFM/LFM boundary in tassel spikelets (O-P). Red arrowheads indicate UFM; blue arrowheads indicate LFM. SPM, spikelet pair meristem; SM, spikelet meristem; UFM, upper floral meristem; LFM, lower floral meristem; Gl, glume; Op, ovule primordia; UF, upper floret; Pa, palea; St, stamen; Si, silk. Scale bars = 50 μm.

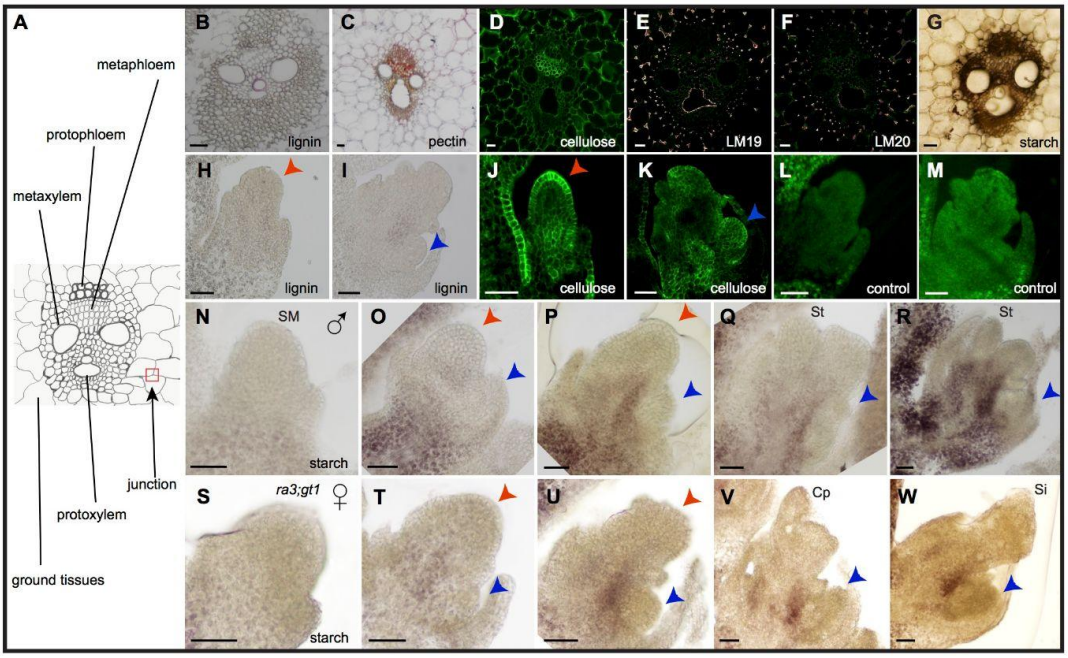

Supplemental Figure S8. Histochemical staining in maize stems and spikelets.

(A) Diagram of maize stem showing organization and cell types. (B) Maize stem stained with phloroglucinol-HCl to detect lignin (pink), which is primarily localized to cell walls of xylem cells. (C) Maize stem cryosection stained with ruthenium red to detect acidic pectin, which is primarily localized to cell walls of phloem and ground tissue. (D) Maize stem stained with calcofluor white/fluorescence brighter 28 to detect cellulose, which is primarily localized in the metaphloem, protophloem, and cell wall of ground tissues. Maize stem stained with LM19 (E) to detect low methylesterified pectin and LM20 (F) to detect high methylesterified pectin; both LM19 and LM20 are primarily localized to the junctions of ground tissues, protoxylem, metaphloem, and protophloem. (G) Maize stem cryosection stained with Lugol's solution to detect starch, which is primarily localized to the vasculature. (H-I) Maize spikelets stained with phloroglucinol-HCl to detect lignin. Very little staining is observed. (J-K) Maize spikelets stained with calcofluor white to detect cellulose. Cellulose surrounds all cells in developing spikelets, but is particularly strong in the L1 layer. (L-M) Tissue processed same as in (J-K), but without calcofluor white to show background autofluorescence. Starch staining in developing tassel (N-R) and *ra3;gt1* (S-W) ear spikelets. Red arrowheads indicate UFM; blue arrowheads indicate LFM. UFM, upper floral meristem; LFM, lower floral meristem; SM, spikelet meristem; St, stamen; Cp, carpel primordia; Si, silk. Scale bars = 50 μm.

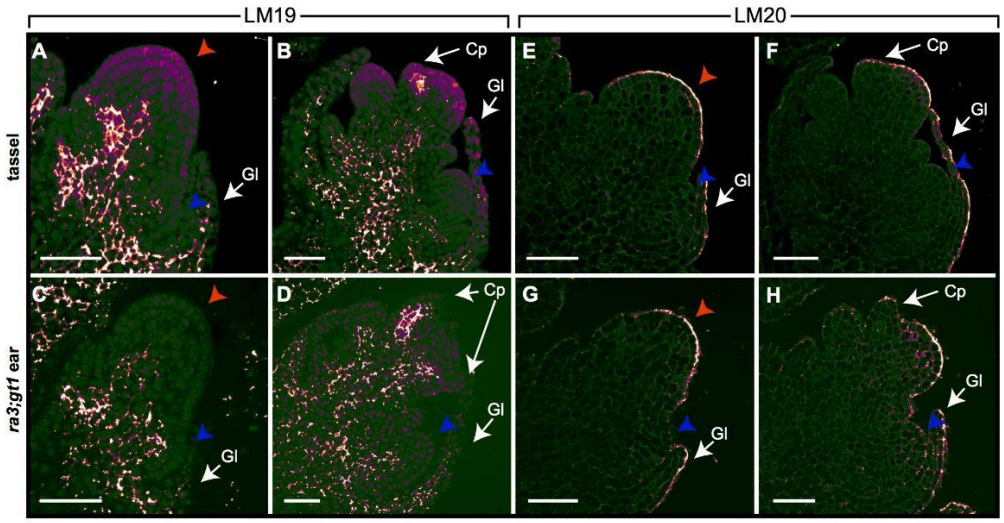

Supplemental Figure S9. The UFM and LFM have distinct cell wall composition regardless of LFM fate.

LM19 (A-D) and LM20 (E-H) preferentially stain upper florets of both tassel (A-B, E-F) and *ra3;gt1* ear (C-D, G-H) spikelets, even though both upper and lower florets develop to maturity. Laser settings are the same as those in Figure 4, C-G for LM19 and Figure 4, I-M for LM20. Red and blue arrowheads indicate UFM and LFM respectively. UFM, upper floral meristem; LFM, lower floral meristem; Cp, carpel primordia; Gl, glume. Scale bars = 50 μm.

Primer name	Sequence
GRMZM2G114552-F	ATGGCAGATGACAAGAAAGCA
GRMZM2G114552-R	GAGACACGAGATCAGCAAGG
AC217050.4_FG006-F1	CCTTCTTCTACTGCTGCTGAAT
AC217050.4_FG006-R1	ACGGACTTAATGCCAACTAGC
GRMZM2G317160-F1	GAGAATGCCGTGACCAACTTC
GRMZM2G317160-R1	TCGTCTGTGGTGAATGCCTTA
GRMZM2G177165-F1	GCTATCTTGCGTCCATTCCTTC
GRMZM2G177165-R1	ATCCTGTCCTCCTCGGTCTG
GRMZM2G131912-F2	GCGTGTCCATCTTCGGTTC
GRMZM2G131912-R2	TGGTGGTGGTGGTGTTGAG
GRMZM2G396553-F2	CCTGTTCGTCGGATTCTCTTC
GRMZM2G396553-R2	CGTAGCCGTCGTCCTTGTA
GRMZM2G069911-F2	CGAAGGAGGTGGTGGAGAAG
GRMZM2G069911-R2	CACGACTACGACGCTGCTA
GRMZM2G180870-F2	CCAGCCAGGTGGTGTTCAT
GRMZM2G180870-R2	CGCAGCATCGTTCTTCGTT
GRMZM2G180246-F	TGAACCCGCAGTCGCTGATG
GRMZM2G180246-R	TCAAAGCTACCTGCTAATCC
GRMZM2G101682-F	ATCATCACACCCAACGCAAC
GRMZM2G101682-R	CACACAAGCCCTAACGTGAC

Supplemental Table S1. Primers used in this study.

Reference

Acosta IF, Laparra H, Romero SP, Schmelz E, Hamberg M, Mottinger JP, Moreno MA, Dellaporta SL (2009) tasselseed1 is a lipoxygenase affecting jasmonic acid signaling in sex determination of maize. Science **323**: 262–265

Anders S, Pyl PT, Huber W (2015) HTSeq--a Python framework to work with high-throughput sequencing data. Bioinformatics **31**: 166–169

Asai K, Satoh N, Sasaki H, Satoh H, Nagato Y (2002) A rice heterochronic mutant, mori1, is defective in the juvenile-adult phase change. Development **129**: 265–273

Baena-González E, Lunn JE (2020) SnRK1 and trehalose 6-phosphate – two ancient pathways converge to regulate plant metabolism and growth. Current Opinion in Plant Biology **55**: 52–59

Baena-González E, Rolland F, Thevelein JM, Sheen J (2007) A central integrator of transcription networks in plant stress and energy signalling. Nature **448**: 938–942

Bai F, Reinheimer R, Durantini D, Kellogg EA, Schmidt RJ (2012) TCP transcription factor, BRANCH ANGLE DEFECTIVE 1 (BAD1), is required for normal tassel branch angle formation in maize. Proc Natl Acad Sci U S A **109**: 12225–12230

Bartlett ME, Thompson B (2014) Meristem identity and phyllotaxis in inflorescence development. Front Plant Sci **5**: 508

Blackburn MR, Haruta M, Moura DS (2020) Twenty Years of Progress in Physiological and Biochemical Investigation of RALF Peptides. Plant Physiol **182**: 1657–1666

Bomblies K, Wang R-L, Ambrose BA, Schmidt RJ, Meeley RB, Doebley J (2003) Duplicate FLORICAULA/LEAFY homologs zfl1 and zfl2 control inflorescence architecture and flower patterning in maize. Development **130**: 2385–2395

Bortiri E, Chuck G, Vollbrecht E, Rocheford T, Martienssen R, Hake S (2006) ramosa2 encodes a LATERAL ORGAN BOUNDARY domain protein that determines the fate of stem cells in branch meristems of maize. Plant Cell **18**: 574–585

Cabib E, Leloir LF (1958) The biosynthesis of trehalose phosphate. J Biol Chem **231**: 259–275

Cacharron J, Saedler H, Theissen G (1999) Expression of MADS box genes ZMM8 and ZMM14 during inflorescence development of Zea mays discriminates between the upper and the lower floret of each spikelet. Dev Genes Evol **209**: 411–420

Cavalier DM, Lerouxel O, Neumetzler L, Yamauchi K, Reinecke A, Freshour G, Zabotina OA, Hahn MG, Burgert I, Pauly M, et al (2008) Disrupting Two Arabidopsis thaliana Xylosyltransferase Genes Results in Plants Deficient in Xyloglucan, a Major Primary Cell

Wall Component. The Plant Cell **20**: 1519–1537

Chen D, Shao Q, Yin L, Younis A, Zheng B (2018) Polyamine Function in Plants: Metabolism, Regulation on Development, and Roles in Abiotic Stress Responses. Front Plant Sci **9**: 1945

Cheng PC, Greyson RI, Walden DB (1983) ORGAN INITIATION AND THE DEVELOPMENT OF UNISEXUAL FLOWERS IN THE TASSEL AND EAR OF ZEA MAYS. American Journal of Botany **70**: 450–462

Chen K-M, Wang F, Wang Y-H, Chen T, Hu Y-X, Lin J-X (2006) Anatomical and chemical characteristics of foliar vascular bundles in four reed ecotypes adapted to different habitats. Flora - Morphology, Distribution, Functional Ecology of Plants **201**: 555–569

Chuck G, Meeley RB, Hake S (1998) The control of maize spikelet meristem fate by the APETALA2-like gene indeterminate spikelet1. Genes Dev **12**: 1145–1154

Chuck G, Muszynski M, Kellogg E, Hake S, Schmidt RJ (2002) The control of spikelet meristem identity by the branched silkless1 gene in maize. Science **298**: 1238–1241

Claeys H, Vi SL, Xu X, Satoh-Nagasawa N, Eveland AL, Goldshmidt A, Feil R, Beggs GA, Sakai H, Brennan RG, et al (2019) Control of meristem determinacy by trehalose 6-phosphate phosphatases is uncoupled from enzymatic activity. Nat Plants **5**: 352–357

DeLong A, Calderon-Urrea A, Dellaporta SL (1993) Sex determination gene TASSELSEED2 of maize encodes a short-chain alcohol dehydrogenase required for stage-specific floral organ abortion. Cell **74**: 757–768

Demesa-Arevalo E, Abraham-Juarez MJ, Xu X, Bartlett M, Jackson D (2021) Maize RAMOSA3 accumulates in nuclear condensates enriched in RNA POLYMERASE II isoforms during the establishment of axillary meristem determinacy. bioRxiv doi: 10.1101/2021.04.06.438639

Du Y, Lunde C, Li Y, Jackson D, Hake S, Zhang Z (2021) Gene duplication at the Fascicled ear1 locus controls the fate of inflorescence meristem cells in maize. Proc Natl Acad Sci U S A. doi: 10.1073/pnas.2019218118

Eveland AL, Goldshmidt A, Pautler M, Morohashi K, Liseron-Monfils C, Lewis MW, Kumari S, Hiraga S, Yang F, Unger-Wallace E, et al (2014) Regulatory modules controlling maize inflorescence architecture. Genome Res **24**: 431–443

Figueroa CM, Lunn JE (2016) A Tale of Two Sugars: Trehalose 6-Phosphate and Sucrose. Plant Physiol **172**: 7–27

Foster T, Veit B, Hake S (1999a) Mosaic analysis of the dominant mutant, Gnarley1-R, reveals distinct lateral and transverse signaling pathways during maize leaf development. Development **126**: 305–313

Foster T, Yamaguchi J, Wong BC, Veit B, Hake S (1999b) Gnarley1 is a dominant mutation in the knox4 homeobox gene affecting cell shape and identity. Plant Cell **11**: 1239–1252

Gallavotti A, Yang Y, Schmidt RJ, Jackson D (2008) The Relationship between Auxin Transport and Maize Branching. Plant Physiology **147**: 1913–1923

Gallavotti A, Zhao Q, Kyozuka J, Meeley RB, Ritter MK, Doebley JF, Pè ME, Schmidt RJ (2004) The role of barren stalk1 in the architecture of maize. Nature **432**: 630–635

Gene Ontology Consortium (2015) Gene Ontology Consortium: going forward. Nucleic Acids Res **43**: D1049–56

Ghiglione HO, Gonzalez FG, Serrago R, Maldonado SB, Chilcott C, Curá JA, Miralles DJ, Zhu T, Casal JJ (2008) Autophagy regulated by day length determines the number of fertile florets in wheat. Plant J **55**: 1010–1024

Gunawardena AHLAN, Arunika H L A, Greenwood JS, Dengler NG (2007) Cell wall degradation and modification during programmed cell death in lace plant, Aponogeton madagascariensis (Aponogetonaceae). American Journal of Botany **94**: 1116–1128

Harholt J, Suttangkakul A, Scheller HV (2010) Biosynthesis of Pectin. Plant Physiol **153**: 384–395

Hay A, Hake S (2004) The Dominant Mutant Wavy auricle in blade1 Disrupts Patterning in a Lateral Domain of the Maize Leaf. Plant Physiology **135**: 300–308

Hinnant TD, Alvarez AA, Ables ET (2017) Temporal remodeling of the cell cycle accompanies differentiation in the Drosophila germline. Dev Biol **429**: 118–131

Hubbard L, McSteen P, Doebley J, Hake S (2002) Expression patterns and mutant phenotype of teosinte branched1 correlate with growth suppression in maize and teosinte. Genetics **162**: 1927–1935

Hu R, Xu Y, Yu C, He K, Tang Q, Jia C, He G, Wang X, Kong Y, Zhou G (2017) Transcriptome analysis of genes involved in secondary cell wall biosynthesis in developing internodes of Miscanthus lutarioriparius. Sci Rep **7**: 9034

Ikeda-Kawakatsu K, Yasuno N, Oikawa T, Iida S, Nagato Y, Maekawa M, Kyozuka J (2009) Expression level of ABERRANT PANICLE ORGANIZATION1 determines rice inflorescence form through control of cell proliferation in the meristem. Plant Physiol **150**: 736–747

Irish EE (1997) Experimental Analysis of Tassel Development in the Maize Mutant Tassel Seed 6. Plant Physiol **114**: 817–825

Irish EE, Nelson T (1989) Sex Determination in Monoecious and Dioecious Plants. The Plant

Cell **1**: 737

Jackson D (1992) In-situ hybridisation in plants. Molecular Plant Pathology: A Practical Approach.

Jackson D, Veit B, Hake S (1994) Expression of maize KNOTTED1 related homeobox genes in the shoot apical meristem predicts patterns of morphogenesis in the vegetative shoot. Development **120**: 405–413

Jamsheer K M, Sharma M, Singh D, Mannully CT, Jindal S, Shukla BN, Laxmi A (2018a) FCS-like zinc finger 6 and 10 repress SnRK1 signalling in Arabidopsis. Plant J **94**: 232–245

Jamsheer K M, Shukla BN, Jindal S, Gopan N, Mannully CT, Laxmi A (2018b) The FCS-like zinc finger scaffold of the kinase SnRK1 is formed by the coordinated actions of the FLZ domain and intrinsically disordered regions. J Biol Chem **293**: 13134–13150

Janzen NR, Whitfield J, Hoffman NJ (2018) Interactive Roles for AMPK and Glycogen from Cellular Energy Sensing to Exercise Metabolism. Int J Mol Sci **19**: 3344

Johnston R, Wang M, Sun Q, Sylvester AW, Hake S, Scanlon MJ (2014) Transcriptomic analyses indicate that maize ligule development recapitulates gene expression patterns that occur during lateral organ initiation. Plant Cell **26**: 4718–4732

Keegstra K (2010) Plant Cell Walls. Plant Physiol **154**: 483–486

Kim D, Pertea G, Trapnell C, Pimentel H, Kelley R, Salzberg SL (2013) TopHat2: accurate alignment of transcriptomes in the presence of insertions, deletions and gene fusions. Genome Biol **14**: R36

Kim JC, Laparra H, Calderón-Urrea A, Mottinger JP, Moreno MA, Dellaporta SL (2007) Cell cycle arrest of stamen initials in maize sex determination. Genetics **177**: 2547–2551

Klein H, Gallagher J, Demesa-Arevalo E, Abraham-Juárez MJ, Heeney M, Feil R, Lunn JE, Xiao Y, Chuck G, Whipple C, et al (2022) Recruitment of an ancient branching program to suppress carpel development in maize flowers. Proc Natl Acad Sci USA **119**: e2115871119

K MJ, Jindal S, Laxmi A (2019) Evolution of TOR–SnRK dynamics in green plants and its integration with phytohormone signaling networks. Journal of Experimental Botany **70**: 2239–2259

K MJ, Laxmi A (2014) DUF581 is plant specific FCS-like zinc finger involved in protein-protein interaction. PLoS One **9**: e99074

K MJ, Laxmi A (2015) Expression of Arabidopsis FCS-Like Zinc finger genes is differentially regulated by sugars, cellular energy level, and abiotic stress. Frontiers in Plant Science. doi:

10.3389/fpls.2015.00746

Le Roux LG, Kellogg EA (1999) Floral development and the formation of unisexual spikelets in the Andropogoneae (Poaceae). Am J Bot **86**: 354–366

Lewis MW, Bolduc N, Hake K, Htike Y, Hay A, Candela H, Hake S (2014) Gene regulatory interactions at lateral organ boundaries in maize. Development **141**: 4590–4597

Liu C, Thong Z, Yu H (2009) Coming into bloom: the specification of floral meristems. Development **136**: 3379–3391

Liu F, Cui X, Horner HT, Weiner H, Schnable PS (2001) Mitochondrial aldehyde dehydrogenase activity is required for male fertility in maize. Plant Cell **13**: 1063–1078

Li Z, Tang J, Srivastava R, Bassham DC, Howell SH (2020) The Transcription Factor bZIP60 Links the Unfolded Protein Response to the Heat Stress Response in Maize. Plant Cell **32**: 3559–3575

Love MI, Huber W, Anders S (2014) Moderated estimation of fold change and dispersion for RNA-seq data with DESeq2. Genome Biol **15**: 550

Lunde C, Kimberlin A, Leiboff S, Koo AJ, Hake S (2019) Tasselseed5 overexpresses a wound-inducible enzyme, ZmCYP94B1, that affects jasmonate catabolism, sex determination, and plant architecture in maize. Communications Biology **2**: 114

Merico D, Isserlin R, Stueker O, Emili A, Bader GD (2010) Enrichment map: a network-based method for gene-set enrichment visualization and interpretation. PLoS One **5**: e13984

Nietzsche M, Landgraf R, Tohge T, Börnke F (2016) A protein–protein interaction network linking the energy-sensor kinase SnRK1 to multiple signaling pathways in Arabidopsis thaliana. Current Plant Biology **5**: 36–44

Nietzsche M, Schießl I, Börnke F (2014) The complex becomes more complex: protein-protein interactions of SnRK1 with DUF581 family proteins provide a framework for cell- and stimulus type-specific SnRK1 signaling in plants. Front Plant Sci **5**: 54

Oszvald M, Primavesi LF, Griffiths CA, Cohn J, Basu SS, Nuccio ML, Paul MJ (2018) Trehalose 6-Phosphate Regulates Photosynthesis and Assimilate Partitioning in Reproductive Tissue. Plant Physiol **176**: 2623–2638

Peaucelle A, Braybrook SA, Le Guillou L, Bron E, Kuhlemeier C, Höfte H (2011) Pectin-induced changes in cell wall mechanics underlie organ initiation in Arabidopsis. Curr Biol **21**: 1720–1726

Peaucelle A, Louvet R, Johansen JN, Höfte H, Laufs P, Pelloux J, Mouille G (2008) Arabidopsis phyllotaxis is controlled by the methyl-esterification status of cell-wall pectins.

Curr Biol **18**: 1943–1948

Pesquet E, Zhang B, Gorzsás A, Puhakainen T, Serk H, Escamez S, Barbier O, Gerber L, Courtois-Moreau C, Alatalo E, et al (2013) Non-cell-autonomous postmortem lignification of tracheary elements in Zinnia elegans. Plant Cell **25**: 1314–1328

Poursarebani N, Trautewig C, Melzer M, Nussbaumer T, Lundqvist U, Rutten T, Schmutzer T, Brandt R, Himmelbach A, Altschmied L, et al (2020) COMPOSITUM 1 contributes to the architectural simplification of barley inflorescence via meristem identity signals. Nat Commun **11**: 5138

Pradhan Mitra P, Loqué D (2014) Histochemical staining of Arabidopsis thaliana secondary cell wall elements. J Vis Exp. doi: 10.3791/51381

Raudvere U, Kolberg L, Kuzmin I, Arak T, Adler P, Peterson H, Vilo J (2019) g:Profiler: a web server for functional enrichment analysis and conversions of gene lists (2019 update). Nucleic Acids Research **47**: W191–W198

Richardson AE, Hake S (2018) Drawing a Line: Grasses and Boundaries. Plants **8**: 4

Roxrud I, Lid SE, Fletcher JC, Schmidt EDL, Opsahl-Sorteberg H-G (2007) GASA4, one of the 14-member Arabidopsis GASA family of small polypeptides, regulates flowering and seed development. Plant Cell Physiol **48**: 471–483

Ruzin SE (1999) Plant Microtechnique and Microscopy. Oxford University Press, USA

Saffer AM (2018) Expanding roles for pectins in plant development. J Integr Plant Biol **60**: 910–923

Sakuma S, Schnurbusch T (2020) Of floral fortune: tinkering with the grain yield potential of cereal crops. New Phytol **225**: 1873–1882

Sampathkumar A, Peaucelle A, Fujita M, Schuster C, Persson S, Wasteneys GO, Meyerowitz EM (2019) Primary wall cellulose synthase regulates shoot apical meristem mechanics and growth. Development **146**: dev179036

Satoh-Nagasawa N, Nagasawa N, Malcomber S, Sakai H, Jackson D (2006) A trehalose metabolic enzyme controls inflorescence architecture in maize. Nature **441**: 227–230

Satterlee JW, Strable J, Scanlon MJ (2020) Plant stem-cell organization and differentiation at single-cell resolution. Proc Natl Acad Sci U S A **117**: 33689–33699

Schläpfer P, Zhang P, Wang C, Kim T, Banf M, Chae L, Dreher K, Chavali AK, Nilo-Poyanco R, Bernard T, et al (2017) Genome-Wide Prediction of Metabolic Enzymes, Pathways, and Gene Clusters in Plants. Plant Physiol **173**: 2041–2059

Schneider CA, Rasband WS, Eliceiri KW (2012) NIH Image to ImageJ: 25 years of image

analysis. Nat Methods **9**: 671–675

Schwacke R, Ponce-Soto GY, Krause K, Bolger AM, Arsova B, Hallab A, Gruden K, Stitt M, Bolger ME, Usadel B (2019) MapMan4: A Refined Protein Classification and Annotation Framework Applicable to Multi-Omics Data Analysis. Mol Plant **12**: 879–892

Sekhon RS, Childs KL, Santoro N, Foster CE, Buell CR, de Leon N, Kaeppler SM (2012) Transcriptional and metabolic analysis of senescence induced by preventing pollination in maize. Plant Physiol **159**: 1730–1744

Sekhon RS, Saski C, Kumar R, Flinn BS, Luo F, Beissinger TM, Ackerman AJ, Breitzman MW, Bridges WC, de Leon N, et al (2019) Integrated Genome-Scale Analysis Identifies Novel Genes and Networks Underlying Senescence in Maize. Plant Cell **31**: 1968–1989

Skibbe DS, Wang X, Borsuk LA, Ashlock DA, Nettleton D, Schnable PS (2008) Floret-specific differences in gene expression and support for the hypothesis that tapetal degeneration of Zea mays L. occurs via programmed cell death. J Genet Genomics **35**: 603–616

Smeekens S (2015) From Leaf to Kernel: Trehalose-6-Phosphate Signaling Moves Carbon in the Field. Plant Physiol **169**: 912–913

Takacs EM, Li J, Du C, Ponnala L, Janick-Buckner D, Yu J, Muehlbauer GJ, Schnable PS, Timmermans MCP, Sun Q, et al (2012) Ontogeny of the Maize Shoot Apical Meristem. The Plant Cell **24**: 3219–3234

Thompson BE, Bartling L, Whipple C, Hall DH, Sakai H, Schmidt R, Hake S (2009) bearded-ear encodes a MADS box transcription factor critical for maize floral development. Plant Cell **21**: 2578–2590

Thompson BE, Hake S (2009) Translational biology: from Arabidopsis flowers to grass inflorescence architecture. Plant Physiol **149**: 38–45

Torode TA, O'Neill R, Marcus SE, Cornuault V, Pose S, Lauder RP, Kračun SK, Rydahl MG, Andersen MCF, Willats WGT, et al (2018) Branched Pectic Galactan in Phloem-Sieve-Element Cell Walls: Implications for Cell Mechanics. Plant Physiology **176**: 1547–1558

Tsai AY-L, Gazzarrini S (2014) Trehalose-6-phosphate and SnRK1 kinases in plant development and signaling: the emerging picture. Front Plant Sci **5**: 119

Verhertbruggen Y, Marcus SE, Haeger A, Ordaz-Ortiz JJ, Knox JP (2009) An extended set of monoclonal antibodies to pectic homogalacturonan. Carbohydr Res **344**: 1858–1862

Vogel J (2008) Unique aspects of the grass cell wall. Curr Opin Plant Biol **11**: 301–307

Wang F, Yuan Z, Zhao Z, Li C, Zhang X, Liang H, Liu Y, Xu Q, Liu H (2020) Tasselseed5

encodes a cytochrome C oxidase that functions in sex determination by affecting jasmonate catabolism in maize. J Integr Plant Biol **62**: 247–255

Wang Q, Hasson A, Rossmann S, Theres K (2016) Divide et impera: boundaries shape the plant body and initiate new meristems. New Phytol **209**: 485–498

Whipple CJ (2017) Grass inflorescence architecture and evolution: the origin of novel signaling centers. New Phytol **216**: 367–372

Wingler A (2002) The function of trehalose biosynthesis in plants. Phytochemistry **60**: 437–440

Xue J, Bosch M, Paul Knox J (2013) Heterogeneity and Glycan Masking of Cell Wall Microstructures in the Stems of Miscanthus x giganteus, and Its Parents M. sinensis and M. sacchariflorus. PLoS ONE **8**: e82114

Yandeau-Nelson MD, Laurens L, Shi Z, Xia H, Smith AM, Guiltinan MJ (2011) Starch-branching enzyme IIa is required for proper diurnal cycling of starch in leaves of maize. Plant Physiol **156**: 479–490

Young TE, Geisler-Lee J, Gallie DR (2004) Senescence-induced expression of cytokinin reverses pistil abortion during maize flower development. Plant J **38**: 910–922

Zhang D, Sun W, Singh R, Zheng Y, Cao Z, Li M, Lunde C, Hake S, Zhang Z (2018) GRF-interacting factor1 Regulates Shoot Architecture and Meristem Determinacy in Maize. The Plant Cell **30**: 360–374

Zhang X, von Mogel KJH, Lor VS, Hirsch CN, De Vries B, Kaeppler HF, Tracy WF, Kaeppler SM (2019) Maize sugary enhancer1 (se1) is a gene affecting endosperm starch metabolism. Proceedings of the National Academy of Sciences **116**: 20776–20785

Zhong C, Xu H, Ye S, Wang S, Li L, Zhang S, Wang X (2015) Gibberellic Acid-Stimulated Arabidopsis6 Serves as an Integrator of Gibberellin, Abscisic Acid, and Glucose Signaling during Seed Germination in Arabidopsis. Plant Physiol **169**: 2288–2303

Zhong R, Cui D, Ye Z (2019) Secondary cell wall biosynthesis. New Phytologist **221**: 1703–1723

Chapter 3

Characterization of translation repression by miRNAs in maize

Introduction

MicroRNAs (miRNAs) are short, non-coding RNAs that repress gene expression in both plants and animals. Plant miRNAs have diverse functions in growth, development, stress response such as flower morphogenesis, flowering time, vegetative growth, leaf polarity, and biotic and abiotic response to environmental signals (Luo et al., 2013; Yu et al., 2019).

Plant miRNA biogenesis has been well-characterized, drawing heavily from experiments in the model plant, Arabidopsis. Endogenous miRNA genes are transcribed by RNA polymerase II into long, hairpin structures, called primary miRNAs (pri-miRNAs). Pri-miRNAs are then cleaved to liberate the hairpin structures, called precursor miRNAs (pre-miRNAs) by DICER-LIKE1 (DCL1) and assistant proteins. DCL1 and assistant proteins carry out a second cleavage on pre-miRNAs to generate a double strand 21-22 nt miRNA/miRNA* duplex with 3' overhangs. Subsequently, the 3' overhangs are methylated by HUA ENHANCER1 (HEN1) (Li et al., 2005; Yu et al., 2005; Yang et al., 2006) and exported to the cytoplasm by the exportin protein HASTY (HST1) (Park et al., 2005).

There are two canonical modes of miRNA-regulated gene expression in plants: mRNA cleavage and translation inhibition.Cleavage and degradation, however, is thought to be the primary mechanism of miRNA-mediated regulation in plants. In the cytoplasm, mature miRNA strand is loaded into ARGONAUTE (AGO) protein to form miRNA-AGO1 RNA-induced silencing complex (RISC), followed by the miRNA* strand degradation (Yu et al., 2019). AGO proteins have two typical domains: PIWI and PAZ. PIWI domain, similar to RNase H, has the endonucleolytic activity while PAZ domain, also found in DICER enzymes, is responsible for binding 3' overhang of small RNAs (Hall and Tanaka Hall, 2005; Ender and Meister, 2010).

Within RISC, miRNAs act as a guide to target specific mRNAs with complementary sequences. In plants, RISC complexes generally cleave mRNA at the position corresponding to 10 and 11 nt of miRNAs in endoplasmic reticulum and cytosol (Rogers and Chen, 2013; Li et al., 2016). On the other hand, RISC complexes potentially repress translation initiation without deadenylation of RNA decay, but also block recruitment or movement of ribosomes, potentially in the membranes like endoplasmic reticulum and in the cytosol including non-membrane structures microtubules and P-body (Brodersen et al., 2008; Yang et al., 2012; Iwakawa and Tomari, 2013; Li et al., 2013).

MiRNA-directed cleavage is thought to be far more common than miRNA-mediated translation repression in plants (Chen, 2008; Iwakawa and Tomari, 2015) because perfect or nearly perfect complementary pairing is present between miRNAs and their targets (Iwakawa and Tomari, 2015). MiRNA-directed cleavage is also easy to detect through cleavage fragments from miRNA targets by multiple approaches such as rapid amplification of cDNA end and degradome sequencing. Translation repression by miRNAs is rarely observed, possibly due to the lack of high-quality antibodies for miRNA targets or sensitive sequencing technology for translation (Rogers and Chen, 2013; Yu et al., 2017).

Importantly, the relative contribution of translational repression versus mRNA degradation by miRNAs is unknown at the genome-level for plants, especially for maize. The maize *fuzzy tassel (fzt)* mutant, encodes DICER-LIKE1 (DCL1), a key enzyme in plant miRNA biogenesis. *fzt* has pronounced inflorescence development defects like floral meristem and sex determination defects due to the decreased levels of miRNAs. While many miRNAs are reduced in *fzt*, the levels of miRNA-targeted mRNAs are not broadly increased, suggesting that translational

regulation by miRNAs may be more widespread (Thompson et al., 2014). To gain insight into repression mechanisms of miRNAs in maize inflorescence development, we combined ribosome profiling and RNA-seq to globally survey miRNA functions in maize tassel primordia.

Results

mRNA stability and translation repression contribute to miRNA repression

To systematically examine miRNA regulation in maize, we used ribo-seq and RNA-seq to compare RNA levels and translation in normal and *fzt* mutant plants (Figure 1). We prepared three biological replicates each for both *fzt* and normal tassel primordia and analyzed samples by ribosome profiling (Riboseq) and RNA sequencing (RNAseq) (Figure 1 and Supplemental Figure 1). In brief, we acquired ~11-23 million unique mapping reads in CDS regions for ribosome footprint and ~60-76 million unique mapping reads in input mRNAs across six libraries, which are comparable to previous reports (Chotewutmontri and Barkan, 2016; Chotewutmontri and Barkan, 2018). Principal component analysis (PCA) confirmed *fzt* and normal siblings clustered together and had high reproducibility (Supplemental Figure S2).

To ensure the isolated ribosome footprints reflected bona fide translation, we examined three hallmarks of ribosome profiling: reads distribution, ribosome footprint length, 3 nucleotide (nt) periodicity. In eukaryotic translation, the 43S preinitiation complex scans the 5' untranslated region (5' UTR) and recruits the 60S large ribosomal subunit to form 80S ribosome at start codon, followed by the active elongation along coding region (CDS) and abrupt termination after stop codon (Iwakawa and Tomari, 2015). As expected, we observed most of filtered riboseq reads are uniquely mapped to CDS regions in both normal and *fzt* mutant samples. In contrast, RNA-seq read distribution was widespread along the length of the mRNA, with a slight 3' bias

due to poly(A) selection for library preparation (Figure 2A). Next, we examined read lengths of ribosome footprints. In eukaryotes, ribosome footprints are typically ~30 nt long, which reflect the occupancy of 60S ribosomal subunits, and more importantly, the stable size of cytoplasmic ribosome footprint by cycloheximide treatment is usually ~30 nt (Jackson and Standart, 2015). Major and minor peaks of 31 and 22 nt, respectively, represent two canonical conformational/rotational stages of translating ribosomes (Lareau et al., 2014; Wu et al., 2019; Gelsinger et al., 2020). Ribosome footprint lengths of normal samples matched this expected distribution (Figure 2B). In *fzt* samples, with reduced levels of miRNAs, ribosome footprints were substantially longer than normal samples, with a major peak at 34 nt. The longer size of ribosome footprints might be generated by different rotated stages of ribosomes (Fujita et al., 2020), suggesting *fzt* mutants may have distinct functional stages of translating ribosomes. Finally, we examined three nucleotide periodicity of ribosome footprints in normal and *fzt* samples. Three nucleotide periodicity reflects the stepwise translocation pattern of ribosomes along each codon of translating mRNAs. Three nucleotide periodicity of 27-36 nt ribosome footprints (Figure 2C) and metagene analysis of peaky ribosome footprints (Figure 2D) show authentic translational features in our six samples. Taken together, these data suggest our ribosome footprints faithfully captured active translating mRNAs.

MiRNAs in plants negatively regulate expression by promoting degradation or inhibiting translation of target mRNAs. To determine the relative contributions of RNA stability and translational repression to miRNA regulation in maize, we determined the global RNA levels, translated mRNA abundance, i.e. ribosome protected fragment (RPF) and translation efficiency (TE) of miRNA targets and non-targets in both normal and *fzt* mutant samples (Figure 3).

Translation efficiency is the rate of protein production per mRNA, which can be reflected by the ratio of ribosome protected fragments to mRNA abundance (Ingolia et al., 2009; Gobet and Naef, 2017). If miRNAs regulate mRNAs primarily at the level of cleavage and degradation, we expect RPF and mRNA abundance of miRNA target to increase proportionately in *fzt* compared to normal siblings. In contrast, if miRNAs regulate mRNAs primarily at the level of translation, we expect an increase in RPF in *fzt* compared to normal samples, but no corresponding increase in mRNA abundance. If miRNA targets undergo mRNA cleavage with additional translation repression, we expect increased RPF levels as well as increases in mRNA abundance and TE in *fzt* compared to normal siblings.

Our data indicate that both RNA degradation and translational repression contribute to most miRNA regulation. To examine distribution differences in RFP, RNA levels, and translational efficiency in *fzt* and normal siblings, we constructed cumulative density plots for both miRNA and non-miRNA targets (Figure 3A-C). In all cases, we observed a significant difference between miRNA targets and non-miRNA targets, consistent with increased protein production of miRNA targets in *fzt* compared to normal samples. Of the 1530 miRNA targets with a significant difference in the RFP, ~70% were increased in *fzt* whereas only 30% were decreased. Of the 5612 non-miRNA targets with a significant difference in the RFP, only 40% of non-miRNA targets had increased RFP (Figure 3A). Similarly, >50% of miRNA targets with a significant difference in the RNA had increased RNA levels in *fzt* compared to normal, whereas only 40% of non-miRNA targets with a significant difference in the RNA had increased RNA levels (Figure 3B) and nearly 80% of miRNA targets with a significant difference in the TE had increased TE in *fzt* compared to normals versus 50% of non-miRNA targets with a significant

difference in the TE (Figure 3C). Additionally, the overall slope of the curve of miRNA targets revealed that effects from most of the increased RPF and RNA for miRNA targets are mild although almost all increased TE are mild effects ($\log_2$(fold change)<1). Together these results indicate that 1) changes in RPF of miRNA targets cannot be attributed solely to changes in RNA levels and 2) translational regulation by miRNAs is likely widespread, but small in magnitude. To understand the overall repression, we used the mean changes of RPF $\log_2$(fold change) to indicate the overall repression which can be explained by RNA degradation and TE repression in remaining RNA. We determined the relative contributions of RNA levels and TE to changes in RPF (Eichhorn et al., 2014) by calculating the mean fold change ($\log_2$) in RPF attributable to changes in RNA and TE, after deducting the mean change of each category in the non-miRNA targets and found approximately equal contribution (Figure 3D). To facilitate the interpretation, we indicated the contribution values of RPF, RNA, and TE with red vertical and horizontal lines in the correlation plot between RPF and RNA as well as RPF and TE for both miRNA targets and non-miRNA targets (Figure 3E-F). Together, these analyses indicate that changes in RNA levels and translational regulation contribute to miRNA-mediated repression.

MiRNA-mediated translation repression could be the result of reduced rates of translation initiation, blocked elongation, or accelerated ribosome drop-off (Bazzini et al., 2012). If miRNAs inhibit translation by reducing initiation, we expect ribosome occupancy to decrease uniformly along the length of the mRNA in the presence of miRNA-mediated repression. In contrast, if miRNAs inhibit translation by blocking elongation or promoting ribosome drop-off, we expect ribosome occupancy to gradually decrease along the length of the mRNA, with the lowest ribosome occupancy at the 3' end. To determine the likely mode of translational regulation in

maize, we analyzed ribosome occupancy of miRNA targets with a RPF $\log_2$(fold change) >0, q <0.05 and all non-miRNA targets along the CDS region (Figure 3G) (Bazzini et al., 2012). We chose to only include miRNA-targeted mRNAs with a significantly increased RFP for this analysis to specifically analyze ribosome occupancy of miRNA targets potentially subjected to translational repression. The increase in RFP of miRNA-targeted mRNAs ($\log_2$(fold change) approximately 0.4) was nearly twice the increase in mRNA levels ($\log_2$(fold change) approximately 0.2) (Figure 3G); no difference was observed in RFP or mRNA levels of non-miRNA targets. Importantly, ribosome occupancy was uniform along the length of the mRNA of both miRNA targets and non-miRNA-targets, suggesting ribosome drop-off did not occur and translation may be regulated primarily at the level of initiation.

Translation repression by miRNAs is dominant in maize

To understand the relationship between the cleavage and translational repression, we analyze different subsets of miRNA targets. Global analysis of miRNA targets indicated that both mRNA stability and translational regulation contribute to miRNA-mediated repression (Figure 3), and indeed more miRNA-targeted mRNAs had significantly increased RFP, RNA levels and TE in *fzt* compared to normals (Figure 4A) than non-miRNA targets, indicating broad upregulation of miRNA target mRNAs in *fzt.* However, the effect of RNA degradation by miRNAs might be overestimated because a certain subset of miRNA targets with higher $\log_2$(fold change)>1 in RNA could potentially lift overall mean fold changes of RNA (Figure 3B and 3D-E). For example, miRNA targets may be regulated 1) primarily at the level of RNA stability, 2) primarily at the level of translation, or 3) a combination of RNA stability and translational regulation. To address this question, we examined the correlation of miRNA targets with significantly increased

RPF, RNA, and TE between *fzt* and normal samples (Figure 4B-H). Specifically, of the 1024 miRNAs targets with a significantly increased RPF in *fzt* , ~30% (312) were regulated primarily at the RNA level (Figure 4B and 4G-H) and ~38% (390) primarily at the translational level (Figure 4B-D). To understand the overall repression of miRNAs at different levels, we also calculated the mean $\log_2$(fold change) of RPF, RNA, and TE for different subsets of miRNA targets (horizontal and vertical lines in Figure 4C-H). We observed a mild increase in RPF with mean $\log_2$(fold change) (0.54) for ~38% (390) of miRNA targets with corresponding increase in TE (0.47) but without a major increase in mRNA (0.02) (Figure 4D and 4E). ~30% (312) of miRNA targets also have seen a more accumulation in RPF with mean $\log_2$(fold change) (0.74) coinciding with a corresponding upregulation in RNA (0.69) without the TE change (0) (Figure 4H and 4I). These data suggest that translation repression or mRNA destability mainly occur on distinct sets of miRNA targets, at least for certain subsets of miRNA targets. Strikingly, ~27% of miRNA targets (281) with a significantly increased RPF, showed no significant difference in RNA or TE (Figure 4B and 4E-F). This suggests that relatively minor changes in RNA levels and TE, which alone did not meet the threshold for significance (adjusted $p < 0.05$), combined to a significant difference in RPF and likely translational output. We also observed a mild increase in RPF with mean $\log_2$(fold change) (0.44) with a more mild non-significant increase in TE (0.28) and a less mild non-significant increase in mRNA (0.16) (Figure 4E and 4F). This suggests a certain subset of miRNA targets have undergone weak mRNA destability with an additional mild translational repression. Thus translational regulation appears as a significant contributor of miRNA regulation for at least 70% of miRNA targets with increased RPF (Figure 4B-H). ~4% of miRNA targets with a significantly increased RPF, showed both significant

differences in RNA and TE level although relative contributions to RPF were variable (Figure 4C). Thus, minor translational repression contributes to the regulation of most miRNA targets and combined small changes in RNA and TE can lead to substantial differences in the amount of translated mRNAs.

Feedback regulation beyond the miRNA repression

To understand how *fzt* affects translation more broadly, we also examined biological patterns of non-miRNA targets with a significant differential RPF. Significant translational accumulation and reduction in non-miRNA targets (Figure 4A) make us wonder if distinct regulatory translation or RNA modules are involved in these feedback regulation. We used MapMan to predict functional groups of RPF up and RPF down categories and especially focused on biological groups and subgroups of protein and RNA (Wilcoxon Rank Sum Test, p value <0.05) (Figure 5A). Generally, genes related to protein biosynthesis, homeostasis, and translocation and RNA processing were enriched in both RPF up and down subsets, suggesting translation is broadly affected in *fzt* compared to normal plants, and reduced miRNA regulation in *fzt* may somehow feedback to affect translation more broadly. In addition, genes related to RNA biosynthesis were also enriched in the RPF down subset, suggesting more RNA regulation and protein modification in translational reduction. Surprisingly, genes in groups like translation elongation and aspartate group amino acid biosynthesis were enriched in the RPF up subset while groups like protein modification, protein quality control, protein folding, endoplasmic reticulum protein translocation were enriched in the RPF down category (Figure 5A), which might represent different feedback mechanisms in translational accumulation and reduction.

The broadness of translation changes in *fzt* mutant compared to normal makes us wonder if these widespread translation changes could be detected by polysome profiles (Figure 5B). Polysome profile is dependent on the rationale: the abundance of translated mRNAs is usually determined by a different number of bound ribosomes because translation is primarily regulated at the initiation step of translation. Actively translated mRNAs have more binding ribosomes (polysomes, indicating more synthesized proteins) while those with less efficient translation have less ribosomes or a single ribosome (less synthesized proteins) (Masvidal et al., 2017). We did not detect obvious differences in the polysome profiles from normal and *fzt* mutant plants (Figure 5C), despite indications of translation being widely affected in *fzt* mutants. Thus, mild changes in global translational state may not have a detectable effect in maize from qualitative methods like polysome profiles.

Discussion

Translational control of plant miRNAs has been underestimated or investigated in small-scale from in vitro assays from plant cell cultures (Iwakawa and Tomari, 2013; Tomari and Iwakawa, 2017) or studies in organelle/membrane protein mutants (Brodersen et al., 2008; Yang et al., 2012; Li et al., 2013). However, the magnitude and broadness of translation repression by miRNAs is still largely elusive in plants. In this study, we observed mild but broad translation changes by miRNAs in maize using Riboseq and RNAseq (Figure 3-4). Polysome profiles data did not detect significant translation changes, indicating the modest translation changes (Figure 5B-C). RNA degradation is still one of the dominant repression modes. However, translation repression contributes to translated mRNA/RPF in almost 70% of miRNA targets with significant differential RPFs in plants despite the overall modest effect. Different from animal

miRNAs, RNA decay has the predominant and broad effect. However, the effect of translation repression by animal miRNAs is also weak (mean of log2(fold change) in TE less than 1) (Guo et al., 2010; Eichhorn et al., 2014). These comparisons suggest eukaryotic miRNAs might have conserved weak translation repression, presumably by inhibition of translation initiation.

The broad range of translation repression in plant miRNAs is likely steady and independent of RNA degradation in plants. We did not observe comparable RNA changes with additional translation repression in most subsets of miRNA targets, suggesting translation repression may have a steady state and may not be a trigger for subsequent RNA degradation in plants (Figure 4). For animal miRNAs, translation repression is also weak but sometimes serves as the trigger for RNA decay. On one common scenario, translation repression by miRNA causes the subsequential RNA decay through the disruption of RNA stability like deadenylation of poly(A) tail and decapping (Bazzini et al., 2012; Djuranovic et al., 2012; Iwakawa and Tomari, 2015). Trigger roles might require translation repression to function temporally and then steady RNA decay emerges predominantly in animal miRNAs (Mathonnet et al., 2007; Fabian et al., 2009; Guo et al., 2010; Bazzini et al., 2012; Iwakawa and Tomari, 2015). Instead, translation repression in plant miRNAs might be stable. Feedback from translation machinery may also facilitate translation repression or alternatively, stable translation repression might be explained by the location of target sites. Whereas binding sites for animal miRNAs typically reside in the 3' UTR, binding sites for plant miRNAs typically reside in the CDS, although a few binding sites exist in the 5' and 3' UTRs (Liu et al., 2014). MiRNAs in 3' UTR might more easily affect the stable structure of translated mRNAs than miRNAs in CDS regions. Certain components might direct different destinies of miRNAs to cleave RNA or repress translation. For example, in

Arabidopsis, the DICER- LIKE1 (DCL1) partnering proteins, DOUBLE-STRANDED RNA-BINDING1 (DRB1) (also known as HYL1) and DRB2 selectively direct RNA cleavage and translation inhibition, respectively (Reis et al., 2015).

Material and Methods

Library construction and sequencing of ribosome footprint and RNA

Tassel primordia (0.5-1 cm) of *dcl1-fzt* and normal siblings were collected from approximately 4 week-old plants grown in Central Crops Research Station in Clayton, North Carolina (three biological replicates), and flash-frozen in liquid nitrogen. Each biological replicate of *dcl1-fzt* and normal sibling was pooled from six and five individual tassel primordia, respectively. Ribosome footprint and total RNA was extracted following the protocol described in (Chotewutmontri et al., 2018) with the following modification. For ultracentrifugation, 1.2 ml digested cell lysate was layered onto the 3.5 ml sucrose cushion and sealed with about 400 ul mineral oil and ultracentrifuged at 33,000 rpm for 5.5 hours at 4 °C using a Beckman SW50.1 rotor in Dupont Sorvall Laboratory Ultracentrifuge OTD-70B (accelerate code 8). Riboseq libraries were constructed using the NEXTFLEX® Small RNA-Seq Kit v3 (PerkinElmer Applied Genomics) following the customized rRNA depletion protocol described in (Chotewutmontri et al., 2018). RNA-seq libraries were constructed using the NEBNext Ultra Directional RNA Library Prep Kit for Illumina with the NEBNext Poly(A) mRNA Magnetic Isolation Module (New England Biolabs). Riboseq and RNAseq libraries are sequenced by Genomic Sciences Laboratory at North Carolina State University with NextSeq 500 v2 with 50 bp SR and NovaSeq 6000 SP with 150 bp PE mode, respectively.

Bioinformatic analysis

Raw Riboseq reads were trimmed using cutadapt (v1.18) to trim 3' adapter (TGGAATTCTCGGGTGCCAAGG), 5’ adapter (GTTCAGAGTTCTACAGTCCGACGATC), and 4 bases from each end of adapter-clipped reads. Trimmed reads (length>1) were then filtered out using bowtie2 (Langmead and Salzberg, 2012) to align against maize ribosomal RNA (retrieved from NCBI Nucleotide) and transfer RNA (retrieved from Ensembl Plants). Remaining clean reads were mapped to maize genome (v4.49) using STAR (v2.7.7a) with recommended parameters except: alignIntronMin 20 --sjdbOverhang 49 --outFilterScoreMinOverLread 0 --outFilterMatchNminOverLread 0 --outFilterMatchNmin 12 --outFilterMultimapNmax 1 --quantMode TranscriptomeSAM --outSAMattributes All. Raw RNAseq reads were trimmed using TrimGalore (v0.6.1) with the paired parameter. Clean reads were mapped using the same setting described for Riboseq except: sjdbOverhang 149 --outFilterMatchNmin 40.

Count tables were generated by htseq-count python package (Anders et al., 2015). Differential expression/translation and PCA analysis was analyzed using DESeq2 (Love et al., 2014) in the R environment. Translation efficiency and differential translation efficiency were calculated based on unique CDS count of Riboseq and unique gene count of RNAseq using xtail (v1.1.5) package (Xiao et al., 2016) in the docker environment. Genes with 10 minimum read count in at least two biological replicates across 12 Riboseq and RNAseq samples and adjusted $P < 0.05$ were considered differentially regulated. Read distribution, three nucleotide periodicity, ribosome footprint length, and metagene analysis were analyzed by using ribominer and ribotricer

packages (Choudhary et al., 2020; Li et al., 2020). Cumulative fraction of RPF, RNA, and TE and scatter plot was analyzed using R ecdf function and ggplot.

MiRNA target prediction was using the psRNATarget web server with default parameters of Schema V2 (2017 release) (https://www.zhaolab.org/psRNATarget/home) (Dai et al., 2018).

Ribosome occupancy and RNA density along the CDS was analyzed using ribominer (Li et al., 2020), custom python script, and R packages. For each gene, the transcript with the longest CDS region (cds length > 60 nt) was used for subsequent analysis. Whole CDS region was divided into 60 bins and the read count of each bin was summed. For each bin, the fold change of every gene was calculated using the DESeq2 package (Love et al., 2014).

Polysome gradient and fractionation

Polysome gradient and fractionation was modified from the protocol (Huggins et al., 2020). Briefly, tassel primordia from greenhouse grown maize (16 h light at 27°C, 8 h dark at 21°C) were dissected and collected in liquid nitrogen. Each biological replicate of *dcl1-fzt* and normal sibling was pooled from 19 and 18 individual tassel primordia, respectively. Primordia were ground in liquid nitrogen and lysates don't thaw by adding more liquid nitrogen, following by adding about 500 µl polysome extraction buffer (50 mM Tris-Acetate pH 8.0, 0.2 M sucrose, 0.2 M KCl, 15 mM $MgCl_2$, 2% polyoxyethylene-10-tridecyl ether, 1% Triton X-100, 20 mM *Beta*-mercaptoethanol, 100 µg/mL chloramphenicol, 100 µg/mL cycloheximide, 2 µl 40 U/µl RNasin® Plus RNase Inhibitor) to further grind and form well-mixed powder. Powder was thawed on ice and centrifuged (15, 000 xg for 10 min at 4 °C). Approximately 500 µl supernatant (about 160 µg RNA; diluted supernatant was quantified with Qubit 2.0 fluorometer using Qubit RNA HS kit) mixed with 1 µl RNasin® Plus RNase Inhibitor and then was loaded on 11 ml 10%

- 45% sucrose gradient (40 mM Tris-Acetate pH 8.0, 0.1 M KCl,15 mM $MgCl_2$, 10 mM *Beta*-mercaptoethanol) made with Biocomp Seton gradient maker (time 4.06 minute, angle 80 degree, speed 8). Tubes were then ultracentrifuged with SW41Ti rotor in Beckman Optima XPN-80 at 38, 000 rpm for 2 hours at 4 °C (accelerate code max and decelerate code 9). The fraction was fractionated into 1 ml/min with recommend parameters (chart speed 150 cm/hour, pump speed 40, absorbance sensitivity 1.0 or 2.0, noise filter 0.5 sec rise time, peak separator off) using a continuous ISCO UA-6 UV-Vis detector (Teledyne Foxy Fractionation System and "TRIS" Peristaltic Pump) at A254 nm.

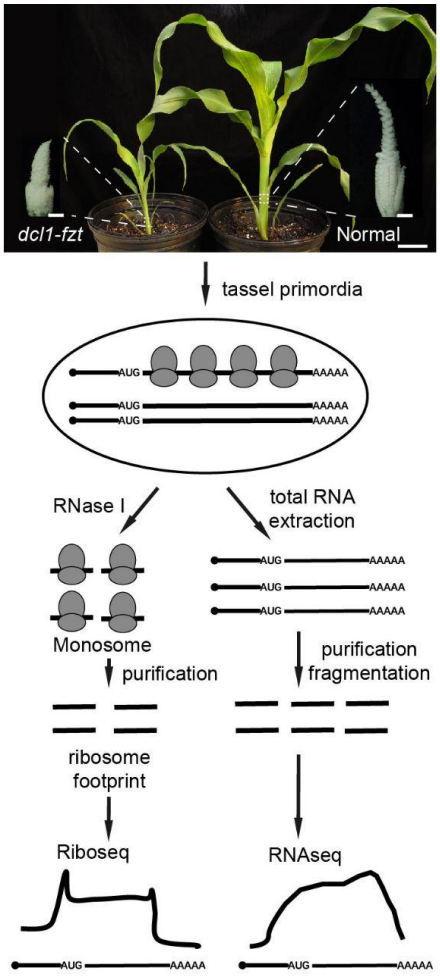

Figure 1. Summary of ribosome profiling and RNAseq.

Tassel primordia are grinded with a polysome extraction buffer and then the lysates are splitted into two parts. One will be extracted with Trizol to get total RNA. Another will be extracted to get ribosome footprint to construct riboseq library for sequencing. Scale bar in plants = 1cm and inset = 1mm.

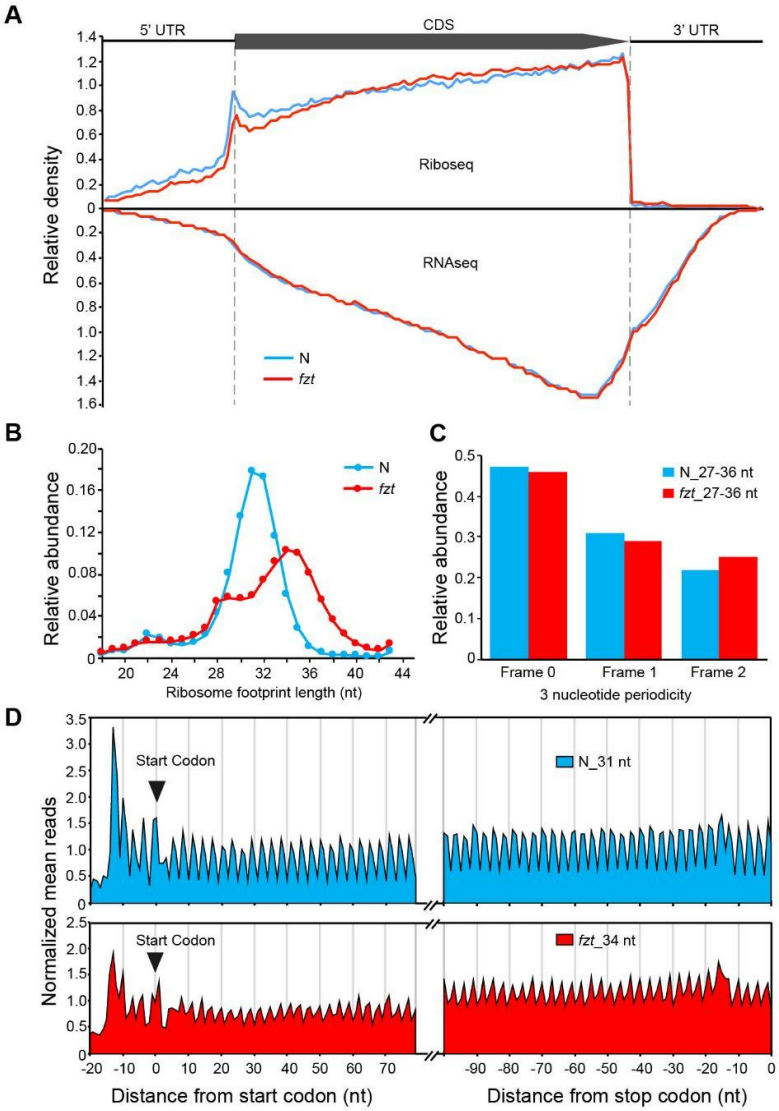

Figure 2. Ribosome footprints reflect the active translation.

A. Read distribution along the mRNA in the riboseq and RNAseq. B. Length distribution of ribosome footprints. C. Read distribution of ribosome footprints in three reading frames. D. Metagene analysis of peaky ribosome footprints close to annotated start and stop codon.

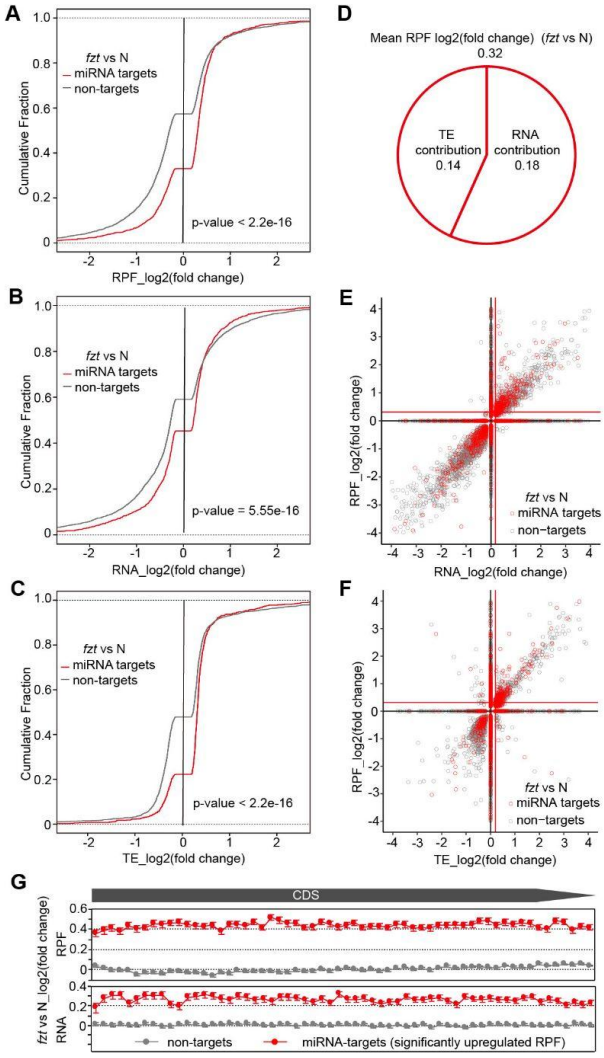

Figure 3. mRNA stability and translation repression contribute to miRNA repression.

A-C. Cumulative density distributions of significantly differential RPF, RNA, and TE $\log_2$(fold change) between *fzt* and normal siblings for predicted miRNA targets (red) and non-miRNA targets (gray). P-values for Kolmogorov–Smirnov tests are shown for miRNA targets (red) and non-miRNA targets (gray). D. Relative contributions of RNA levels and TE to RPF changes in miRNA targets. Mean $\log_2$(fold change) in RPF attributable to changes in RNA and TE is calculated after deducting mean $\log_2$(fold change) of each category in the non-miRNA targets. E-F. Scatter plots show $\log_2$(fold change) of significantly differential RPFs (y axis) and RNA or TE (x axis) between *fzt* and normal siblings. Predicted miRNA targets are in red and non-miRNA targets in gray. Calculated mean $\log_2$(fold change) after deducting mean $\log_2$(fold change) of non-miRNA targets are indicated as lines. 120 and 82 data were not present in scatter plots due to exceeding $\log_2$(fold change) space limit. G. Relative RPF read density (top) and RNA density (bottom) along the coding regions of miRNA targets with a significantly increased RFP (red) and

all non-miRNA targets (gray). Each point shows mean +/− SEM $\log_2$ (fold change) in 60 bins spanning the whole coding regions.

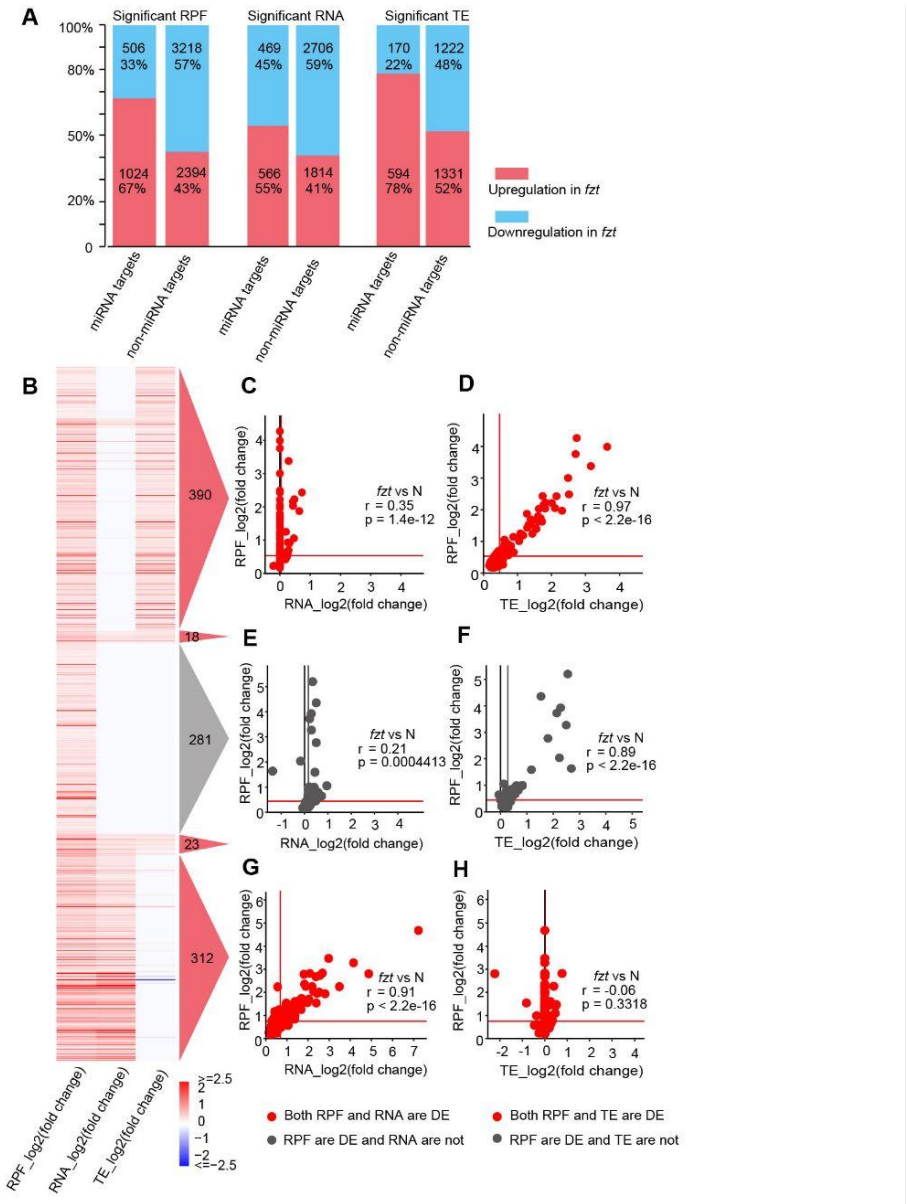

Figure 4. Translation repression by miRNAs is dominant in maize.

A. Summary of significantly differential RPF, RNA, and TE between *fzt* and normal siblings for predicted miRNA targets and non-miRNA targets. B. Correlation of RPF, RNA, and TE changes for miRNA targets with a significantly increased RFP in *fzt*. Categories (triangles) are classified based on correlation heatmap. Red triangle indicates RPF and one of RNA or TE are both significantly regulated. Grey triangle indicates RPF is significantly regulated and none of RNA or TE are significantly regulated. C-H. Correlation plots show $\log_2$(fold change) of significantly differential RPFs (y axis) and RNA or TE (x axis) for each category. Calculated mean $\log_2$(fold change) are indicated as gray or red lines.

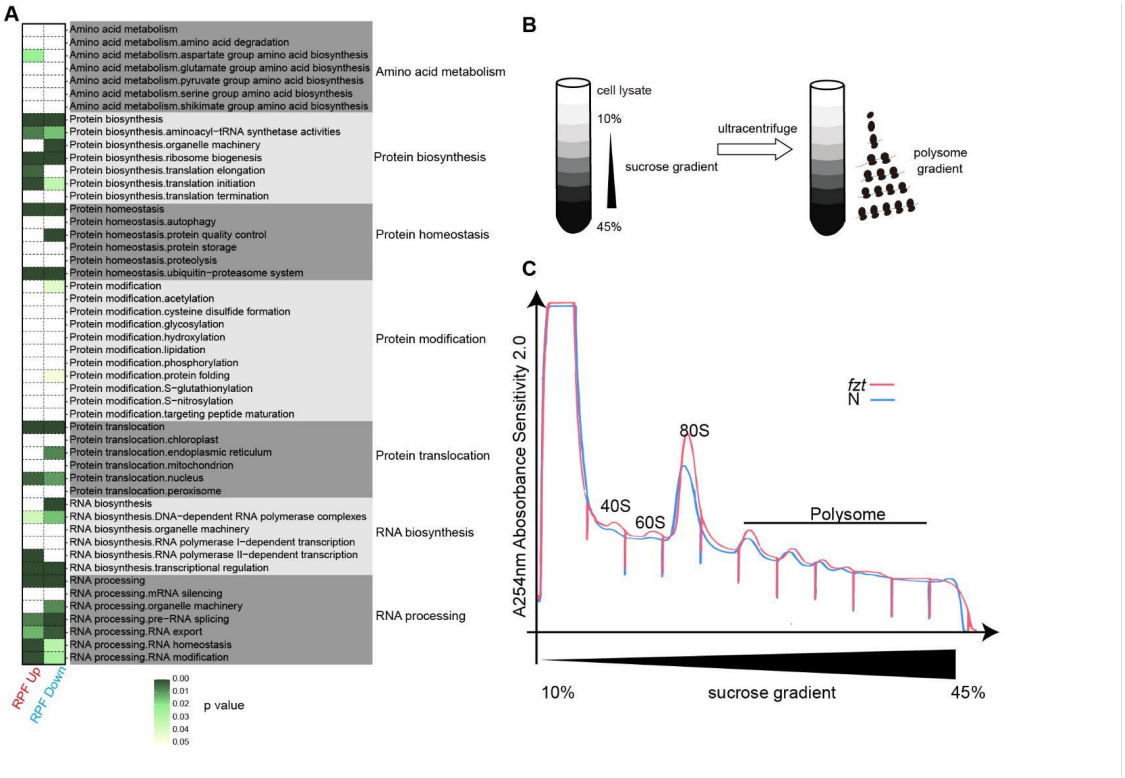

Figure 5. Feedback regulation beyond the miRNA repression.

A. Heatmap of MapMan-annotated functional groups from significantly upregulated and downregulated RPF of non-miRNA targets between *fzt* and normal siblings. P value is calculated in Wilcoxon rank sum test. Blank grids in heatmap are not statistically significant. B. Polysome profile assays. Extracted cell lysate is loaded on 10% - 45% sucrose gradient and detected with continuous UV detector at A254 nm. C. Polysome profile from *fzt* and normal tassel primordia. Two independent biological replicates show consistent results.

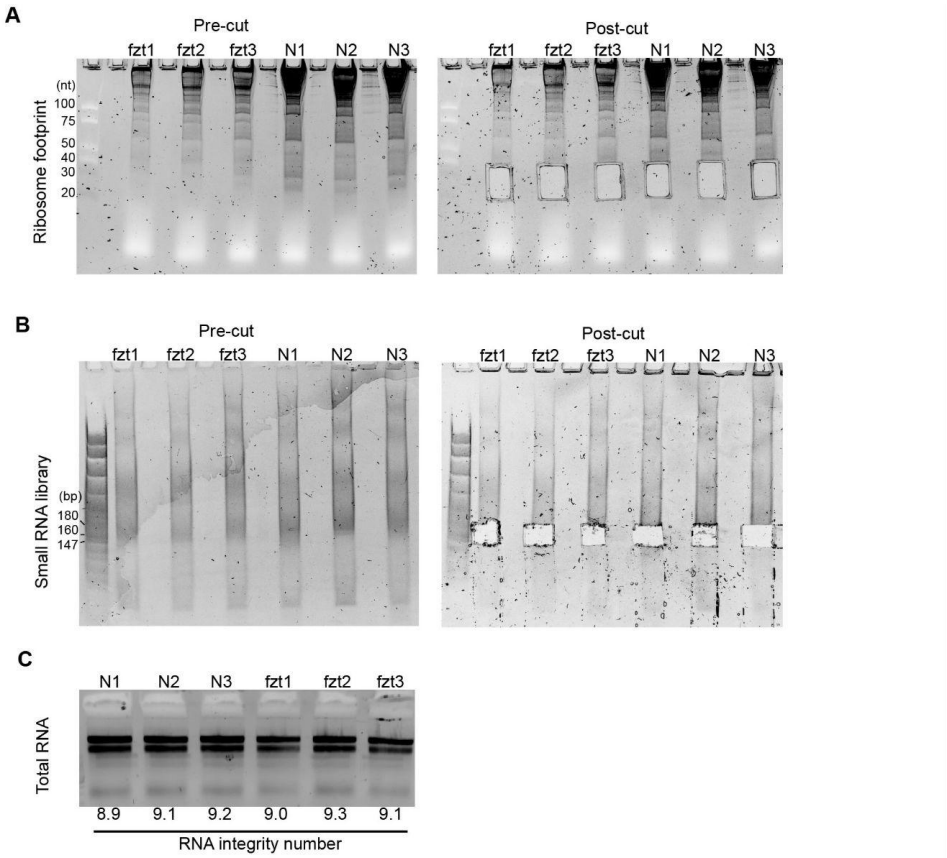

Supplemental Figure 1. Preparation of ribosome footprints, riboseq libraries, and total RNA from *fzt* and normal tassel primordia.

A. Preparation of ribosome footprints. The ethidium bromide (EB) staining denaturing-PAGE gel is indicated with prestained small RNA marker. The range of excised ribosome footprints is from 20 nt to 40 nt. B. Preparation of small RNA libraries for ribosome footprints. The ethidium bromide (EB) staining nature PAGE gel is indicated with pBR322 DNA-MspI Digest marker. The range of targeted library fragments is from 147 to ~170 bp corresponding to 20 – 40 nt ribosome footprint. C. Total RNA for RNAseq has high quality detected by Bioanalyzer.

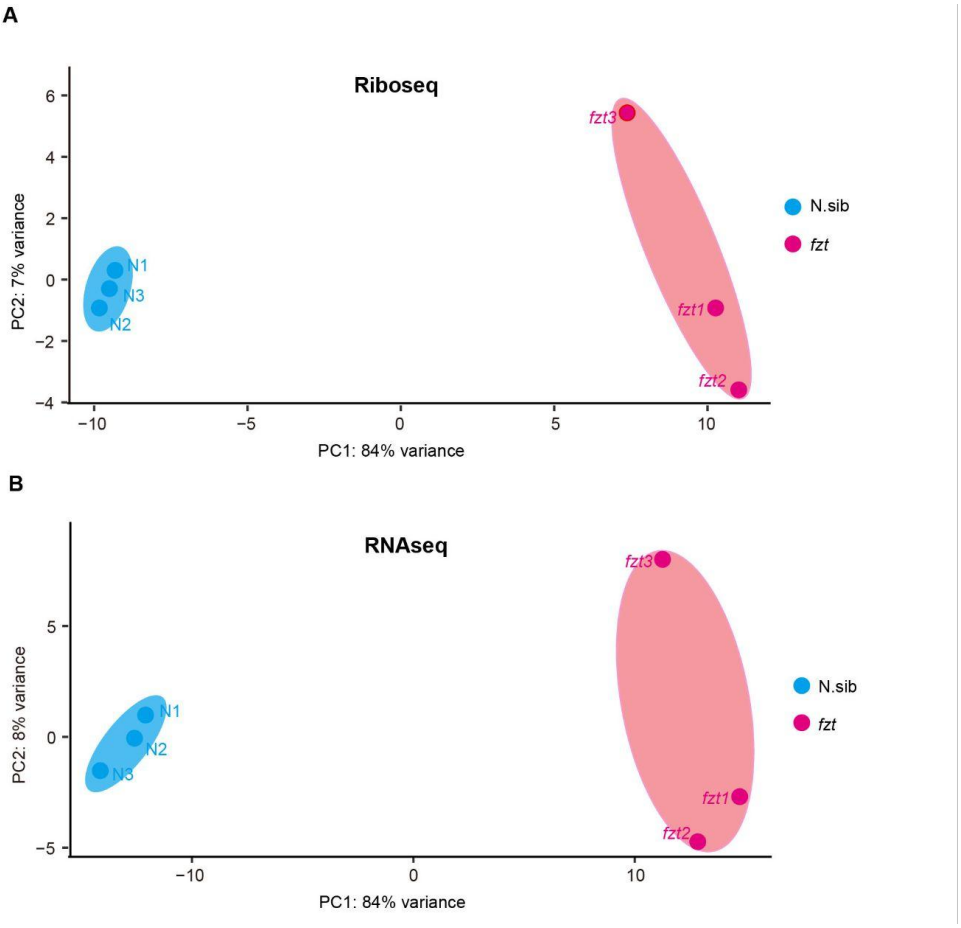

Supplemental Figure 2. Cluster and reproducibility analysis.

A-B. PCA analysis of riboseq samples and RNAseq samples in *fzt* and normal biological replicates.

Reference

Anders S, Pyl PT, Huber W (2015) HTSeq--a Python framework to work with high-throughput sequencing data. Bioinformatics **31**: 166–169

Bazzini AA, Lee MT, Giraldez AJ (2012) Ribosome profiling shows that miR-430 reduces translation before causing mRNA decay in zebrafish. Science **336**: 233–237

Brodersen P, Sakvarelidze-Achard L, Bruun-Rasmussen M, Dunoyer P, Yamamoto YY, Sieburth L, Voinnet O (2008) Widespread translational inhibition by plant miRNAs and siRNAs. Science **320**: 1185–1190

Chen X (2008) MicroRNA Metabolism in Plants. RNA Interference 117–136

Chotewutmontri P, Barkan A (2016) Dynamics of Chloroplast Translation during Chloroplast Differentiation in Maize. PLoS Genet **12**: e1006106

Chotewutmontri P, Barkan A (2018) Multilevel effects of light on ribosome dynamics in chloroplasts program genome-wide and psbA-specific changes in translation. PLoS Genet **14**: e1007555

Chotewutmontri P, Stiffler N, Watkins KP, Barkan A (2018) Ribosome Profiling in Maize. Maize 165–183

Choudhary S, Li W, D Smith A (2020) Accurate detection of short and long active ORFs using Ribo-seq data. Bioinformatics **36**: 2053–2059

Dai X, Zhuang Z, Zhao PX (2018) psRNATarget: a plant small RNA target analysis server (2017 release). Nucleic Acids Res **46**: W49–W54

Djuranovic S, Nahvi A, Green R (2012) miRNA-mediated gene silencing by translational repression followed by mRNA deadenylation and decay. Science **336**: 237–240

Eichhorn SW, Guo H, McGeary SE, Rodriguez-Mias RA, Shin C, Baek D, Hsu S-H, Ghoshal K, Villén J, Bartel DP (2014) mRNA destabilization is the dominant effect of mammalian microRNAs by the time substantial repression ensues. Mol Cell **56**: 104–115

Ender C, Meister G (2010) Argonaute proteins at a glance. Journal of Cell Science **123**: 1819–1823

Fabian MR, Mathonnet G, Sundermeier T, Mathys H, Zipprich JT, Svitkin YV, Rivas F, Jinek M, Wohlschlegel J, Doudna JA, et al (2009) Mammalian miRNA RISC recruits CAF1 and PABP to affect PABP-dependent deadenylation. Mol Cell **35**: 868–880

Fujita T, Yokoyama T, Shirouzu M, Taguchi H, Ito T, Iwasaki S Anatomy of footprint extension in ribosome profiling reveals translational landscape mediated by S1 protein in

bacteria. doi: 10.21203/rs.3.rs-41219/v1

Gelsinger DR, Dallon E, Reddy R, Mohammad F, Buskirk AR, DiRuggiero J (2020) Ribosome profiling in archaea reveals leaderless translation, novel translational initiation sites, and ribosome pausing at single codon resolution. Nucleic Acids Res **48**: 5201–5216

Gobet C, Naef F (2017) Ribosome profiling and dynamic regulation of translation in mammals. Curr Opin Genet Dev **43**: 120–127

Guo H, Ingolia NT, Weissman JS, Bartel DP (2010) Mammalian microRNAs predominantly act to decrease target mRNA levels. Nature **466**: 835–840

Hall TMT, Tanaka Hall TM (2005) Structure and Function of Argonaute Proteins. Structure **13**: 1403–1408

Huggins HP, Subash JS, Stoffel H, Henderson MA, Hoffman JL, Buckner DS, Sengupta MS, Boag PR, Lee M-H, Keiper BD (2020) Distinct roles of two eIF4E isoforms in the germline of. J Cell Sci. doi: 10.1242/jcs.237990

Ingolia NT, Ghaemmaghami S, Newman JRS, Weissman JS (2009) Genome-wide analysis in vivo of translation with nucleotide resolution using ribosome profiling. Science **324**: 218–223

Iwakawa H-O, Tomari Y (2013) Molecular insights into microRNA-mediated translational repression in plants. Mol Cell **52**: 591–601

Iwakawa H-O, Tomari Y (2015) The Functions of MicroRNAs: mRNA Decay and Translational Repression. Trends Cell Biol **25**: 651–665

Jackson R, Standart N (2015) The awesome power of ribosome profiling. RNA **21**: 652–654

Langmead B, Salzberg SL (2012) Fast gapped-read alignment with Bowtie 2. Nat Methods **9**: 357–359

Lareau LF, Hite DH, Hogan GJ, Brown PO (2014) Distinct stages of the translation elongation cycle revealed by sequencing ribosome-protected mRNA fragments. Elife **3**: e01257

Li F, Xing X, Xiao Z, Xu G, Yang X (2020) RiboMiner: a toolset for mining multi-dimensional features of the translatome with ribosome profiling data. BMC Bioinformatics **21**: 340

Li J, Yang Z, Yu B, Liu J, Chen X (2005) Methylation protects miRNAs and siRNAs from a 3’-end uridylation activity in Arabidopsis. Curr Biol **15**: 1501–1507

Li S, Le B, Ma X, Li S, You C, Yu Y, Zhang B, Liu L, Gao L, Shi T, et al (2016) Biogenesis of phased siRNAs on membrane-bound polysomes in Arabidopsis. Elife. doi:

10.7554/eLife.22750

Li S, Liu L, Zhuang X, Yu Y, Liu X, Cui X, Ji L, Pan Z, Cao X, Mo B, et al (2013) MicroRNAs inhibit the translation of target mRNAs on the endoplasmic reticulum in Arabidopsis. Cell **153**: 562–574

Liu Q, Wang F, Axtell MJ (2014) Analysis of complementarity requirements for plant microRNA targeting using a Nicotiana benthamiana quantitative transient assay. Plant Cell **26**: 741–753

Love MI, Huber W, Anders S (2014) Moderated estimation of fold change and dispersion for RNA-seq data with DESeq2. Genome Biol **15**: 550

Luo Y, Guo Z, Li L (2013) Evolutionary conservation of microRNA regulatory programs in plant flower development. Dev Biol **380**: 133–144

Masvidal L, Hulea L, Furic L, Topisirovic I, Larsson O (2017) mTOR-sensitive translation: Cleared fog reveals more trees. RNA Biol **14**: 1299–1305

Mathonnet G, Fabian MR, Svitkin YV, Parsyan A, Huck L, Murata T, Biffo S, Merrick WC, Darzynkiewicz E, Pillai RS, et al (2007) MicroRNA inhibition of translation initiation in vitro by targeting the cap-binding complex eIF4F. Science **317**: 1764–1767

Park MY, Wu G, Gonzalez-Sulser A, Vaucheret H, Poethig RS (2005) Nuclear processing and export of microRNAs in Arabidopsis. Proc Natl Acad Sci U S A **102**: 3691–3696

Pratt AJ, MacRae IJ (2009) The RNA-induced silencing complex: a versatile gene-silencing machine. J Biol Chem **284**: 17897–17901

Reis RS, Hart-Smith G, Eamens AL, Wilkins MR, Waterhouse PM (2015) Gene regulation by translational inhibition is determined by Dicer partnering proteins. Nat Plants **1**: 14027

Rogers K, Chen X (2013) Biogenesis, turnover, and mode of action of plant microRNAs. Plant Cell **25**: 2383–2399

Thompson BE, Basham C, Hammond R, Ding Q, Kakrana A, Lee T-F, Simon SA, Meeley R, Meyers BC, Hake S (2014) The dicer-like1 homolog fuzzy tassel is required for the regulation of meristem determinacy in the inflorescence and vegetative growth in maize. Plant Cell **26**: 4702–4717

Tomari Y, Iwakawa H-O (2017) In Vitro Analysis of ARGONAUTE-Mediated Target Cleavage and Translational Repression in Plants. Methods Mol Biol **1640**: 55–71

Wu CC-C, Zinshteyn B, Wehner KA, Green R (2019) High-Resolution Ribosome Profiling Defines Discrete Ribosome Elongation States and Translational Regulation during Cellular

Stress. Mol Cell **73**: 959–970.e5

Xiao Z, Zou Q, Liu Y, Yang X (2016) Genome-wide assessment of differential translations with ribosome profiling data. Nat Commun **7**: 11194

Yang L, Wu G, Poethig RS (2012) Mutations in the GW-repeat protein SUO reveal a developmental function for microRNA-mediated translational repression in Arabidopsis. Proc Natl Acad Sci U S A **109**: 315–320

Yang Z, Ebright YW, Yu B, Chen X (2006) HEN1 recognizes 21-24 nt small RNA duplexes and deposits a methyl group onto the 2’ OH of the 3' terminal nucleotide. Nucleic Acids Res **34**: 667–675

Yu B, Yang Z, Li J, Minakhina S, Yang M, Padgett RW, Steward R, Chen X (2005) Methylation as a crucial step in plant microRNA biogenesis. Science **307**: 932–935

Yu Y, Jia T, Chen X (2017) The “how” and “where” of plant microRNAs. New Phytol **216**: 1002–1017

Yu Y, Zhang Y, Chen X, Chen Y (2019) Plant Noncoding RNAs: Hidden Players in Development and Stress Responses. Annu Rev Cell Dev Biol **35**: 407–431

Chapter 4

Future Directions

Understanding the regulatory mechanisms of gene expression in floral development is critical for agricultural practice. My thesis work is focusing on gene expression regulation in maize floral development from transcription and translation level. Chapter 2 describes the role of downstream physiological modules in maize floral development, likely caused by upstream transcription regulation. Floral meristems are typically regarded as functionally equivalent, regardless of where they are initiated on the plant. Maize and other members of the Andropogoneae tribe, however, produce spikelets with two florets that are typically dimorphic. In maize ears, the upper floral meristem develops into a fertile female floret, but the lower floret aborts. Importantly, floral abortion and sterility is common in the cereals and the mechanisms that regulate lower floret growth in maize may also apply to other cereal crops. While a handful of regulators of floret abortion/sterility have been identified, almost nothing is known about the genes/physiological processes that function downstream of these high level regulators. Moreover, recent decades have seen much more popular identification and characterization of key genetic regulators in floral development compared to examination in physiological modules. Thus, it is critical to not only identify the physiological processes that function specifically in grass florets, but also how these processes vary between florets with different fates.

Chapter 2 investigates the downstream physiological modules in floral development, particularly connected to floral fertility or abortion. I did not identify genes likely to function as master regulators of upper versus lower floral meristem fate, suggesting that “selector” genes that determine meristem fate may not exist. It is also possible that some non-meristematic genes function as non-cell-autonomous pathways to regulate the floral meristem fates from cell-to-cell

communication. Upstream quantitative gene expression changes were predicted to function in core cell physiological processes, including the cell wall, sugar and energy homeostasis. I found that cell wall modifications and sugar accumulation differed between the upper and lower florets, indicating differential gene expression is reflective of changes in cell physiology and function. Importantly, demethylesterified pectin is assocated with carpel abortion, which might serve as the trigger or accompanying process during floral abortion. Early in spikelet development, pectin distribution is similar in all spikelets examined with both methylesterified and demethylesterified pectin preferentially accumulating in the upper floret, regardless of lower floret fate. Later in spikelet development, however, demethylesterified pectin was strongly associated with aborting carpels in both the upper and lower floret of tassel spikelets and in the lower floret of ear spikelets. Pectin modification in the carpel abortion were unexpected and very novel in cell wall study. To our knowledge, this is the first indication that pectin functions in programmed cell death in plants and may be a critical factor in floret fertility.

I also identified a novel boundary domain between the upper and lower floret including RNA localization (like *BBTI*, *pectate lysate*, *adc1*) and sugar localization (starch staining). This also triggers us to pursue the cell wall function (like pectin) in this unique boundary. This boundary domain might serve the regulatory hub, which is probably important for floral meristem activity. It is likely relevant to other species in the Andropogoneae tribe, which includes key crops such as sorghum and sugarcane in addition to maize, and may be broadly applicable in the grasses.

Chapter 3 describes the role of translational regulation in maize floral development, likely caused by miRNA translation repression. Relative contribution of mRNA degradation and translational repression by maize miRNAs point to two distinct modes of gene expression

regulation. RNA degradation has a small scale (less targets) but dramatic effect (higher fold changes) and translational repression has large scale (more targets) but modest effect (lower fold changes). In multiple possible regulatory contexts by animal miRNAs, RNA decay can be caused by transient or rapid translation repression and forms the lag of detectable destabilization; RNA decay sometimes is also independent of translation repression. This raises several questions about plant miRNAs: why do plants need this broad and mild translation repression? What is the relationship between RNA degradation and translation repression? Are RNA degradation and translational repression happening parallel or cause-and-effect?

The biological effect by translation repression in plant miRNAs might be underestimated. Direct quantifying the fold changes to interpret overall silencing by RNA degradation and translation repression might miss the feedback regulation as a whole. When miRNA regulation is disrupted (for example, in a miRNA biogenesis mutant), the cell responds with broad changes to the translational landscape, beyond direct miRNA targets. Thus, the biological effect of mild translational changes by miRNAs might be more powerful than expected. The fate of RNA cleavage is degradation, but the fate of translation repression is unknown. Translation repression may be reversible to ensure the presence of template mRNAs in case that translational-repressed targets are required to be reactivated. It is also noticeable that translation repression by plant miRNAs is associated with cytosol, membrane or organelles compartments. The compartmentalization of translation repression might be more efficient and specific for gene expression regulation.